PHOTONICS Research

Epsilon-near-zero photonics: infinite potentials

Jiaye Wu,[1] Ze Tao Xie,[1] Yanhua Sha,[1] H. Y. Fu,[2] and Qian Li[1,*]

[1]School of Electronic and Computer Engineering, Peking University, Shenzhen 518055, China
[2]Tsinghua Shenzhen International Graduate School, Tsinghua University, Shenzhen 518055, China
*Corresponding author: liqian@pkusz.edu.cn

Received 7 April 2021; revised 28 May 2021; accepted 28 May 2021; posted 1 June 2021 (Doc. ID 427246); published 30 July 2021

With its unique and exclusive linear and nonlinear optical characteristics, epsilon-near-zero (ENZ) photonics has drawn a tremendous amount of attention in the recent decade in the fields of nanophotonics, nonlinear optics, plasmonics, light-matter interactions, material science, applied optical science, etc. The extraordinary optical properties, relatively high tuning flexibility, and CMOS compatibility of ENZ materials make them popular and competitive candidates for nanophotonic devices and on-chip integration in all-optical and electro-optical platforms. With exclusive features and high performance, ENZ photonics can play a big role in optical communications and optical data processing. In this review, we give a focused discussion on recent advances of the theoretical and experimental studies on ENZ photonics, especially in the regime of nonlinear ENZ nanophotonics and its applications. First, we overview the basics of the ENZ concepts, mechanisms, and nonlinear ENZ nanophotonics. Then the new advancements in theoretical and experimental optical physics are reviewed. For nanophotonic applications, the recent decades saw rapid developments in various kinds of different ENZ-based devices and systems, which are discussed and analyzed in detail. Finally, we give our perspectives on where future endeavors can be made.

https://doi.org/10.1364/PRJ.427246

1. INTRODUCTION

Epsilon-near-zero (ENZ) materials are a category of near-zero-index (NZI) materials [1–3] that are regarded as a novel platform for integrated photonics and nanophotonic devices [4]. Generally, there are four main mechanisms to realize ENZ [4], namely, first, to utilize the collective motion of free carriers at bulk plasma frequency in semiconductors [5]; second, to implement photonic multilayer design via the media mixing of alternating layers of dielectric and metal materials [6,7] and create an effective medium [8]; third, to use a metallic shell to force and confine electromagnetic (EM) energy in a waveguide below cutoff frequency so as to obtain a near-zero effect [9–11]; and last, to exploit the photonic Dirac cone in the Brillouin zone [12–14]. Among these, the first mechanism is more widely used, because heavily doped silicon-based semiconductors [5], III-V group semiconductors [15], metals [4,5], and transparent conducting oxides (TCOs) [1,2,4,5,16] can easily realize ENZ by adjusting their free carrier concentration. Most of the ENZ materials operate in a wide range of the spectrum, from ultraviolet (UV), visible, near-infrared (NIR), to the mid-infrared (MIR) and far-infrared (FIR), making them perfect candidates to be used in applications of visible light communications (VLC) and the IR telecommunication windows of 1.3, 1.55, and 2 μm.

In the recent two decades, novel phenomena have been found in ENZ materials, such as EM energy squeezing and tunneling [10,17], slow light trapping [18], pulse shaping [19–21], enhanced electric fields [22–25], enhanced optical nonlinearity [16,26–28], complex pulse dynamics [20,29–36], second- [37–43], third- [40,44,45], high-harmonic generations (SHG, THG, HHG), and cascaded HHG [46–51], efficient frequency conversion and translation [52,53], MIR nonlocality [54], super-coupling effects [55], novel optical modes [56–59], spin-orbit interactions [60,61], and enhancement of spatial nonlocality [62,63]. In the last couple of years, new methods to tune the ENZ properties have emerged, such as electro- and all-optical tuning [64–66], controlled annealing [67,68], laser-induced tunability [69], and supercritical fluid (SCF) treatments [70]. The exclusive optical properties and advanced experimental techniques have given rise to numerous applications including manipulation of thermal emissions [71], passively Q-switched solid-state lasers [72], on-chip quantum networks [73], electro- and all-optical switches [65,74–79], optical modulators [64,66,80–89], absorbers [90–97], optical isolators [98], photonic memory [99,100], on-chip light sources [101–104], circuit elements [105], terahertz [106–108] and radio-frequency range operation [109], wireless communications [110], beam generation and shifts [111–116], and improving the resolution of lithography [117–119]. These mentioned works are only an overview and brief examples of the progress in the ENZ community, and more literature is discussed in detail in the following sections of this review.

Previous review papers [1,2,4,5,16] discussed ENZ photonics in the aspects and perspectives of plasmonics [5], integration platforms [4], NZI conditions [1,2], and nonlinear optical effects [16]. In this review, we focus on the recent progress of theoretical and experimental researches on ENZ photonics, typically in the realm of the rapidly developing nonlinear ENZ nanophotonic physics and its applications in the last two years. This review is structured as follows. In Section 2, the basics, mechanisms, and nonlinearity of ENZ materials are introduced. In Section 3, the recent advances in optical physics of ENZ are summarized, especially with nanostructures and subwavelength setups. In Section 4, the progress of ENZ nanophotonic applications in the recent couple of years is discussed. In Section 5, we share our perspectives and visions on future researches on ENZ photonics. Finally, in Section 6, conclusions are drawn for this review.

2. BASICS OF ENZ PHOTONICS

A. ENZ-Induced Linear Optical Phenomena

The refractive index n is a fundamental, simple, yet fascinating constant to manipulate and play with. Departing from the "normal" dielectric materials where n is always larger than one, resembling the idea of "negative index" (e.g., Refs. [120–123]), NZI materials begin with a conception that n can be tuned smaller than one and near zero, according to the relation that n equals the square root of the product of permeability μ and permittivity ε. This means that three options are available to realize NZI: μ-near-zero (MNZ), ε-near-zero (ENZ), and ε-μ-near-zero (EMNZ). MNZ and EMNZ involve the manipulation of μ, and they form their own category. Compared with them, ENZ seems to be a more intensively studied topic, and this might be due to its easier implementation, which is introduced in Section 2.C. Generally, the exact spectral (frequency/wavelength) point where the permittivity (or its real part) approaches zero is called an ENZ frequency/wavelength, or ENZ point. The vicinity of the ENZ point is called an ENZ region or ENZ zone, but by far, there is no clear definition of the width of the ENZ region. It is possible to define the spectral area where $-1 \le \varepsilon \le 1$ or $0 \le n \le 1$ to be the ENZ region based on a classical optics sense. Figure 1(a) shows the measured complex permittivity of an ENZ indium tin oxide (ITO) with an ENZ wavelength at ~1400 nm [108], and Fig. 1(d) is a photograph of an ENZ ITO nanolayer. In some materials such as TCOs, inevitable intrinsic loss exists in the ENZ region, and therefore their permittivity and refractive index are complex. Assume that $\mu \approx 1$, for complex ε and complex $n_C = n + ik$, $\varepsilon = n_C^2$ still holds. By expanding it, one can

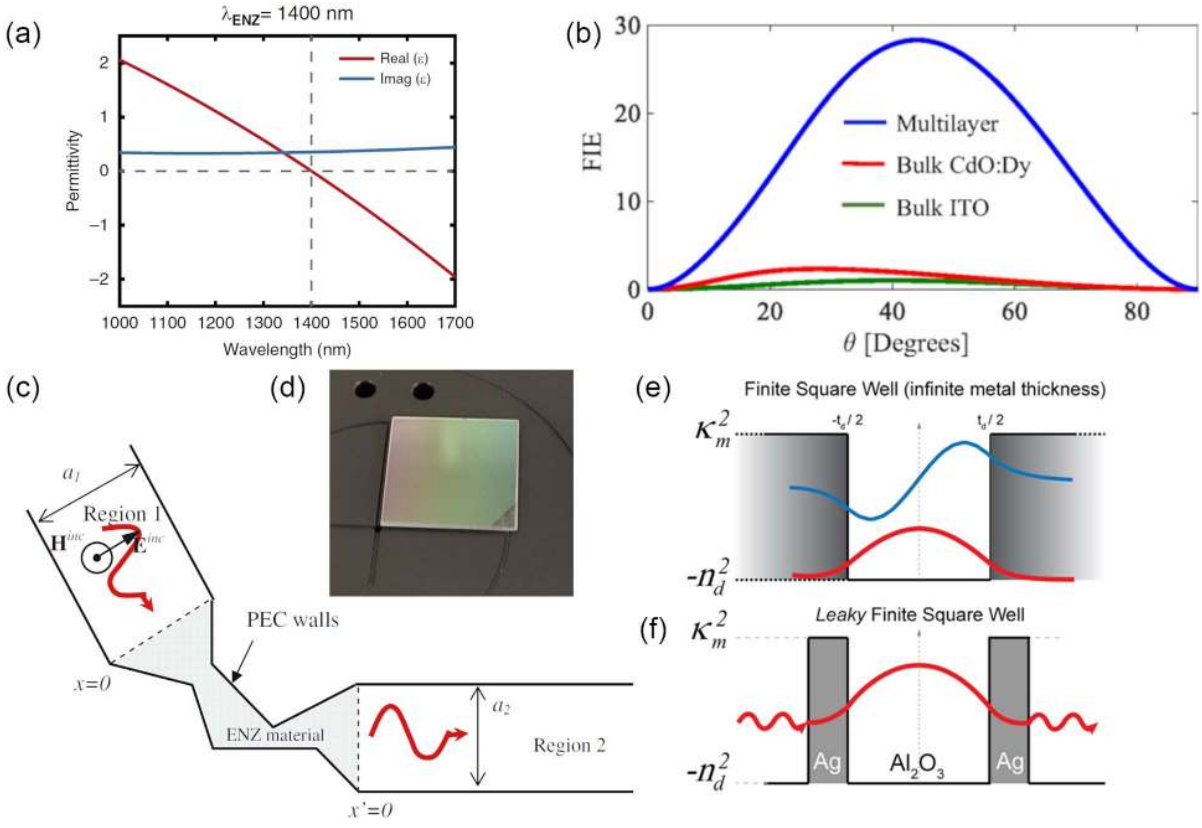

Fig. 1. (a) Measured complex permittivity of ENZ ITO nanolayer. The ENZ wavelength is observed at 1400 nm [108]. (b) Field intensity enhancement factor versus incident angle for multilayer, CdO:Dy, and ITO [124]. (c) Schematic diagram of a waveguide structure with an ENZ section [125]. (d) Photograph of an ITO nanolayer deposited on a silica glass substrate. (e) Square quantum well model of the MIM structure with thick metal layers [126]. (f) Double barrier system of the quantum well model for MIM structure with thin metal layers [126]. (a) Springer Nature and Changchun Institute of Optics, Fine Machines and Physics (CIOMP), under a Creative Commons CC BY License; (b), (c) American Physical Society; (e), (f) American Chemical Society.

obtain $\Re(\varepsilon) = n^2 - k^2$ and $\Im(\varepsilon) = 2nk$. This means that no matter what value $\Re(\varepsilon)$ is, as long as $\Im(\varepsilon) > 0$, n will always be greater than zero. It also indicates that, if the loss is too high, even if $\varepsilon \to 0$, a "dielectric-like" n that is greater than one is likely. In this case, ENZ cannot create an NZI effect, and NZI can be used to describe materials with a lower intrinsic loss [1,2].

From a classical standpoint, $n \to 0$ can allow many phenomena to occur that cannot be found in dielectric materials. Consider the Snell's law $n_1 \sin\theta_1 = n_2 \sin\theta_2$; if $n_1 \to 0$ and $n_2 \neq 0$, no matter what the incident angle is, the angle of output $\theta_2 \to 0$, meaning a normal departure/emission. Therefore, for ideal and near-ideal ENZ materials, the direction of emission can be controlled and engineered by the shape of the media, and achieve directive emission as an antenna [127]. Similarly, the continuity condition of electric fields at the boundaries of media gives $\varepsilon_1 E_1 = \varepsilon_2 E_2$. When one side of the equation has ENZ, it also needs a large electric field intensity to balance. This is called the electric field enhancement effect at the interfaces, and it has been reported under different setups and scenarios [22,24,25,124]. In different ENZ materials, the differences of the field enhancement effect are significant, which are schematically shown in Fig. 1(b). This figure is a comparison of field intensity enhancement factors in multilayers, ITO, and dysprosium-doped cadmium oxide (Dy: CdO) [124].

Due to a near-zero n, the optical distance $L' = nL$ is also quite small. Consider the simplest case, a one-dimensional plane wave with the form $E = A\exp i(\omega t - \beta L + \varphi_0)$, where A is the amplitude, ω is the angular frequency of the EM wave, t is time, $\beta = 2\pi n/\lambda$ is the wavenumber, and φ_0 is the initial phase. After propagating for an actual distance L, the phase change is $\Delta\varphi = \beta L = 2\pi nL/\lambda$, which means that when $n \to 0$, $\Delta\varphi \to 0$. Also, consider that when near-zero conditions are satisfied, the phase velocity $v_p = c/\sqrt{\varepsilon\mu}$ results in a seemingly "infinite" value, or a "static-like" electric field distribution [1]. These indicate that, ideally, when the EM wave is incident into the ENZ material, the phase at the output end almost continues the phase at the input end, producing a "tunneling" effect [125,127]. This effect enables high fidelity transmission and arbitrary bending in ENZ materials [17,125], which is schematically shown in Fig. 1(c). In 2019, Mousavi Khaleghi *et al.* extended the ENZ tunneling effect for microstrip lines matching with different impedance characteristics using a substrate integrated waveguide [128]. Besides phase and field tunneling, in 2019, Caligiuri *et al.* further introduced a semi-classical view on the ENZ resonant tunneling modes in metal-insulator-metal (MIM) nanocavities. They describe the MIM cavity as a quantum well and use quantum mechanics to explain the relationship between the complex refractive index and cavity resonances. Figures 1(e) and 1(f) are illustrations of their quantum model. By experiments, they discovered that resonances in the cavity can be stimulated by illumination-induced resonant tunneling through the metal, which can be regarded as a photonic analog to a tunnel diode in microelectronics [126].

On the other hand, the group velocity is defined as $v_g = \partial\omega/\partial\beta$, and when the ENZ condition is satisfied, one can obtain the slow light effect [18,129,130] as in other nonlinear metamaterials [131], which allows adequate interaction time between the light and the matter. This has a role to play in part of the famous pulse shaping and radiation tailoring effects (e.g., Refs. [19,132]), and the enormous enhancement of optical nonlinearity (e.g., Refs. [27,28]). These two aspects are discussed in detail in the following sections. Recently, ENZ materials were found to possess their own confinement modes [133,134] and quasi-confined modes [135], which could allow EM waves to propagate or localize under certain circumstances. These extraordinary physical phenomena have sparked and inspired many novel discoveries in nanophotonics, nonlinear optics, light-matter interactions, and their applications.

B. Nonlinear ENZ Nanophotonics

The enhancement of optical nonlinearity is also another fascinating subtopic of ENZ photonics that attracts much scientific attention. Due to its relatively stronger intensity, the third-order nonlinearity first came into the sight of the ENZ community. For Kerr nonlinearity, the nonlinear-index coefficient n_2 in $n = n_0 + n_2 I$ has the following relation with the third-order susceptibility $\chi^{(3)}$:

$$n_2 = \frac{3}{4\varepsilon_0 c n_0^2}\Re\left(\chi^{(3)}_{xxxx}\right). \tag{1}$$

Here, for linearly polarized light, only one component of the fourth-rank $\chi^{(3)}$ tensor has the contribution to n. In this relation, a near-zero n_0 results in a large n_2, and considering the field enhancement effect of ENZ, the change in refractive index can be as significant as 170% in ENZ ITO [27]. A detailed comparison of n_2 and $\chi^{(3)}$ among Ag, Au, AZO, ITO, and some metamaterials was done using various pulse widths and techniques at different probe wavelengths [16], and for the second-order nonlinear effects, recently, the bulk and surface second-order susceptibility for ENZ AZO was obtained by Tian *et al.* [136]. The second- and third-order nonlinearity can influence the EM wave via the nonlinear polarization terms in Maxwell's equations [137]:

$$\mathbf{P}_{NL} = \varepsilon_0(\chi^{(2)}\!:\!\mathbf{EE} + \chi^{(3)}\!\vdots\!\mathbf{EEE}). \tag{2}$$

The large nonlinear optical response is not limited to TCO materials, but effective media as well. Through the endeavors and investigations of many authors, the community's understandings of ENZ materials' nonlinearity, its mechanisms, and implications have become deeper and deeper. Here we provide a glance at the progress made in the past two years. Kinsey and Khurgin expressed their opinion that nonlinear ENZ materials possess two key features of simultaneous enhancements of both extrinsic and intrinsic light-matter interactions that make them unique and exclusive, and distinguish them from other conventional slow light media [138]. Nahvi *et al.* studied the nonperturbative magnetic nonlinearity in doped ENZ media [139], which provides a novel mechanism for designing nanoscale optical switches and modulators. By constructing a metamaterial of alternating layers of metal and TCO, Vincenti *et al.* demonstrated that a high degree of anisotropy is likely to be the necessity of boosting nonlinear processes effectively [140]. They also showed that the nonlocal effects and

hot electron nonlinearity can greatly affect the linear and nonlinear responses. For highly degenerated semiconductors such as TCOs, the second-order nonlinearity can be significantly reduced, yet the second-order nonlinear process can still be enhanced via the designed multilayers. Deng *et al.* also demonstrated that the second-order nonlinearity can be enhanced by an engineered plasmonic-ENZ metasurface, which exhibits a 10^4-fold SHG enhancement [141]. For the nonlinear mechanism itself, in several seminar works, Benis *et al.* studied the spectral and angular dependence of nonlinear refraction in ENZ ITO [142]; Solis *et al.* gave a theoretical explanation of the nonlinear response enhancement in ENZ media [143] and found that when the linear ϵ decreases, the conversion efficiency increases; and Liu *et al.* investigated the loss and thickness dependency of ENZ ITO's nonlinear responses, where the surface response is significantly larger than the bulk [144]. The role of hot electron scattering in ENZ ITO's nonlinearity was discussed by Wang *et al.*, where they proposed an electron scattering model that considers the distribution situations in a non-parabolic band. They found that the ionized impurity scattering and acoustic phonon scattering are the major factors that can contribute to a deeper understanding of the ENZ ITO's optical nonlinearity [145]. Resembling the situation in ENZ TCOs, for multilayered ENZ metamaterials, Suresh *et al.* demonstrated that an alternating stack of Ag-SiO_2 layers can have its ENZ wavelength tuned anywhere in the visible spectrum [146,147]. They also discovered that, besides generating an effective zero-permittivity, this structure can also exhibit a large nonlinear-index coefficient of $n_2 = 1.2 \times 10^{-12}$ m^2/W and a nonlinear absorption coefficient of -1.5×10^{-5} m/W. Niu *et al.* realized a coupled system with large and broadband optical nonlinearity, consisting of ENZ material and gold dolmens. This polarization-selected optical nonlinearity transition system demonstrates a more than three orders of magnitude enhancement in susceptibility and nonlinear refractive index [148]. Besides the recent progress, some earlier works can bring new insights into the intriguing nonlinear ENZ phenomena, such as transmissivity directional hysteresis [149], solitons [29,30,150], and optically induced metal-to-dielectric transition [151].

C. Realization of ENZ

Realizing a near-zero permittivity by utilizing different mechanisms and materials has been another heated aspect of ENZ photonics. The current realization methods can be categorized into four types, namely, the bulk plasmon frequency induced by free carriers (plasmonic ENZ materials); the effective media implemented by photonic multilayers (subwavelength anisotropic ENZ materials); Dirac cone in the center of Brillouin zone [Γ point in an all-dielectric photonic crystal (PC)]; and metallic hollow waveguides (ENZ effect at the cutoff frequency).

For plasmonic ENZ materials, metals and semiconductors are commonly used. The collective movements of free carriers create the bulk plasma effect, where ENZ is a result of the carriers' response to a certain frequency range of the electric field oscillation in the EM waves. Their behavior can be modeled by the famous Drude model [152]

$$\varepsilon_R = \varepsilon_b - \frac{\omega_p^2}{\omega^2 + i\gamma\omega} = \varepsilon_b - \frac{\omega_p^2}{\omega^2 + \gamma^2} + i\frac{\omega_p^2\gamma}{(\omega^2 + \gamma^2)\omega}, \quad (3)$$

where the high frequency (also called "background") permittivity ε_b, electron scattering rate (or Drude damping rate, Drude relaxation rate) γ, and plasma frequency ω_p are related to fabrication methods, conditions, and processes. Specifically, $\omega_p = \sqrt{Ne^2/(\varepsilon_0 m^*)}$ and $\gamma = e/\mu m^*$, where N is the free carrier concentration, μ is the mobility of the material, e is the charge of an electron, and m^* is the effective mass of the electron. Plasmonic ENZ materials often suffer from large intrinsic (ohmic) loss, which greatly limits their applications in large-scale devices. However, most of them are compatible with the state-of-the-art complementary metal oxide semiconductor (CMOS) platform for on-chip integration and suitable for nanoscale photonic devices. Also, the fabrication technologies, such as magnetron sputtering, chemical vapor deposition, and atomic layer deposition (ALD), of these materials are relatively mature, which can greatly reduce their costs. The most popular materials in this category are TCOs. In the consumer electronics industry, TCOs are vastly implemented in nano-electronic devices or used as transparent electrodes in touchscreens. In such products, transparency and conductivity are the main concerns; in optics, the electric properties serve as a conduit to help realize and tune the intended optical properties, such as EM field strength, phase, velocity, nonlinearity, and loss. In ENZ studies, the commonly used TCOs include ITO [153], aluminum-doped zinc oxide (Al:ZnO, AZO) [154], gallium-doped ZnO (Ga:ZnO, GZO) [155], indium-doped cadmium oxide (In:CdO, ICO) [156–158], fluorine-doped CdO (F:CdO, FCO) [159] whose atomic force microscopic (AFM) scanning is shown in Fig. 2(a), and many other dopants used in CdO [4,160,161]. Recently, the ultra-large optical nonlinear response in ITO [27] has led to extensive studies in nonlinear nanophotonics, and the possibilities for AZO, GZO, and ITO to form Tamm plasmon polaritons in NIR are demonstrated [162]. Realizing ENZ by the bulk plasma is "natural" and does not require subtle engineering; therefore, the implementations of this mechanism come in various forms, for example, thin film, two- and three-dimensional (2D and 3D) structures, and metasurfaces (e.g., Ref. [163]), and recent advances in plasmonic ENZ focused more on the optical science and applications, which are discussed in Sections 3 and 4.

Since the discovery of the photonic bandgap [164,165], until now the concepts, design methods, and applications of PCs have been greatly expanded and enriched. Over the decades, PCs, quasi-crystals, or more generally, multilayers have been proven to possess high flexibility, versatility, and tunability from UV to FIR [166–169]. They can also be used for ENZ realizations and applications by three different mechanisms: (i) metal-dielectric multilayers to form effective media [8], which have an equivalent near-zero permittivity; (ii) stacked ENZ-dielectric materials to help enhance the ENZ characteristics; and (iii) exploiting the band structure and using a Dirac cone at the Γ point in an all-dielectric PC to realize ENZ. For effective media, the permittivity can be well described by the Maxwell-Garnett equations

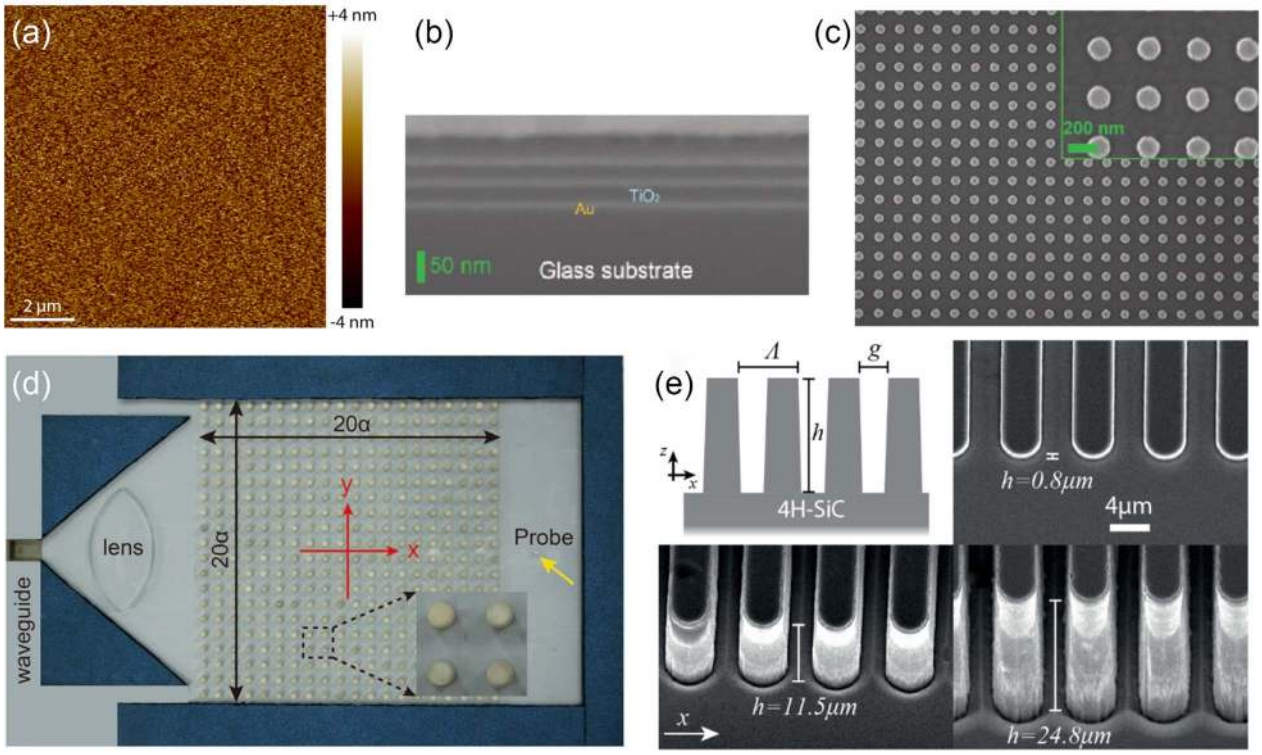

Fig. 2. (a) AFM scanning of F:CdO thin film [159]. (b) Scanning electron microscopy (SEM) image of the cross section of the multilayer structure [170]. (c) SEM image of the nanodisks [170]. (d) Photograph of the all-dielectric PC design and setup [21]. (e) SEM image of the deep-etched 4H-SiC gratings [171]. (a) American Chemical Society; (b), (c) De Gruyter, under a CC BY Creative Commons Attribution 4.0 International License; (d) Springer-Nature, under a Creative Commons CC BY License; (e) American Chemical Society.

$$\varepsilon_{\parallel} = \frac{\varepsilon_{\text{dielectric}} d_{\text{dielectric}} + \varepsilon_{\text{metal}} d_{\text{metal}}}{d_{\text{dielectric}} + d_{\text{metal}}},$$
$$\varepsilon_{\perp} = \frac{\varepsilon_{\text{dielectric}} \varepsilon_{\text{metal}} (d_{\text{dielectric}} + d_{\text{metal}})}{\varepsilon_{\text{dielectric}} d_{\text{metal}} + \varepsilon_{\text{metal}} d_{\text{dielectric}}}, \quad (4)$$

where the parameters d are the thicknesses of the respective materials. The combinations of the materials can be diverse and tailored for certain needs. In 2011, Rizza *et al.* demonstrated a kind of gain-assisted nanocomposite multilayer with an ENZ modulus in the visible wavelengths [172]. In 2013, Maas *et al.* realized ENZ at visible range using multilayers [173]. Besides previous endeavors, in 2019, Zhao *et al.* designed an ENZ multilayer medium to achieve the isotropic equivalent ENZ effects using alternating layers of Ag and SiC [174]. Kelley *et al.* experimentally demonstrated that multiple ENZ resonances can be supported in the individually tuned CdO multilayered optical thin film [175]. Simultaneous IR emissions from each layer were observed in such a structure, which opens new opportunities in absorber and light emitter designs. For light propagation and confinement, optical mode hybridization has been discussed and studied in silicon photonics [176]. Interestingly, the hybridization of ENZ modes was also found in ENZ photonics by utilizing resonant tunneling in layered MIM structures of Ag and Al_2O_3 [177]. From this standpoint, ENZ MIM cavities can be a new playground for light-matter interactions with high coupling efficiency. In 2020, for a deeper insight into the light-matter interactions, Rashed *et al.* studied the hot electron dynamics in an ENZ multilayer by the two-temperature model (2TM) [178]. They discovered the ultrafast effective permittivity modulation and a relaxation time of 3.3 ps in an Ag-TiO_2 stack. Localized plasmon resonance (LPR) is another intriguing aspect of the interaction, and it is known to be related to multiple factors such as the environment, shapes, and sizes. Habib *et al.* showed that by engineering the multilayer structure, the size dependence of LPR can be greatly reduced, and LPR itself can be controlled by the ENZ parameters of the structure [170]. The cross section of their multilayer design and the subwavelength nanodisks are illustrated in Figs. 2(b) and 2(c). The photonic multilayer design can also help enhance the ENZ properties of the original ENZ TCO materials by manipulating their transmission, reflection, and absorption [179]. For other mechanisms of ENZ realization, by using a metallic rods structure, 2D PCs can also operate at a constant cutoff frequency [180], and by a carefully constructed all-dielectric PC, shown in Fig. 2(d), dual zero-index can be obtained via a triply degenerated Dirac cone at the center of the Brillouin zone [21].

Apart from the effective NZI media induced by subwavelength multilayers, an equivalent ENZ can be realized by exploiting the cutoff frequency of a waveguide. From Maxwell's equations [137], one knows that in a waveguide there exists a cutoff frequency determined by the smallest dimension and the refractive index. Below the cutoff frequency, the EM waves can neither propagate nor localize in the structure; instead, they radiate in the so-called radiation mode. However, if a PEC boundary condition is satisfied, the EM energy is "forced" back

to the waveguide and forms an ENZ mode with the effective index equal to zero. With $\mu_{\text{eff}} = \mu_0$, the effective permittivity here can be expressed as

$$\varepsilon_{\text{eff}} = \varepsilon_0\left(n^2 - \frac{c^2}{4\nu^2 w_{\text{H}}^2}\right). \tag{5}$$

Here w_{H} is the H-plane width of the waveguide. In this scenario, the phase velocity is infinite, and the phase in the structure becomes constant. The past two decades saw the theoretical and experimental verifications of this concept [9–11]. Recently, Zhou and Li demonstrated that by using a substrate-integrated waveguide, the cutoff frequency can operate at 3.5 GHz with an efficiency higher than 63% [181]. As shown in Fig. 2(e), Folland *et al.* fabricated high aspect ratio gratings using 4H-SiC with strong IR absorption, >90 high Q-factor, and effective permittivity of $0.0574 + 0.008i$ [171]. They show that the modes can be supported in both aqueous and anhydrous surroundings. Ji *et al.* designed an extremely anisotropic waveguide with two types of dielectric materials and metal wires [182]. In this design, the focusing of energy at a size smaller than 0.2 times the wavelength was observed, besides the directive emission and bending phenomena already reported by earlier reports on effective ENZ waveguides.

3. ADVANCES IN OPTICAL PHYSICS

A. Velocities and Dispersions

In Section 2, it is shown that for an ideal ENZ material, a near-infinite phase velocity and a low group velocity ("slow light") can be obtained. The velocities here can have deeper implications and thus deeper influences on other physical characteristics, which contributes to a more profound understanding of the optical physics of ENZ photonics. Benis *et al.* studied the effect of these velocities on the large nonlinear phase shift in ENZ TCO materials [183,184]. They found that the slowed group velocity and the enhanced phase velocity can form a condition that can greatly increase the material-permittivity-related phase sensitivity. They demonstrated that the contributions of the two velocities can be concluded into a formalism that explains the nonlinear phase shift. Additionally, they conducted an experiment that shows that even when the nonlinear index is not necessarily altered, at ENZ, the nonlinear phase change of the probe beam can be as close as $\pi/2$. The authors carried out their measurements via the nondegenerate beam deflection method, which is implemented at a normal incidence. The cross-phase modulation (XPM) experiment is also conducted. These measurements show no sign of polarization-related dependence because the effects of third-order nonlinearity are significantly weaker than those of the sub-picosecond carriers. The observed frequency shift, however, is greatly dependent on the nonlinear-phase-shift-induced temporal dynamics of the pulse, meaning that shorter pulses could help create greater frequency shifts in ENZ materials.

Regarding the group velocity, it also has an important role to play in the aforementioned frequency shift phenomenon in ENZ materials, which can hopefully be exploited in the applications of optical signal processing. Khurgin *et al.* studied the group velocity's impact on the adiabatic frequency shift (AFS) under the ENZ setup [52]. They showed that the AFS can be realized in the ENZ region with a shorter length. For the optically induced refractive index change, the efficiency of the AFS is higher when the pump operates at the ENZ wavelength. These effects result from the slow light effect and electron relaxation dynamics near the ENZ wavelength, which is caused by the low group velocity. They then verified their theoretical predictions with experiments using an ENZ AZO thin film and revealed that TCOs near their corresponding ENZ point can be suitable for realizing frequency conversions; a more detailed discussion on this topic is presented in Section 3.C.

In nonlinear optics, another important concept originated from group velocity is the high-order chromatic dispersions. These chromatic dispersions are the Taylor expansion factors of the propagation constant, which are defined as $\beta_\xi \equiv \mathrm{d}\beta^\xi/\mathrm{d}^\xi\omega$, where ξ is the order of the dispersion. From this definition, each order is the "dispersion" (the variation of the value with wavelength or frequency) of the previous order, which reflects the variation trend and speed of the curve with high-order perturbations and fixes. If one tries to calculate the chromatic dispersion near the ENZ wavelengths of the ENZ materials, the obtained values can be very large due to their dispersive nature. By symbolic computations, Wu *et al.* numerically showed [33] that these high values of the second- and third-order dispersions are orders of magnitude greater than those of the highly dispersive InP waveguide [185] and the commonly used or dispersion-engineered silica fibers [137,186,187]. This is also mentioned by Kelley and Kuznetsova in their modeling of pulse interactions in ENZ AZO [188]. It seems that these chromatic dispersion values are useful for designing a high-efficiency nanophotonic dispersion compensator by using the dispersion management technique [189].

However, the situations for higher orders of dispersions with the ENZ materials are not that "classical," and the realization of dispersion compensation based on this mechanism faces a great challenge due to the complex dispersion patterns between orders and another deeper difficulty. By analytical deduction and mathematical analyses, Wu *et al.* demonstrated a more in-depth investigation into chromatic dispersion [35]. They found that in both physical and mathematical senses, the concept of high-order chromatic dispersions based on the Taylor expansion definition is not applicable near the ENZ wavelength for at least the ENZ TCO materials with Drude-like permittivity dispersion, because the chromatic dispersions are essentially derived parameters rather than fundamental physical quantities, and they do not converge near the ENZ point. This situation is illustrated in Fig. 3. In other words, the descriptions by the finite orders of chromatic dispersions of ENZ materials near the ENZ wavelength do not contain sufficient information to illustrate the whole picture—the effects of high-order dispersions exist, but it is just not suitable to apply the concept here. This is also demonstrated by the authors' comparison between the permittivity-based finite-difference time-domain (FDTD) method and the dispersion-based nonlinear Schrödinger equation, which showed that the results of FDTD are more realistic under the ENZ setup. It is worth mentioning that, in previous researches, the inapplicability issue of higher orders of chromatic dispersions also occurs in

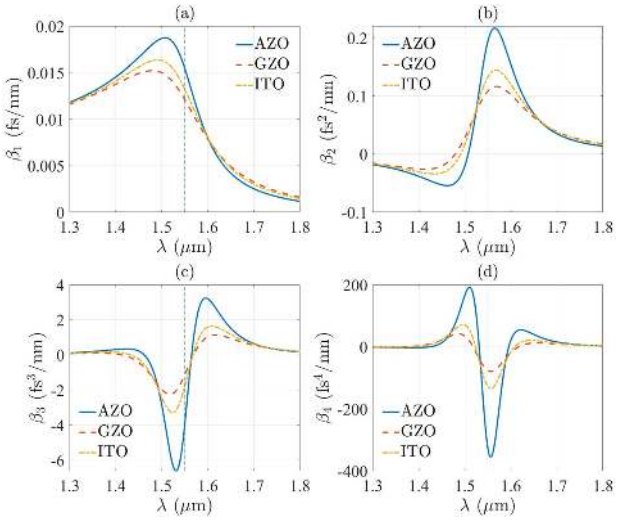

Fig. 3. Calculated (a)-(d) first- to fourth-order chromatic dispersions in the ENZ region of AZO, GZO, and ITO by symbolic calculation. The values of dispersions do not decline with the increment of the order for the Drude-like permittivity ENZ materials [35]. (a)–(d) American Physical Society.

the effective media and metamaterials with engineered permittivity [190–192], which might indicate that the inapplicability of high-order chromatic dispersions can also happen under certain circumstances in effective-media-based multilayered anisotropic ENZ materials [79,178], as long as their permittivity curves cause divergence near the ENZ wavelength.

B. Pulse Dynamics and Light-Matter Interactions

The behavior of an optical pulse in a medium is different from that of a plane wave. Pulse dynamics and light- (pulse-) matter interactions can take various forms and have been fascinating to researchers for a long time. Previously, the linear and nonlinear light-matter interactions were studied under the near-subwavelength and longer-than-wavelength setups based on ideal ENZ materials [19,22,28]. For a more realistic setup considering complex dispersions, high absorption and optical nonlinearity, reflection and scattering of light in a subwavelength structure, interesting new patterns can happen [32]. Recently, Wu *et al.* demonstrated this idea a step further with ultrashort chirp-free and chirped pulses in ENZ ITO [34], and the combination of these factors forms the pulse self-interaction, where in both spectral and temporal senses, the studied ITO slab is "sub-pulse," and allows the pulse to interact with its reflected part linearly and nonlinearly, creating superposition results of evolution patterns that are exclusive to ENZ materials. They also found a quasi-standing-wave pattern induced by two identical but counterpropagating pulse sources, which can be used in a nanoscale resonator's design. Kelly and Kuznetsova demonstrated the modeling of pump-probe modulation and interactions in an ENZ AZO/ZnO multilayer metamaterial [36] and also the adaptive ultrashort pulse re-shaping in that material [20] using a modified FDTD algorithm.

At the nanoscale, localized surface plasmon resonance (LSPR) is a typical representative of light-matter interactions in a subwavelength structure. It is already known that the wavelength and intensity of LSPR are related to the shapes, sizes, compositions, dopant or free carrier concentrations of the studied optical structure, and also the ambient environment [4,5,193–195]. In metals such as Au nanorods and Ag nanoparticles, LSPR is found to be dependent on the wavelengths and bandwidths of the light sources [196,197]. Wu *et al.* numerically illustrated the differences in localized resonance patterns between a 10 fs pulse and a 100 fs pulse [35]. They mentioned that in a real-world scenario, the underlying mechanism can be even more complex, and more physical processes might be involved, such as the 2TM in multilayered ENZ metamaterials [178]. A so-called non-thermal process [198–200] can occur when the pulse's temporal width is shorter than the scattering relaxation time of the free carriers [52,201] between each excitation between bands [52,202]. For the influence of engineered optical structures on light-matter interactions, Yildiz and Caglayan showed that by using plasmonic nanorods strongly coupled to the ENZ waveguide operating at the cutoff frequency, the aforementioned control limitations can be overcome, and the waveguide exhibits two hybrid modes of guided ENZ modes and LSP modes [203]. The dispersion curve and the field distributions of an infinite rectangular hollow silver waveguide, as an example, are shown in Figs. 4(a)–4(c). This coupling can create a strong Rabi splitting according to their FDTD simulations, which can be inspiring for the manipulation of modes in ENZ media. Habib *et al.* used a nanodisk array to eliminate the size dependence of the plasmon resonance and assumed effective control over the phase distribution by tuning the ENZ region of the substrate material [170], whose phase distributions of the electric field of different parameters are illustrated in Figs. 4(d)–4(g). These findings can be very helpful in precise control in flat optical designs and applications.

The interactions of light with matter are, per se, the interactions of fields. Arnoldus and Xu studied the force on an electric dipole near an ENZ surface [204]. This force is induced by the reflected evanescent EM field of its own from the ENZ medium, which is repulsive and perpendicular to the ENZ interface. On the other hand, Nefedov and Rubi investigated the Casimir forces in ENZ boron nitride, which emerges from the transverse-magnetic (TM) waves [205]. For isotropic absorptive ENZ materials, the force is larger than hyperbolic materials, which makes it a good candidate for applications in nanotechnology. Castro *et al.* studied the local optical density of states in the vicinity of ENZ materials [206]. For a dipole emitter, they established criteria for assessing the threshold of radiative and non-radiative processes. Their results show that the complete cancellation of the local optical density of states stems from the near field of radiative modes in a lossless case, and for the real-life lossy samples, they also evaluated their performances and the limits of the cancellation effects.

C. Frequency Generation and Harmonic Waves

The group velocity of ENZ materials can help improve the AFS efficiency near the ENZ wavelength [52], as shown in Fig. 5(a). The frequency conversion operation can produce new frequency components and redistribute energy within the spectrum, which is very useful in applications such as on-chip ultra-compact multiwavelength light sources. Recently, Zhou *et al.* demonstrated a broadband frequency translation in an

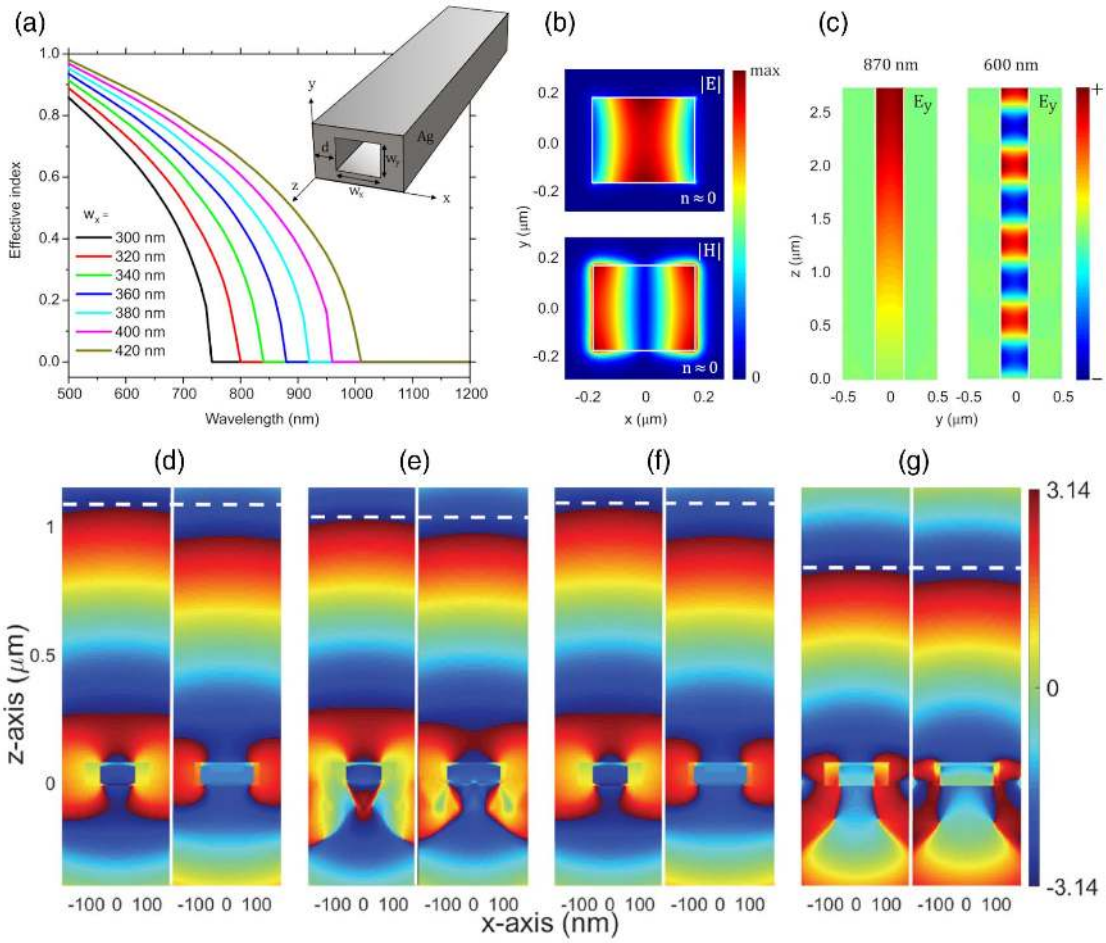

Fig. 4. Influence of optical structure on light-matter interactions [203]. (a) Effective index dispersion of the fundamental mode for ENZ waveguides with different core sizes w_x. (b) Electric **E** field and magnetic **H** field distribution at the cutoff frequency on xy plane. (c) y component of the **E** field along the waveguide axis at the ENZ wavelength of 870 nm and a shorter wavelength of 600 nm. Influence of the substrate [170]: phase distribution profiles of the x component of **E** field for ENZ nanodisk diameters of 120 nm (left) and 180 nm (right) (d) on glass at the wavelength of 684 nm; (e) on hyperbolic metamaterial at 684 nm; (f) on glass at 751 nm; and (g) on hyperbolic metamaterial at 751 nm. (a)–(c) American Physical Society, under a Creative Commons Attribution 4.0 International License; (d)–(g) De Gruyter, under a Creative Commons Attribution 4.0 International License.

ENZ ITO by time refraction [53,207]. For materials that exhibit significant refractive index differences in time, this effect can be used to realize a changed EM frequency with an unchanged wave vector. This refractive index change can be induced optically in a sub-picosecond time scale. The schematic diagrams on utilizing this time-refraction phenomenon are illustrated in Figs. 5(b)–5(d). By experiments, they demonstrated a controllable and broadband shift up to 14.9 THz in the ENZ region. This finding allows for one more dimension of control and manipulation in ENZ materials. The expansions of the Kerr-nonlinearity-induced time-varying refraction enabled frequency shift can be found in the seminar works of the same group [208–210]. Bruno *et al.* studied the broad frequency shift of parametric processes in ENZ AZO [211]. Specifically, they looked into the frequency shift for four-wave-mixing (FWM) generated fields. Their experiments show that the shift is as significant as 60 nm compared with the 40 nm pulse. They further demonstrated the negative refraction by a time-varying plasmonic nanoantenna metasurface [212]. The strong coupling and interactions result in a Rabi splitting of 30% and a 2× frequency generation with nonlinear polarization. The negative refraction has a conversion efficiency four orders of magnitude higher than the ENZ film alone. In 2021, Jia *et al.* realized 3 THz broadband generation in both transmission and reflection signals in ENZ ITO under the illumination of an NIR ultrafast Ti-sapphire pump source [108].

Another well-known frequency generation effect is harmonic generation. For heavily doped degenerated semiconductors such as ENZ TCOs, the second-order susceptibility $\chi^{(2)}$ is greatly reduced, which is related to SHG and sum-frequency generation (SFG). However, experiments by different groups have shown that the effects of second-order nonlinearity exist. In 2015, Capretti *et al.* demonstrated SHG in ENZ ITO and TiN [38] and enhanced THG in ENZ ITO [45]; in the same year, Luk *et al.* investigated THG in ultrathin ENZ films [44]. In 2019, Passler *et al.* studied SHG from ENZ Berreman

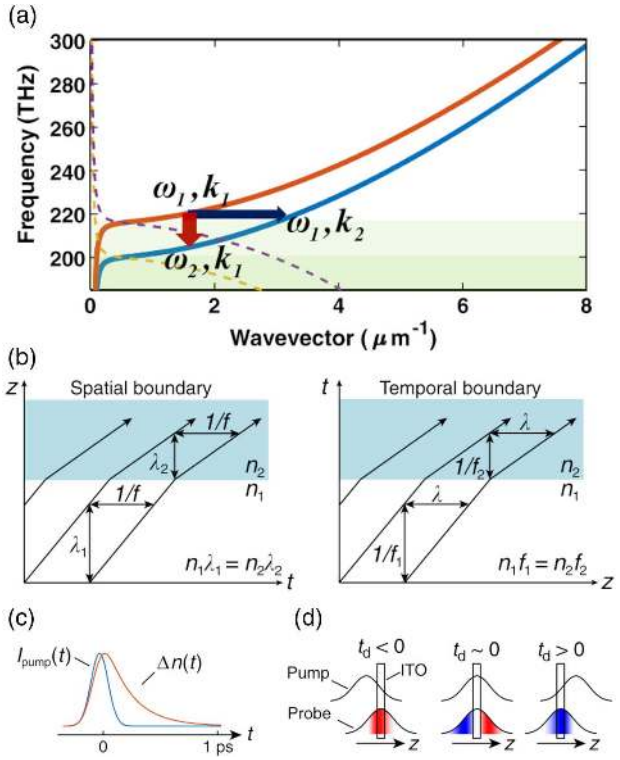

Fig. 5. (a) AFS in ENZ materials with Drude-like dispersion [52]. (b) Refractive-index-change-defined spatial boundary and a refractive-index-change-defined boundary defined by time-refraction [53]. (c) Temporal change in refractive index and light intensity [53]. (d) Redshift or blueshift of the frequency of the probe when the pump beam falls behind or leads the probe [53]. (a) Optical Society of America. (b)–(d) Springer-Nature, under a Creative Commons CC BY License.

modes in polar crystal films [41]; in 2020, Kolmychek *et al.* investigated the SHG spectroscopy in ENZ gold nanorods [43], Vianna *et al.* demonstrated SHG enhancement in an ENZ substrate [42], and Dass *et al.* discovered the gap-plasmon-enhanced SHG in ENZ nanolayers [39]. Rodríguez-Suné *et al.* investigated the impacts of hot electrons and nonlocal effects in ENZ ITO's SHG and THG [40]. For HHGs, in non-ENZ materials, up to the 15th order has been reported [213,214], extending from UV to IR. In ENZ materials, HHGs up to the ninth order in ICO pumped by a solid-state Ti:sapphire laser were experimentally demonstrated [46] by Yang *et al.* For numerical simulations, by considering the cascaded effects, Xie *et al.* discussed the giant enhancement of THG and fifth-harmonic generation in an ENZ Au-ITO metasurface [50], and Wu *et al.* studied HHGs in an ENZ AZO nanopyramid array [49] and nanolayer [48]. These simulations show the potentials of ENZ TCOs, but the conditions to realize in experiments remain to be explored. In 2021, Tian *et al.* experimentally realized UV HHG up to the fifth order in ITO pumped by an Yb-based fiber laser, with two orders of magnitude higher efficiency than previous reports [51].

D. Nonlinearity and Loss

Gigantic optical nonlinearity in ENZ materials is an intriguing optical property that distinguishes them from other nonlinear materials. In 2016, Alam *et al.* obtained a large nonlinear response in ENZ ITO [27]. In 2018, they found that large optical nonlinearity can be enhanced by a gold nanoantenna coupled to an ENZ ITO metasurface [215]. Later, it was unveiled that the huge nonlinear response is not exclusive to plasmonic ENZ materials, but also multilayered ENZ metamaterials where an effectively high nonlinearity can be exhibited [146]. Khurgin *et al.* revealed that slow and fast nonlinearities exist in ENZ materials [130]. Compared with conventional materials, although their strength is not significantly larger, the advantages are obvious, namely, the response time, enhancement of the slow light effect, and broad bandwidth, which are important attributes to ultrafast optics.

While high nonlinearity is a "good" property that scientists are pursuing, the accompanied relatively high loss is the "bad" property that should be minimized in the most non-loss-operated applications. However, the relation between the two properties seems to be symbiosis. In their seminar works, Kinsey's group proposed a carrier kinetic model [216] and analyzed the role of loss in optical nonlinearity [217]. They then found that the band non-parabolicity and absorptive loss are the sources of large nonlinear effects [218]. According to their explanation, the absorption of EM energy takes two forms, namely, the interband absorption, which increases the number of free electrons through excitation and blueshifts the ENZ wavelength, making the material more metallic, and the intraband absorption, which elevates the energy of the free-electron cloud, redshifts the ENZ wavelength, and reduces the material's ability to interact with an external field. They found that the conduction band's non-parabolicity has a contribution to intraband nonlinearity, which is also the origin of the free carriers' effective mass dispersion. The schematic diagram of their explanation model is illustrated in Fig. 6. On the other hand, Rocco *et al.* investigated the influence of loss on second-order nonlinearity by implementing a dielectric AlGaAs nanoantenna on an ENZ substrate [219]. They discovered that the conversion efficiency highly relies on the damping of the substrate when compared to the impacts of optimization.

However, the intrinsic high loss present in plasmonic ENZ materials, such as TCOs, and in metals, which affects MIM

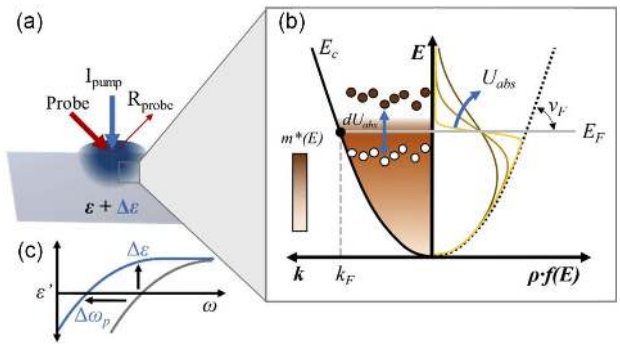

Fig. 6. Schematic diagram of (a) intraband nonlinearity of ENZ materials: pump-induced permittivity change, which in turn alters the reflectivity; (b) electron effective mass modification (elevation) by pump energy absorption (absorptive loss); (c) effective-mass-change-induced plasma frequency redshift [218]. (a)–(c) Optical Society of America.

ENZ structures, limits the scale of nanophotonic devices and their applications. On the contrary, for loss-operated applications, the loss needs to be controlled, adjusted, and manipulated. By inserting an ENZ thin film into the MIM structure, Liu *et al.* demonstrated a method to tailor and widen the absorption spectrum [220]. Li *et al.* proposed theoretically and numerically an approach to reduce the loss in ENZ materials by adjusting the structural dispersion, and thus the effective parameters, rather than the material itself [221]. They demonstrated two usage scenarios: the propagation of plane waves in a bulk medium and a surface plasmon polariton (SPP) at the ENZ interface. In experiments, Wu *et al.* introduced the SCF treatment technique into ENZ photonics for the first time and used CO_2 to lower the intrinsic loss (linear loss) of the ENZ ITO nanolayer by 10.52% in its ENZ region [70]. In 2021, Ma *et al.* proposed principles for controlling the nonlinear saturable and reverse saturable absorption of ENZ TCOs [222].

E. Aligning the ENZ Wavelength

The extraordinary characteristics of ENZ materials happen only within its ENZ region, or even only at the small proximity of the ENZ wavelength. Also, the bandwidths of many optical devices and components are only tens of nanometers. Therefore, there is an urgent need to align the ENZ wavelength of the material with the light source. For multilayered ENZ metamaterials, it is already demonstrated that by changing the layer design and materials, with state-of-the-art high precision manufacturing, the ENZ wavelength can be stably placed anywhere in the spectrum [146]. Nevertheless, for plasmonic ENZ materials, especially TCOs, this is a whole different story. By the Drude model, one can discover that with only a fraction change in the free carrier concentration, the ENZ wavelength will drift through a wide range of the spectrum. This situation is illustrated in Fig. 7(a), where with a small change in the steep *N* curve, the permittivity will be very different and results in an ENZ wavelength elsewhere. The more severe thing is that many factors during the fabrication of TCOs can lead to significantly different results, such as the air pressure, airflow, target purity, humidity, temperature, time, ambient atmosphere, and annealing conditions. Recently, a study by Xian *et al.* showed the effects of oxygen stoichiometry on the optical structure and ENZ properties of ITO films [223]. Obviously, ENZ TCOs are less stable than multilayers in terms of ENZ wavelength. The past years saw many beneficial attempts to address this

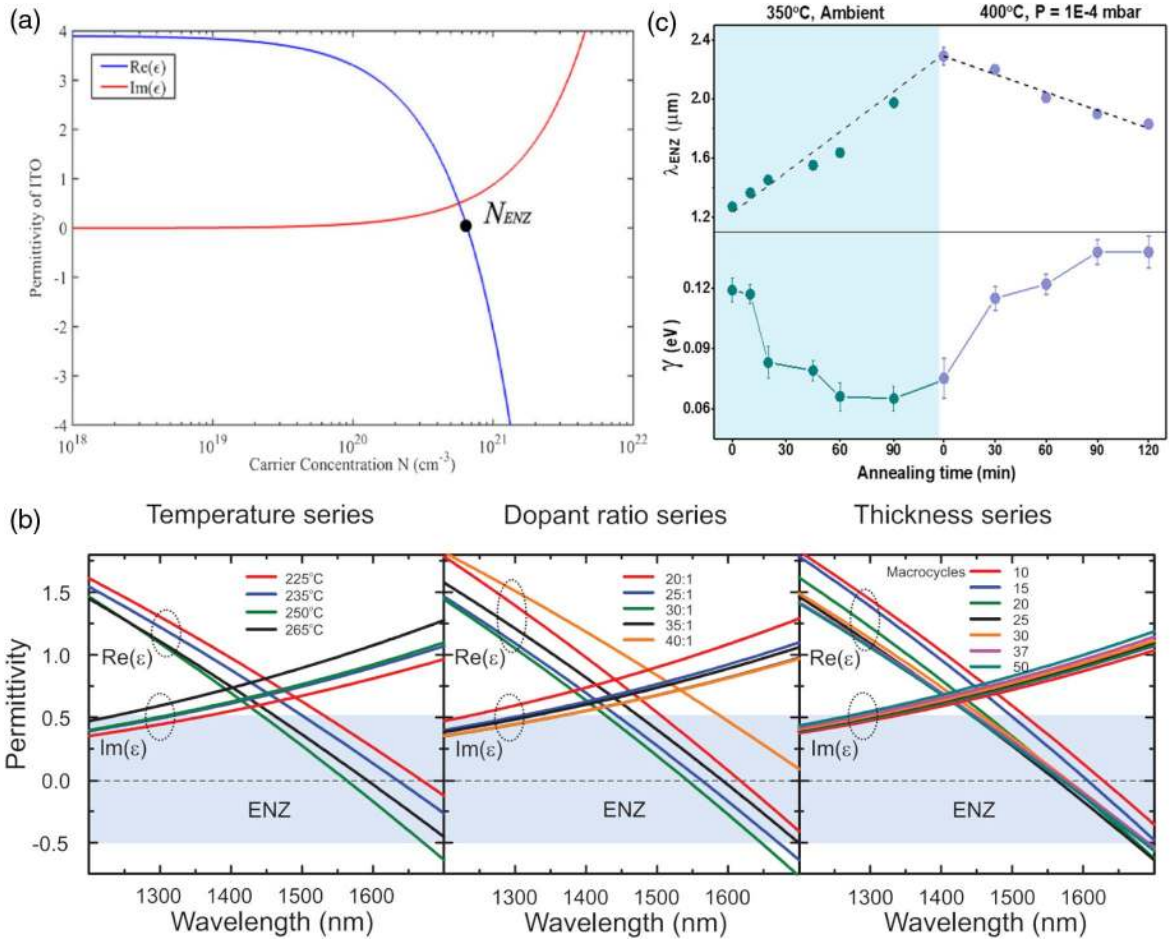

Fig. 7. (a) Relation between complex permittivity of ENZ ITO and free carrier concentration [80]. (b) Controlled annealing protocol (temperature) for ITO for ENZ wavelength tuning [68]. (c) Temperature, dopant ratio, and thickness dependence of ENZ AZO in ALD fabrication and condition control [224]. (a) IEEE, under a Creative Commons Attribution 4.0 License; (b) AIP Publishing; (c) John Wiley and Sons.

problem, and they can be categorized into two groups: temporary methods and semi-permanent methods.

For the temporary measures, it was previously discovered that the ENZ wavelength can be adjusted optically, electrically, and thermally [170]. For the optical method, the temporary permittivity change can also be observed in time refraction phenomena. By working the nonlinear refractive index back to the equivalent permittivity, a Kerr-induced permittivity change can be obtained. It is worth noting that when the laser is too strong, permanent changes might happen within the material, making this so-called temporary method irreversible. For the electrical control scheme, by applying an external electric field [225,226], the voltage can redistribute the free carriers, thus changing the ENZ wavelength. This is basically the mechanism of electro-optical modulators [64]; the redistribution of free carrier concentration happens only within several nanometers beneath the interface [80], and the permittivity change is very limited. For the thermal approach, if the temperature is not too high, the heating of the material can help excite more electrons, resulting in a change in permittivity. For higher temperatures, heating becomes annealing—a semi-permanent method.

However, the temporary methods have a significant drawback: they require external support, i.e., pump, electric source, or heater. These can limit their applications in integrated platforms and chips. For the semi-permanent approaches, all that is needed is pre-, in-, or post-fabrication processing. An optical solution is also available: Hong *et al.* investigated the laser-induced permittivity tunability in ENZ ITO films [69]. They found that the pulsed laser irradiation introduces some defects that alter the optical properties of ENZ ITOs. Their FDTD simulations agree with the experiments and prove their method effective. Zheng *et al.* [227] and Gurung *et al.* [224] used ALD to assume tunability and controllability over the ENZ properties of AZO nanolayers, whose condition dependence is illustrated in Fig. 7(b). The two groups of Wang *et al.* [67] and Johns *et al.* [68] separately and independently investigated controlled annealing protocols to manipulate and tune the ENZ wavelength of ITO. The tunability curve is shown in Fig. 7(c). Annealing requires a relatively higher temperature (hundreds of degrees Celsius), and longer time (several hours), and the tuning results are less stable and can jump over a wider range of the spectrum. Considering the use scenario where a small spectral adjustment is required, such as aligning into the gain band of the erbium-doped fiber amplifier, the controlled annealing protocols are not as flexible as the SCF treatment, because in the NIR range, the ENZ wavelength can change dramatically when a slight change occurs in free carrier concentration. SCF [228,229] is a state of a material that above a certain temperature and pressure point becomes indistinguishable between gas and fluid. Due to its ability to fix defects and improve the performance of microelectronic devices [230–235], recently Wu *et al.* introduced this technique to ENZ photonics and demonstrated that the low temperature (120°C) and time-saving (1 h) SCF oxidation technology can stably shift the ENZ wavelength for nanometer grade [70], which can be useful in the final fine-tuning of ENZ wavelength alignment. Other SCF processing techniques, such as oxidation and nitridation, hold the key to unveil deeper connections between electric and optical properties.

4. ENZ SYSTEMS FOR NANOPHOTONIC APPLICATIONS

A. Optical Isolators

An optical isolator can be regarded as the photonic counterpart of an electronic diode. By breaking Lorentz reciprocity, an optical isolator can allow the EM wave to propagate from one direction but block the other [236].

There is a trend in the world of ENZ nanophotonics to explore the realization of all on-chip integration signal processing and logic (operation) elements using ENZ, and an optical isolator is no exception. Davoyan *et al.* proposed two distinctive designs of ENZ-enabled optical isolators by merging ENZ material with magneto-optical materials [98], as illustrated in Figs. 8(a) and 8(b). For a given handedness of circularly polarized EM waves, the forward propagating one experiences a transparent medium, while the backward propagating one sees an opaque medium. They explored two possible implementations of this idea, namely, a metal-dielectric multilayer stack and a rectangular waveguide operating at its cutoff frequency.

However, recent years did not witness much progress in this topic by "conventional" mechanisms, except for incorporating non-Hermitian optics, for example, in Ref. [237], shown in Fig. 8(b). We suspect the main reason is that the benefits and enhancement brought by implementing ENZ materials do not significantly outperform the optical isolators realized by other mechanisms. The use of magneto materials is essential in this application, meaning that the "normal" non-magnetic ENZ material itself cannot achieve the optical isolation effect alone. Yet, it is too early to conclude that ENZ isolators, and hopefully, other linear and nonlinear effects of ENZ materials, can be implemented into the design for performance optimizations, or achieve properties that cannot be found in other kinds of optical isolators.

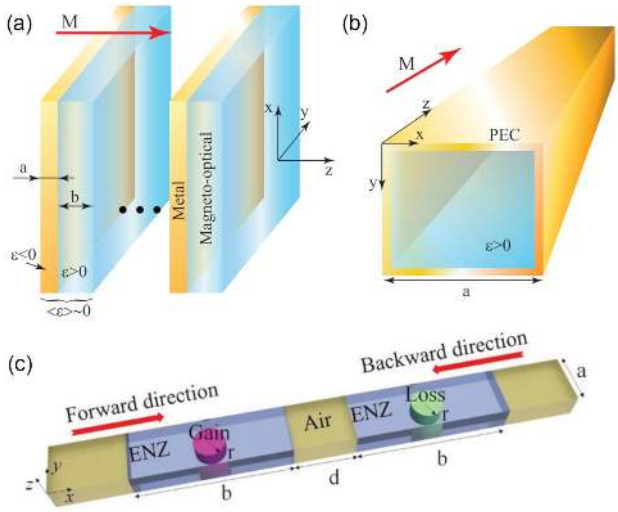

Fig. 8. Schematic diagrams of (a) multilayered metal-MO stack isolator [98]; (b) waveguide-based isolator [98]; (c) non-Hermitian ENZ optical isolation scheme [237]. (a), (b) Optical Society of America; (c) John Wiley and Sons.

B. All-Optical Switches

Optical switches are essential components of optical signal processing units and optical logic gates, holding the key to the optical computing system as well as integrated optics. The current state-of-the-art design of ENZ-based optical switches includes all-optical switches and electro-optical switches. The main working principle of all-optical switches depends on the unprecedented optical nonlinearity of the natural ENZ TCO material. In 2017, Guo *et al.* experimentally demonstrated an all-optical switch based on ITO nanocrystals synthesized by a wet-chemistry route [74]. Their results show that ITO nanocrystals exhibit a short recovery time of ≈450 fs (corresponding to a response speed of ≈2 THz) and modulation depth ≈160% in the ENZ region, which benefits from the surface trap states of ITO nanocrystals. By integrating ITO and poly(methyl methacrylate) film into a fiber waveguide, an all-optical fiber switch enabling to convert the continuous wave (CW) into ultrafast femtosecond laser pulses has been demonstrated as a proof of concept. In 2018, Jiang *et al.* showed an ITO film that achieves an optical amplitude modulation of 7.4% under the incident light intensity of 306 MW · cm^{-2} in the experiment [238]. Using ITO film as a saturable absorber in integrated waveguide chip lasers for optical switches at 1.9 μm is shown in Fig. 9(a). They also realized *Q*-switched mode-locked and stable pulse laser output with a repetition rate of 6.4 GHz and an average output power of 28.6 mW. In 2019, Zhang *et al.* presented an investigation into the nonlinear saturable absorption of ITO thin film and realized passively *Q*-switched lasers with wavelengths of 1063, 1340, and 1410 nm [77]. Hu *et al.* numerically showed an all-optical switch by using high-mobility CdO integrated into a Bragg microcavity, which has a reflectance of 94% under a pump fluence of 7 μJ · cm^{-2} [76], as plotted in Fig. 9(b). In addition, Saha *et al.* demonstrated an optical switching platforms-based yttrium-doped CdO [239]. With pump-probe experiments, the CdO film achieves a maximum reflectance change of 135% in the MIR region with a relaxation time of 45.6 ps under a pump fluence of 1.3 mJ · cm^{-2}. In 2020, Zhang *et al.*

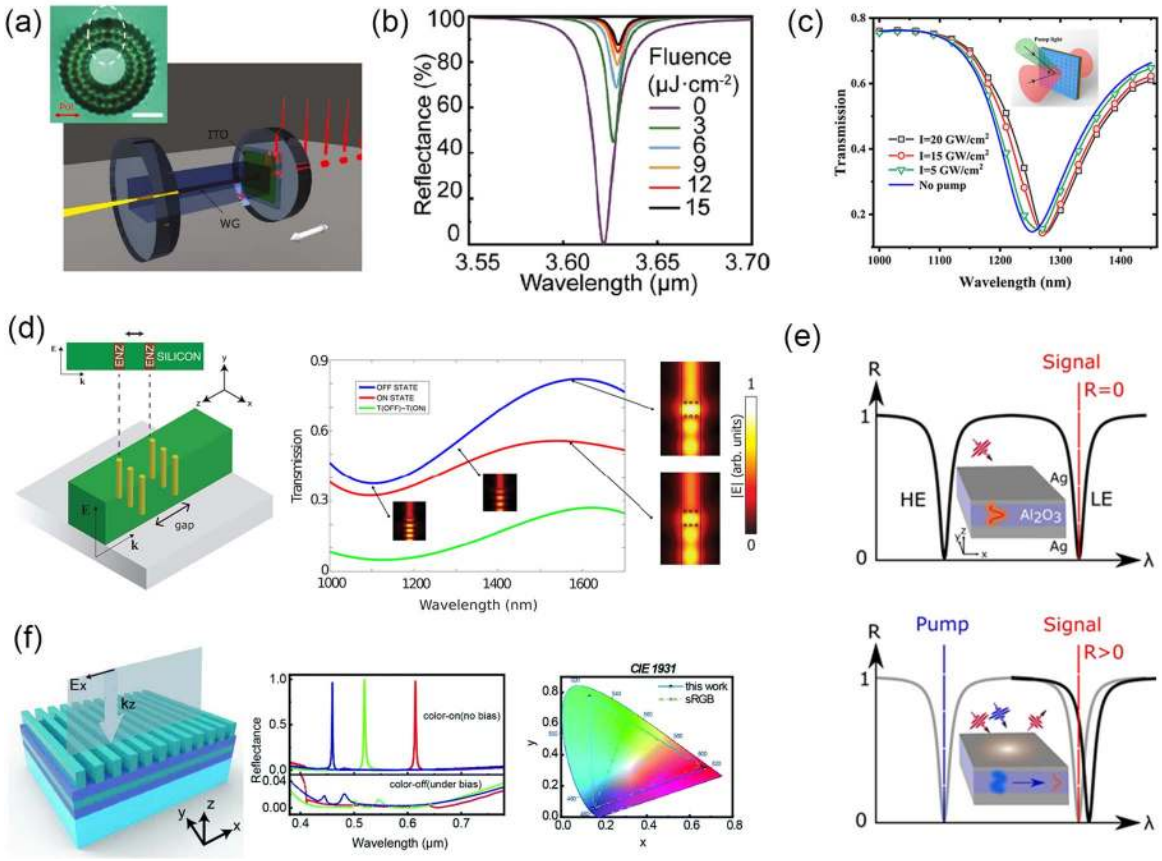

Fig. 9. (a) Layout of the *Q*-switched waveguide using the ENZ ITO [238]. (b) Reflectance spectra of CdO-based Bragg microcavity under different pump fluences at a 45° incident angle [76]. (c) Transmission of the all-optical switch under different pump light intensities at 30° incident angle; the inset is the schematic of the all-optical switch [65]. (d) Schematic of the Si photonic waveguide, and transmission of the device in ON and OFF states [240]. (e) Schematic of the MIM nanocavity with two ENZ modes. The high energy (HE) and low energy (LE) resonances display low reflectance at the ENZ points (top). Change of *R* for the signal probe pulse upon optical pumping of the HE ENZ mode; the gray curve represents the equilibrium positions of the resonances [79]. (f) Schematic of the dielectric guided-mode resonance gratings. The reflectance of the three primary color devices at the color-on state (no bias) and color-off state (under bias). CIE 1931 coordinates calculated by the proposed device (solid line) and the color gamut of the sRGB triangle (dashed line) [241]. (a) De Gruyter, under a Creative Commons Attribution 4.0 International License; (b) Optical Society of America; (c) IEEE, under a Creative Commons Attribution 4.0 International License; (d) Chinese Laser Press; (e) Spring-Nature, under a Creative Commons Attribution 4.0 International License; (f) Royal Society of Chemistry.

studied the ENZ ITO as an optical switch at 2.06 μm in experiments [72]. Xie *et al.* designed an all-optical switch based on a metasurface utilizing the large nonlinearity of ITO near the ENZ point, which has an extinction ratio (ER) exceeding 5 dB with a response time of ∼650 fs under the control of the pump light, as shown in Fig. 9(c) [65]. In 2021, Li *et al.* numerically proposed a femto-joule all-optical switch based on an electrically tunable plasmonic-CdO-Si waveguide [78]. High-mobility CdO has ENZ-enhanced optical nonlinearity in the telecom wavelength region. Their design has a modulation depth of 15.9 dB/μm and a switching time of 230 fs at the cost of switching energy of 13.5 fJ. Bohn *et al.* studied the all-optical switching of ENZ plasmons via pump-probe experiments in the Kretschmann-Raether configuration [242]. Their results demonstrate that a thermal switching mechanism leads to a shift in the plasmon resonance frequency of 20 THz for a TM pump intensity of 70 GW · cm^{-2}, and additional two-beam coupling is observed for degenerate pump and probe frequencies. The aforementioned two mechanisms combine to result in a measured change in reflection of the probe from 1% to 45% for a pump intensity of 70 GW · cm^{-2} in a 60 nm ITO thin film [242].

Another principle of all-optical switches depends on the artificial structure with effective ENZ parameters. An ultrafast on-chip remotely triggered nanoscale all-optical switch, which consists of two silicon PC nanocavities, silicon PC waveguides, multicomponent nanocomposite, and a control waveguide, was demonstrated by Chai *et al.* in 2017 [243]. The multicomponent nanocomposite nano-Au:(Er^{3+}:Al_2O_3) was designed to achieve large optical nonlinearity enhancement with effective ENZ parameters. The proposed device has an ultralow threshold control intensity of 560 kW · cm^{-2}, ultrafast switching time of 15 ps, and high switching efficiency of 60% in the experiment. In 2018, Neira *et al.* designed an artificial effective ENZ cavity by implementing a few Au nanorods inside a Si photonic waveguide, as shown in Fig. 9(d) [240]. The designed structure has strong nonlinearity with switching energies below 600 fJ, a modulation depth of about 30 dB/μm, and a loss of less than 0.8 dB. In 2020, Kuttruff *et al.* proposed an approach for ultrafast all-optical switching based on the MIM nanocavity, which can be described as effective ENZ resonances [79]. They used an antisymmetric optical pumping in the UV region in the MIM nanocavity, to achieve an approach for ultrafast all-optical switching in the NIR, as illustrated in Fig. 9(e). The results show the MIM nanocavity approaching a sub-3 ps control of the reflectance with a relative modulation depth of 120%.

C. Electro-Optical Switches

For electro-optical switches, the electro-optical functionality is realized by tuning the electron density of TCOs via applying a bias voltage. In 2019, Hu *et al.* constructed a solid-state electro-optical switch using a high-Q CdO Bragg microcavity [76]. The reflectivity of the device can be switched from close to zero to 89% with a low bias electric field, and the transmittance of the device can be modulated from 4% to 44%. An electro-optical metasurface switch based on ENZ ITO, which has a large modulation depth of up to ∼17 dB, was proposed by Xie *et al.* in 2020 [65]. Finally, in 2021, Wang *et al.* numerically demonstrated an electrically switching reflective structural color display, which combined ENZ ITO with dielectric guided-mode resonance (GMR) gratings, as displayed in Fig. 9(f) [241]. The device can be electrically turned on or off by switching between a narrowband reflector and a transparent film. A large color gamut beyond sRGB (∼161%) and a modulation speed of ∼10 MHz were estimated in their research.

D. Electro-Optical Modulators

In natural ENZ materials such as TCOs, the free carrier concentration of TCOs can be tuned under an applied voltage, which in turn results in a dramatic change in the ENZ point and the optical property of the TCOs materials. This effect results from the accumulation (or depletion) layer of these materials and can be built up when TCOs are bounded by a dielectric as a response to an electrostatic field. TCOs are emerging as attractive active materials for electro-optical modulators due to their electrically tunable physical property.

In 2012, Lu *et al.* numerically presented an ENZ electroabsorption modulator by sandwiching a thin ENZ AZO film into a Si slot waveguide [244]. Their results show that the proposed modulator can achieve over 3 dB modulation depth in a 250 nm long waveguide. In 2013, Vasudev *et al.* proposed an ENZ ITO modulator and provided its operating principles [66]. The modulator consists of a Si strip waveguide coated with a HfO_2 layer and an ITO layer. They found that the transmission of an optical mode through the waveguide can be diminished by altering the local index and increasing the carrier absorption of the ENZ region, and an electric field concentration exactly in the region of highest free carrier absorption under ENZ condition. The modulator allows for 3 dB in an under 30 μm long waveguide, and energy consumption of 100 fJ/bit. In 2014, Lee *et al.* experimentally demonstrated an ultra-compact plasmon slot waveguide field-effect modulator based on ENZ ITO [245]. They realized a high dynamic range of 2.71 dB/μm and a low loss of ∼0.45 dB/μm. In 2015, Zhao *et al.* investigated butt-coupling and evanescent-coupling schemes for a slot waveguide ENZ ITO modulator [246]. In the butt-coupling scheme, the modulator has demonstrated an insertion loss (IL) below 1.3 dB and an ER above 6.0 dB for a wavelength range from 1.25 to 1.42 μm. In the evanescent-coupling scheme, the modulator has achieved an ER greater than 6.0 dB and an IL less than 1.7 dB for a wavelength ranging from 1.25 to 1.39 μm. In the same year, Baek *et al.* proposed an ultra-compact integrated phase modulator that consists of two vertically stacked Si layers and a core with ultrathin HfO_2/ITO/HfO_2 multilayers. When a voltage bias between the ITO thin film and the Si layer is applied, the ENZ effect leads to a dramatic change in the fundamental TM-like mode of the input light, resulting in both phase and amplitude modulation. Their computer simulations show that the proposed phase modulator has a modulation efficiency of $V_\pi L \sim 0.0071$ V · cm and bandwidth of ∼70 GHz [247]. In 2016, Koch *et al.* studied the carrier accumulation process of TCO-based plasmonic absorption modulators [248]. They employed the stationary quantum hydrodynamic to get an inhomogeneous carrier distribution in the TCO layer and predicted the transfer functions of plasmonic absorption modulators by solving Maxwell's equations. The results show that the

digital modulation characteristic arises from carrier accumulation in the thin TCO layer. In 2017, Sinatkas *et al.* comprehensively studied and evaluated electro-optical modulators developed on the Si-rib and Si-slot waveguides [249]. They achieved an integration of Maxwell wave theory and solid-state physics, by employing the drift-diffusion model for the description of free carrier dynamics in semiconductors, and the electro-optic effect was introduced using a unified finite element method (FEM). The results show that the Si-slot waveguide outperforms the Si-rib design in all metrics and is proven comparable to the performance of the plasmonic waveguide. Campione *et al.* numerically proved that CdO shows better modulation performance than indium oxide [250].

In 2018, Liu *et al.* experimentally demonstrated a chip-scale slot waveguide modulator exploiting ENZ ITO [84]. As shown in Fig. 10(a), the modulator consists of a Si strip waveguide covered with 8 nm of HfO_2 and a 15 nm ITO film, which forms a metal oxide semiconductor (MOS) capacitor. A tapered grating coupler is used to couple a normally incident, free-space laser beam into and out of the waveguide. Simulation and experiment results show that the ENZ effect can increase the overlap of the guided mode with the ITO layer. They also created a 50 nm wide slot in the center of the Si strip waveguide, and performance measurements show the modulator with the slot has greater benefits compared to the modulator without a slot. Wood *et al.* reported a design of a fast, compact electro-absorption modulator composed of $Si/HfO_2/TCO/Au$ on a Si rib waveguide in the experiment illustrated in Fig. 10(b) [64]. The proposed modulator has an operation with a 6.5 dB ER from 1530 to 1590 nm, a 10 dB IL, and achieved digital modulation at rates of 2.5 Gb/s. A modulator based on a plasmonic slot waveguide was investigated by Gao *et al.* [82]. The device is composed of an active Au plasmonic slot waveguide with electrodes between two silicon waveguides, and 10 nm thick HfO_2 is deposited on top of the Au slot waveguide followed by filling the slot with 200 nm thick ITO [82]. The modulator experimentally demonstrated a uniform modulation with 70 nm optical bandwidth across the 1530–1600 nm band, modulation of 2.62 and 1.5 dB/μm, and dynamic modulation speed at 40 MHz. In Li *et al.*'s experimental investigation, their device was composed of a Si/oxide/ITO MOS capacitor built at the center of a one-dimensional silicon PC nanocavity on a Si strip waveguide [251]. By applying a gate voltage, the modulator can work in dual mode of cavity resonance and optical absorption by

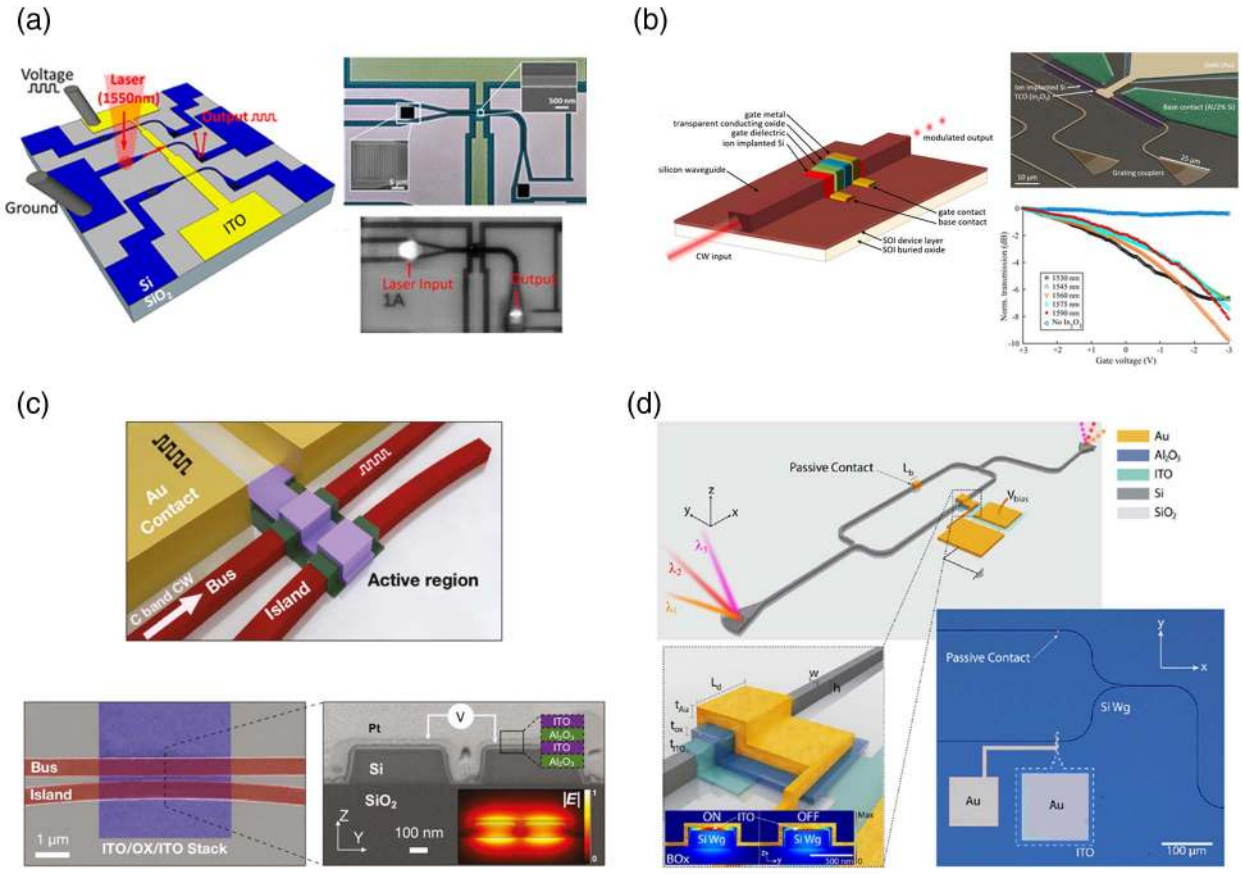

Fig. 10. (a) Schematic of the chip-scale electro-absorption modulator and SEM image of fabrication result [84]. (b) Schematic and SEM image of the gigahertz speed ENZ modulator, and transmission of the modulator under DC electro-optical characterization [64]. (c) Schematic and SEM image of coupling-enhanced dual-gated ITO modulator, cross-sectional image, and mode profile illustrating the device layers and operating mechanism of the active region [252]. (d) Schematic of the Mach-Zehnder modulator; $Si/ITO/Al_2O_3/Au$ active device region, and corresponding eigenmode profiles to light ON and OFF states; optical microscope image of the Mach-Zehnder modulator [253]. (a) American Chemical Society; (b) Optical Society of America; (c) De Gruyter, under a Creative Commons Attribution 4.0 International License; (d) Optical Society of America.

utilizing the change in refractive index from both the conductive oxide and the Si strip waveguide. The modulator demonstrates 0.5 dB extra optical loss, moderate Q-factor above 1000, and energy efficiency of 46 fJ/bit. A comparative analysis of TCO electro-absorption modulators was presented by Gao *et al.* in 2018 [254].

In 2019, Gao *et al.* used a high mobility In_2O_3 gate to replace low mobility ITO to lower the voltage swing of the modulator [255]. Experimental results show that the device can achieve a small voltage swing of only 2 V to obtain an ER of 1.2 dB/μm. Tahersima *et al.* experimentally demonstrated a compact coupling enhanced dual-layer ITO modulator consisting of a Si photonic bus waveguide and short coupling island waveguide separated away from the bus [252]. As shown in Fig. 10(c), two waveguides are covered by an active ITO/Al_2O_3/ITO stack. The concept of the proposed modulator allows utilizing the normally parasitic Kramers-Kronig relations synergistically. The island waveguide enables a higher ER compared to the traditional absorption-only case in the absorptive state of the modulator; the bus waveguide enables high optical transmission in the light-ON state, because the coupling between two waveguides is minimized, and the absorption losses are also minimized due to the non-plasmonic mode and dielectric-like dual-gated ITO/oxide/ITO stack atop both waveguides. As a result, the authors indicated that a 2 dB ER modulation with an IL of 2 dB for 4 V of applied bias can be achieved using the proposed device. Forouzmand *et al.* performed a study of an electro-optical amplitude and phase modulator [256]. The modulator is designed by the ENZ ITO into a GMR mirror metasurface, which consists of a high-index Si nanograting placed on top of a Si guiding core followed by a Si dioxide optical buffer layer and a highly reflective substrate. A modulation depth as high as ∼0.80 and a phase variation of ∼210° in the 0.45–0.6 range can be realized by the proposed structure.

Additionally, in 2020, Rajput *et al.* realized a modulator with a Si-ITO heterojunction between p-type silicon and n-type ITO [257]. The reported Si-ITO heterojunction waveguide-based modulator exhibits more change in k, making it more suitable for intensity modulation, compared to the ITO-oxide-silicon hybrid waveguide. An ER of 7 dB for the 1.7 mm long device can be achieved at a maximum low voltage of −5 V in their experiment. Zhou *et al.* designed and demonstrated an ENZ modulator based on an Au/ITO/HfO_2/p-Si MOS capacitor [88]. The device has an energy efficiency of 100 fJ/bit, modulation bandwidth of 3.5 GHz, data rate of 4.5 Gb/s, and optical bandwidth from 1515 to 1580 nm wavelength in the experiment. By replacing ITO with higher mobility TCO materials, the device can achieve 40 GHz modulation bandwidth and 0.4 fJ/bit energy efficiency. As plotted in Fig. 10(d), Amin *et al.* demonstrated a spectrally broadband, gigahertz-fast Mach-Zehnder interferometric modulator, and integrated it into Si photonic integrated circuits [253]. Experimental measurements indicate the modulator reveals minuscule $V_\pi L$ of 95 V · μm, and an ER of ∼3 to > 8 dB. Unlike lithium niobite optoelectronics, the proposed ITO optoelectronics is crystal-orientation independent and synergistic to enhancing electrostatics from transistor technology. In 2021, Sha *et al.* presented a comparative study on the designs and optimizations of ENZ multi-slot waveguide modulators [258].

As a summary, the performance characteristics of the ENZ TCOs-based amplitude modulators are listed in Table 1 with Refs. [64,66,80,82,84,85,87,88,244–246,248–253,255–257,259–266]. Some values have been recalculated using parameters given in the references.

E. Perfect Absorbers

A perfect absorber (PA) is a device designed to control the absorption spectrum in terms of intensity, bandwidth, and resonance, and is crucial in the field of optical signal processing. However, PA faces the challenge of a high material loss or large thickness. Recent studies have shown that ENZ materials have strong electric field enhancement and resonant light absorption in thin layers due to the continuity requirement for the boundary conditions at the interface for ENZ materials. Therefore, ENZ materials have emerged as an ideal candidate to create PA in ENZ photonic researches for both theory and experiment.

In 2012, Feng *et al.* demonstrated PA in ENZ-metal structures when the material is arbitrarily thin (thickness-to-wavelength ratio < 1) and with arbitrarily low loss [267]. Their numerical and analytical solutions reveal that there is a linear relationship between the thickness and the loss at perfect absorption, meaning the thickness can be pushed to zero when the material approaches zero. The exotic phenomenon can be understood in terms of coherent perfect absorption. In 2014, Luk *et al.* experimentally demonstrated that perfect absorption occurs slightly above the ENZ frequency of ITO, and all incoming energy is absorbed in the $\lambda/50$ thin film ITO material, not in the metallic substrate [268]. The authors indicated that similar behavior can be expected for any material with similar dielectric properties, greatly expanding the list of materials that can be considered for use as ultrathin PAs. Zhong *et al.* showed that an anisotropic ENZ thin metamaterial with a metallic substrate has perfect absorption of an incident plane wave at a specific angle while the metamaterial can be arbitrarily thin and have arbitrarily low loss [269]. Experimental results demonstrate an absorber working at 5.35 GHz using ENZ metamaterial with a thickness of $\lambda/56$ and an absorption peak of 95% at a 60° incidence angle.

TCO materials with natural ENZ effects and the compatibility with current semiconductor fabrication techniques can be used as absorbers. Thereinto, the simplest structure of an absorber is TCO films or with a substrate. In 2015, Yoon *et al.* experimentally implemented a PA based on ITO thin films that work in an attenuated total reflection configuration [270]. The multilayer of ITO films has an absorption close to 100% over a wide NIR wavelength range of 1450–1750 nm at a 48.9° incidence angle. In 2016, Kim *et al.* also considered an ITO double layer sandwiched between two ZnSe prisms, and achieved an absorption >99% in 1443–1576 nm [271]. In 2017, Rensberg *et al.* used an ultrathin film of vanadium dioxide on an AZO substrate to completely suppress the reflection of light, and control the wavelength with minimal reflection over the entire MIR range by changing the free carrier concentration of the AZO substrate [272]. Bruno *et al.* also reported that the air/AZO/glass system can exhibit an absorption close to 60% across the ENZ region in 2020 [273].

Table 1. Comparison of ENZ Electro-Optical Modulators[a]

Year	Reference	Structure	Extinction Ratio (ER)	Insertion Loss (IL)	FoM	Speed	Energy	Bias (V)
2012	[244]	$Si/SiO_2/AZO/Si$ (Si slot-wg)	17.4 dB/μm	1 dB/μm	17	RC 7.28 ps	N.A.	N.A.
2013	[66]	$Si/HfO_2/ITO/Si$ (Si strip-wg)	0.11 dB/μm	0.0029 dB/μm	37.3	N.A.	100 fJ/bit	0 to 2.3
2014	[245]	**$Au/Al_2O_3/ITO$ (plasmonic slot-wg)***	2.7 dB/μm	0.45 dB/μm	6	100 GHz	4 fJ/bit	0 to 2.2
	[259]	$Si/TiN/HfO_2/ITO/Cu$ (Si strip-wg)	19.9 dB/μm	2.9 dB/μm	6.9	11 GHz	0.4 pJ/bit	−2 to 4
		$Si_3N_4/TiN/HfO_2/ITO/Cu$ (Si_3N_4 stripe-wg)	4.13 dB/μm	1.575 dB/μm	2.6	N.A.		
2015	[246]	$Si/SiO_2/ITO/SiO_2/Si$ (butt-coupled, Si slot-wg)	6 dB/μm	1.3 dB/μm	4.6	N.A.	N.A.	2 to 4
		$Si/SiO_2/ITO/SiO_2/Si$ (evanescent-coupling, Si slot-wg)	4 dB/μm	1.13 dB/μm	3.54			
2016	[260]	$Si/HfO_2/ITO/Au$ (Si rib-wg)	4.3 dB/μm	2.6 dB/μm	1.65	40 GHz	22.5 fJ/bit	0 to 1.3
	[261]	$Si/HfO_2/ITO/Au$ (Si strip-wg)	9.86 dB/μm	0.4 dB/μm	24.65	88 GHz	50 fJ/bit	0 to 3.4
	[248]	$Si/HfO_2/ITO/Au$ (plasmonic wg)	1.7 dB/μm	0.47 dB/μm	3.7	30 GHz	60 fJ/bit	0 to 5
	[262]	Single layer (Si wg)	5 dB	0.87 dB	5.75	257 GHz	330 fJ/bit	0 to 4
2017	[249]	$Si/HfO_2/ITO$ (Si rib-wg)	0.30 dB/μm (TE) 0.25 dB/μm (TM)	0.1 dB/μm	3 2.5	184 GHz 219 GHz	1.6 pJ/bit 2.4 pJ/bit	0 to 4
		$Si/HfO_2/ITO$ (Si slot-wg)	1.11 dB/μm	0.11 dB/μm	111	175 GHz	0.6 pJ/Bit	
	[250]	$Si/HfO_2/CdO/Au$ (Si rib-wg)	>4 dB/μm	N.A.	N.A.	N.A.	N.A.	N.A.
2018	[84]	**$Si/HfO_2/ITO$ (Si slot-wg)***	0.15 dB/μm	N.A.	N.A.	117 kHz	2 pJ/Bit	−5 to 5
	[263]	Hybrid (plasmonic slot-wg)	0.29 dB/μm	0.0029 dB/μm	100	47.5 GHz	67.1 fJ/bit	0 to 2.35
			0.34 dB/μm	0.049 dB/μm	6.94	140 GHz	22.7 fJ/bit	
	[64]	**$Si/HfO_2/ITO/Au$(Si rib-wg)***	1.63 dB/μm	2.5 dB/μm	0.652	RC 180 ps	2.1 pJ/bit	−3 to 3
	[82]	$Au/HfO_2/ITO$ (plasmonic slot-wg)	2.62 dB/μm	0.58 dB/μm	4.52	250 GHz	30 fJ/bit	0 to 3.5
		$Au/HfO_2/ITO$ (plasmonic slot-wg)*	1.5 dB/μm	N.A.	N.A.	40 MHz	N.A.	−2 to 2
	[264]	$Si/HfO_2/ITO$ (Si rib-wg)	0.25875 dB/μm (TE) 0.25625 dB/μm (TM)	0.009125 dB/μm (TE) 0.010625 dB/μm (TM)	28.36 (TE) 24.12 (TM)	16 GHz	N.A.	0 to 5
		$Si/HfO_2/ITO/HfO_2/Si$ (Si rib-wg)	1.066 dB/μm (TE) 1.063 dB/μm (TM)	0.0041 dB/μm (TE) 0.0043 dB/μm (TM)	260 (TE) 247.21 (TM)	N.A.		
	[251]	**$Si/SiO_2/ITO$ (Si strip-wg)***	14.93 dB/μm	1.33 dB/μm	11.23	87 GHz	46 fJ/bit	0 to 19.5
	[265]	$Si/ITO/SiO_2/Au$ (Si strip-wg)	1.62 dB/μm (TE) 1.59 dB/μm (TM)	N.A.	N.A.	N.A.	N.A.	N.A.
2019	[255]	**$Si/HfO_2/In_2O_3/Au$ (Si strip-wg)***	1.2 dB/μm	N.A.	N.A.	55 MHz	110 fJ/bit	−6 to 12
	[80]	$Si/HfO_2/ITO$ (Si slot-wg)	1.44 dB/μm	0.037 dB/μm	38.92	20 GHz	2.93 pJ/bit	0 to 5
	[87]	Si (access wg) Si/ITO/Ag (ring wg)	22.8 dB	1.6 dB	14.25	1.3 THz	3.25 fJ/bit	0 to 2
	[266]	$Si/SiO_2/Si$ (access wg)	14 dB	0.076 dB	185	48.67 GHz	4.35 fJ/bit	0 to 2.35
		$Si/SiO_2/ITO/HfO_2/Si$ (ring wg)						
	[252]	**$Si/Al_2O_3/ITO/Al_2O_3/ITO$ (Si strip-wg)***	0.5 dB/μm	0.5 dB/μm	1	5.4 GHz	200 fJ/bit	0 to 4
	[85]	$Ag/HfO_2/ITO/Ag$ (plasmonic stub-resonator wg)	> 10 dB	N.A.	N.A.	78 GHz	90 fJ/bit	0 to 5
	[256]	$Au/SiO_2/Si/Al_2O_3/HfO_2/ITO/Al_2O_3/HfO_2/Si$ (metasurface)	N.A.	N.A.	N.A.	N.A.	N.A.	−15 to 24
2020	[257]	**Si/ITO (Si rib-wg)***	0.0041 dB/μm	N.A.	N.A.	N.A.	N.A.	−5 to 5
	[88]	**$Si/HfO_2/ITO/Au$ (Si rib-wg)***	0.4 dB/μm	2.7 dB/μm	0.15	15 GHz	64 fJ/bit	0 to −10
	[253]	**$Si/ITO/Al_2O_3/Au$ (Si rib-wg)***	> 8 dB	6.7 dB	> 1.19	1.1 GHz	2046 fJ/bit	−10 to 10

[a]Figure of merit (FoM) is defined as ER/IL. "*" denotes experimental works, and those without "*" are theoretical/simulation-based works. "wg" is short for waveguide.

In addition, artificial structures based on ENZ TCO materials are widely used for building PAs, such as metasurfaces and metamaterials [90,92,274–277], plasmonic cavities [157], and multilayers [93,175,227]. By embedding ITO film into an Au grating metasurface, Park *et al.* designed a PA that can be controlled by applying a voltage bias, as illustrated in Fig. 11(a)

[90]. With electric biases, the carrier concentration of ITO can be either decreased (depletion) or increased (accumulation), leading to changes in the optical properties of the ITO. The proposed PA has large modulation around the ENZ wavelength and achieves a 125 kHz modulation rate of absorption. Another example of an ENZ-TCO-material-based metasurface is a patterned metal squares MIM structure, depicted in Fig. 11(b) [274]. Due to the coupling between an ENZ mode and gap plasmon mode, the proposed device has shown a 240 nm wide, flattop perfect (>98%) absorption at around 1550 nm wavelength. In 2017, Yang *et al.* constructed an ultrafast tunable high-*Q*-factor PA utilizing CdO with a Berreman mode plasmonic cavity [157]. Experimental results show that Berreman-type perfect absorption occurs at 2.08 μm. The perfect absorption resonance strongly redshifts on sub-bandgap optical pumping due to the transient, which leads to a change in the p-polarized reflectance from 1.0% to 86.3%. In addition, Kelley *et al.* demonstrated a new class of IR nanophotonic materials based on multilayered CdO thin films in 2019 [175].

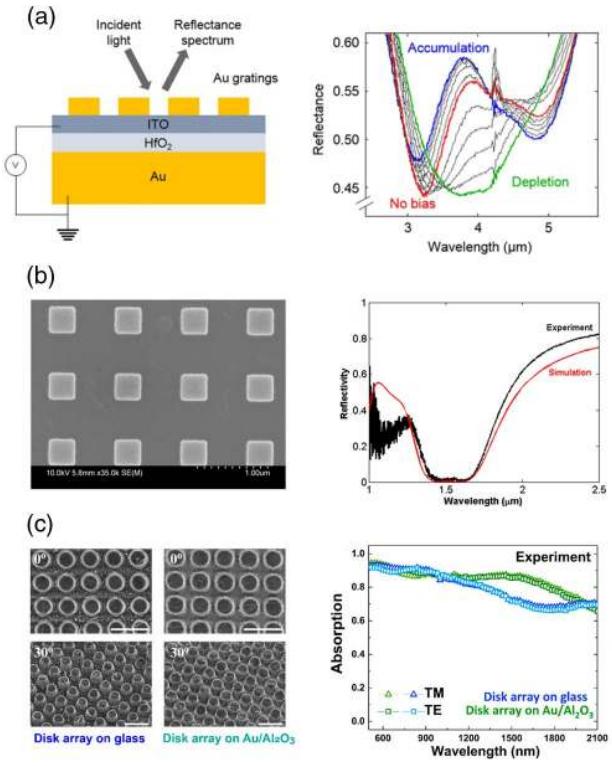

Fig. 11. (a) Illustrations of an electrically tunable absorber, and the reflectance spectra measured using a Fourier-transform IR microscope. The red, blue, and green lines represent the reflectance of the device under 0 V for no bias, −5 V for accumulation, and +5 V for depletion, respectively; the gray curves represent reflectance with an incremental step size of 1 V [90]. (b) SEM image of the fabricated device and experimentally measured absorption spectrum compared with simulated absorption spectrum [274]. (c) SEM images from the fabricated $Ti_3C_2T_x$ disk array on glass, $Ti_3C_2T_x$ disk array on Au/alumina, and experimentally measured absorption spectra for transverse-electric (TE) and TM polarizations for two designs [278]. (a) Springer-Nature, under a Creative Commons CC BY License; (b), (c) American Chemical Society.

The structure consists of three CdO layers, each individually tuned for the resonant perfect absorption condition, which achieves 90%–97% peak absorption with peak widths as narrow as 307 cm^{-1}. IR reflectivity measurements reveal that the optical response of the multilayer structure combines with an ENZ plasmonic polaritonic mode of each CdO layer [175].

Other materials and their artificial structures are also used to construct PAs. The two-dimensional (2D) material graphene is revealed to be a good candidate for efficient absorbers due to its remarkable optical properties in the gigahertz regime. Lee *et al.* introduced ENZ graphene within a plasmonic nanocavity structure for a tunable absorber [279]. Because a periodic nanocavity composed of a metal grating and metal substrate supports a strongly localized mode inside the cavity, greatly enhanced absorption (~80%) is achieved in ultrathin graphene. The absorption wavelength can be tuned by electrically controlling the Fermi level of graphene, and achieve a large enhancement (~35 times) of graphene absorption over universal graphene absorption at ENZ wavelength in a Fermi level of 0.7 eV. Lobet *et al.* designed a device made of graphene sandwiched between poly(methyl methacrylate) thin films on ENZ metamaterial substrate and achieved perfect absorption for normal incidence without a metal grating to couple incident light to ENZ graphene [280]. Mirshafieyan *et al.* used InSb with an ENZ point at 35.17 μm to build an Ag/n-InSb/TiO_2/Ag thin-film-layered absorber [281]. Halterman *et al.* theoretically proved that ENZ Weyl semimetals can be employed as coherent PAs for nearly any incident angle by choosing the proper geometrical and material parameters [282]. Nahvi *et al.* introduced nonlinear doped ENZ structures to design a nonlinear absorber, which exhibits significantly enhanced nonlinearity and tailorable intensity-dependent absorption characteristics [91]. Artificial structures based on other ENZ materials or effective ENZ structures are also used to design PAs; among them, the most important are metasurfaces and metamaterials. For example, 2D $Ti_3C_2T_x$ (T_x represents surface functional groups) MXene is used to design metasurfaces exhibiting broadband absorption by Chaudhuri *et al.*, as shown in Fig. 11(c) [278]. The proposed metasurface achieves absorption (~90%) over a broad bandwidth of ≈1.55 μm, which is attributed to strong LSPRs at NIR frequencies and the optical losses inherent to $Ti_3C_2T_x$. Other metasurfaces such as TiN/SiO_2/InAsSb/Au [283], Al/SiO_2/$Bi_{1.5}Sb_{0.5}Te_{1.8}Se_{1.2}$/Au [284], and Al/$MgF_2$/$SiO_2$/Al have also been numerically studied. Multilayers with an effective ENZ effect are another type of structure used in PAs [97,285]. Also, Li and Argyropoulos proposed nonlinear ENZ plasmonic waveguides composed of narrow periodic rectangular slits carved in a silver screen, to realize tunable nonlinear coherent perfect absorption [286].

F. Light-Emitting Devices

Light-emitting devices hold the key to optical connection networks, which can control the direction of emission and enhancement of emission rates. However, the light emission of natural bulk materials is usually omnidirectional and unpolarized, and constitutes a broad spectrum, which impedes the efficient utilization of light-emitting devices. ENZ materials exhibiting exotic and directed emission behaviors due to the

unique properties of effective permittivity have become the most promising candidates for light-emitting devices. Enoch *et al.* had a seminar work on ENZ directive emission devices [127]. Their results indicate that the energy radiated by a source will be concentrated in a narrow cone in the surrounding media, and emitted with high directivity when the metamaterial has an NZI parameter. Since then, ENZ-based light-emitting devices have been extensively studied [1,4,287]. For recent studies, in 2018, Liberal and Engheta theoretically demonstrated that directional thermal emission from ENZ bodies can be resonantly enhanced with the addition of dielectric particles to excite spatially static fluctuating fields, as shown in Fig. 12(a) [71]. The results indicate that the directional thermal emission is insensitive to any particular geometry or structural resonance of the ENZ host, which is different from previous works. Metal/dielectric nanocavities with $CsPbBr_3$ perovskite nanocrystal film were designed to be resonant with the absorption and emission bands of the employed fluorophores by Caligiuri *et al.* [288]. By special tailoring and ellipsometry measurement, the proposed nanocavity has double ENZ wavelength at 375 and 510 nm. The authors indicated that the spontaneous emission and decay rate have been significantly enhanced by the surface plasmon (SP) enhanced absorption and SP coupled emission. In 2019, Davoyan and Engheta studied and showed theoretically that the interaction of magneto-optical activity and ENZ optical wave dispersion significantly alters radiation [289]. Duan *et al.* demonstrated a nanocavity with different sizes in the coupled Ag nanorod and ENZ film with the spectral accumulation of large spontaneous emission [290]. The nanocavity can achieve about 3400 times the spontaneous emission enhancement at ENZ frequency, and 80.3% of the far-field radiation is radiated forward with a small solid angle. The results originate from the slowing down of the spectral shift of resonant nanocavities at the ENZ point. In 2020, Caligiuri *et al.* demonstrated both theoretically and experimentally the emission of a fluorophore consisting of a push-pull chromophore by embedding it into an ENZ MIM nanocavity [291]. Sakotic *et al.* proposed realistic silicon carbide structures based on Berreman embedded eigenstates in ENZ layered materials [292]. As shown in Fig. 12(b), the proposed structures give rise to quasi-coherent and highly directive thermal emission around the embedded eigenstate.

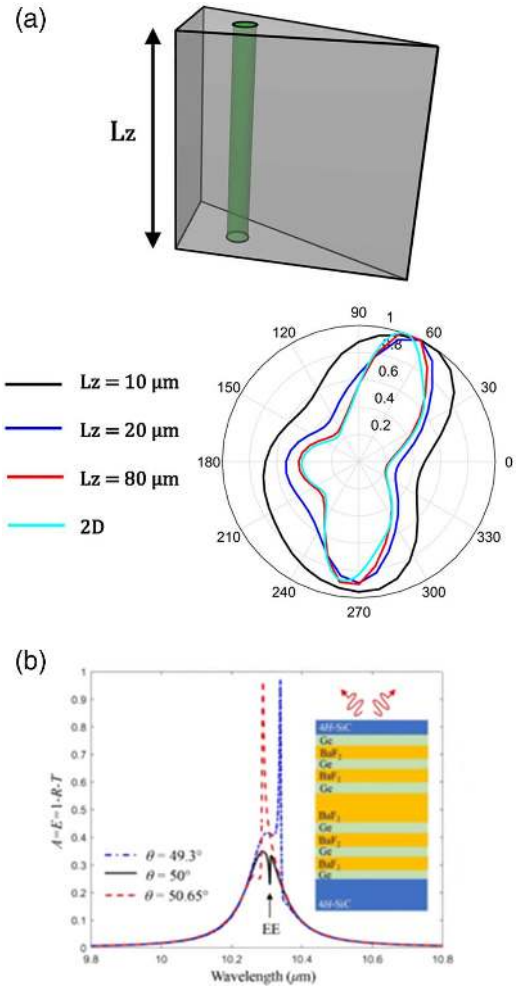

Fig. 12. (a) Sketch of ENZ bodies, numerical prediction radiation pattern based on the normalized emission pattern at the ENZ wavelength [71]. (b) Thermal emission around embedded eigenstate [292]. (a) National Academy of Sciences; (b) American Physical Society.

G. Sensors and Sensing

ENZ materials can also be applied in sensing and sensors. Among them, the ENZ waveguide channel is the most common kind of structure. Alù and Engheta reported an idea to exploit the dramatic field enhancement associated with energy squeezing and tunneling in metamaterial-inspired ultranarrow waveguide channels with the ENZ effect to sense small permittivity variations in a tiny object [293]. By modeling the super coupling effect in the ENZ waveguide, the closed-form expression of describing the presence of defects or permittivity perturbations along the channel is obtained, which shows how the high-intensity electric field in the channel can be successfully used for sensing applications. Lobato-Morales subsequently presented the waveguide channels with the ENZ effect for dielectric permittivity characterization with high sensitivity (error of characterized dielectric values within 3% and 13%) in the experiment [294]. Jha *et al.* numerically and experimentally utilized ENZ waveguide channels to design a sensor for testing the permittivity of various dispersive liquids, which typically demonstrates a 6% error under ideal conditions [295]. Pacheco-Peña *et al.* theoretically realized an ENZ-based sensor with a sensitivity up to 0.03 m/RIU, which is capable of detecting changes in the permittivity/refractive index or position with deep subwavelength analyte sizes [296].

Additionally, Fusco *et al.* reported the engineering of nonperiodic sodium tungsten bronze (Na_xWO_3) nanocrystals with the ENZ effect and designed an efficient optical sensor of Na_xWO_3 relying on a nonresonant sensing mechanism based on refractive index matching [297]. By exposing ENZ metamaterials in different environments, their device can achieve an optical sensitivity as high as 150 nm/RIU. Meng *et al.* proposed and demonstrated numerically an electrical tunable refractive index sensor based on an ENZ ITO metasurface [298]. In the glucose solution, the figure of merit (FoM) of

the sensor reached 24.7 with a sensitivity of 213.3 nm/RIU. Yang *et al.* designed a single-polarization single-mode PC fiber (PCF) with ENZ SiC [299]. The proposed fiber is based on a triangular lattice of air holes distributed in the cladding region, and SiC is deposited into four air holes. It is found that the resonance is sensitive to the relative ε variation of the material filling the fiber's air holes. The results show that the fiber sensor has a sensitivity of 566.4 nm/RIU.

H. Within the New Communication Window of 2 μm

The past 50 years saw the evolution of optical communication wavelengths, from the first and experimental 850 nm original band (O band, 1260–1360 nm), extended band (E band, 1360–1460 nm), short-wavelength band (S band, 1460–1530 nm), conventional band (C band, 1530–1565 nm), longer-wavelength band (L band, 1565–1625 nm), all the way to the ultralong-wavelength band (U band, 1625–1675 nm). Now a novel and potentially useful communication window, 2 μm, has become the academic hotspot of optical communications, ultrafast fiber optics, and mode-locked lasers.

For ENZ photonics, the "MIR" band of 2 μm is relatively new. The benefits of operating at the longer wavelength of 2 μm are that the heavy doping of the dopant is not required according to the Drude model, which can result in a potentially lower intrinsic loss and electron scattering rate, and a potentially larger second-order nonlinearity due to its weaker degrading and fewer dopant-induced defects. In 2017, Yang *et al.* used an ICO film with an ENZ wavelength of 2.10 μm for PA in polarization switching purposes [157]. In 2018, Zheng *et al.* fabricated AZO films using ALD techniques with ENZ wavelength of 2204 and 2390 nm [227], and Jiang *et al.* implemented ENZ ITO for optical switches in a waveguide at 1.9 μm [238]. In 2019, Wu and Li numerically calculated the linear pulse propagation at 2 μm in an ENZ ITO [31]; Yang *et al.* experimentally demonstrated HHG in ENZ ICO with an ENZ wavelength of 2.08 μm [46]. In 2020, Zhang *et al.* successfully fabricated and first used ENZ ITO as an optical switcher at 2.06 μm [72]. They achieved a 312 mW maximum average output power with a repetition rate of 20.53 kHz and a pulse temporal width of 2.42 μs. The pulse energy is 15.20 μJ with a peak power of 6.28 W. This experiment proves that ENZ ITO is a good candidate for a saturable absorber in a solid-state laser. For the 2 μm implementation, ENZ materials' high tunability and flexibility are full of potential.

5. PERSPECTIVES

A. Measurements of Physical Parameters

As can be seen in the previous sections, besides experiments, theoretical and numerical works can provide predictions and explanations for the underlying physical processes and mechanisms of the phenomena. They can also provide insights into the potentials and possibilities of certain setups and design schemes. Their contributions to the science community are not neglectable. Although some data are available in previous reviews [1,2,4,5,16], the current theoretical and simulation studies in ENZ photonics still suffer from the lack of measured experimental data. Many linear and nonlinear optical parameters of commonly used materials are still nowhere to be found. This greatly affects creativity and novelty in the fields because experimental verifications can take years to finally be realized due to laboratory conditions and equipment limitations. Here we call for the measurement and characterization of the fundamental properties of commonly seen ENZ materials, such as their background permittivity, damping rate, effective electron mass, mobility, free carrier concentration, Lorentz correction terms, second- and third-order susceptibilities, and nonlinear absorption coefficient. It is worth noting that a novel method for measuring the optical frequency field-effect mobility in TCOs is proposed based on a microring resonator [300]. These parameters could help build more realistic models, and the models will in turn assist future experiments, implementations, and applications. We encourage our colleagues in this community to consider publishing their main investigations along with these experimentally obtained data as supplementary information or depositing them in professional data journals and deposit archives. We also suggest systematic and comparative studies over ENZ materials, which could also benefit the community to a great extent.

B. Possibilities in Other Novel Materials

Besides naturally occurring materials such as semiconductors and metals, and the engineered metamaterials such as multilayered MIM stacks and all-dielectric stacks, other materials can exhibit exclusive, different, and exotic ENZ properties. It has been discovered that 2D materials [301], organic compounds [109], perovskites [302–305], etc., can demonstrate ENZ or even multiple ENZ points in the spectrum. Kharintsev *et al.* introduced TiON nano-composites that show double ENZ behavior [306]. Ran *et al.* also realized double ENZ using NbN_x films [307]. Lin *et al.* used black phosphor for ENZ that operates at the terahertz regime [106]. Dai *et al.* experimented with graphene/polyolefin elastomer ENZ metamaterials that work with radiofrequency [109]. Li *et al.* demonstrated a low-loss ENZ material consisting of stacked subwavelength layers of polymer and silver [308]. Novel materials may overcome the shortcomings of conventional ENZ materials, or even develop into their own categories such as flexible ENZ materials.

C. Focus on Novel Mechanisms

Novel mechanisms to realize ENZ, or to process and enhance ENZ properties, are another interesting aspect that we believe future endeavors in the field of ENZ photonics may focus on. These novel mechanisms can hopefully help ENZ materials to outperform other materials and become more practical in real-life applications and products.

Resembling acoustic soft surfaces, Nahvi *et al.* introduced EM soft surfaces with an enhanced nonlinearity. This is realized by doping the ENZ media with zero-area perfect electric conductor dopants [309]. These dopants can be used to control the media's response to TE waves, leaving the response to TM waves unaffected. The involvement of magnetization could bring new characteristics into ENZ photonics. Shen *et al.* studied giant magnetoimpedance in magnetized ENZ materials [310], Davoyan and Engheta investigated the nonreciprocal emission in magnetized ENZ media [289], and Zhao *et al.* demonstrated the EM properties of dielectric-doped magnetic

ENZ media [311]. For double ENZ, except for using new materials, Forouzmand and Mosallaei used ITO thin layers and Si nano-bars to construct an electrically tunable dual-band amplitude modulation metasurface exhibiting double ENZ [312]. For other physical and optical mechanisms, Popov *et al.* studied the Brewster effect near the exceptional points (EPs) of degeneracy in ENZ media [313] and found that the constant phase propagation does not demand the diminishing of real permittivity. Ito *et al.* engineered mushroom-like silica nanopillars to exploit phonon polaritons to realize an effective ENZ response in MIR [314], and this design is claimed to be suitable for mass production. Kolmychek *et al.* demonstrated enhanced magneto-optical effects and anomalous birefringence in ENZ nanorod arrays [315].

It can be seen from the examples above that the idea of new mechanisms to realize extraordinary ENZ effects can be inspired from other fields of photonics, and these new designs can exhibit exclusive physical and optical phenomena that can be very useful, for example, by introducing non-Hermitian optics [316] and aperiodic structures [168,317,318]. This is expected to be one of the popular trends in future ENZ studies.

D. Tunability of ENZ Wavelength

From Section 3.E, one knows that the tunability issue of ENZ materials, especially TCOs, is in a very early stage of development. Most commonly used TCOs show their ENZ wavelengths in the NIR to MIR range, combining their CMOS compatibility, simple fabrication, and low loss, making them the natural candidates for optical communications and optical signal processing, especially in the form of on-chip nanophotonic devices. Highly affected by their manufacturing process and storing environment, TCOs are more like complex mixtures rather than stable crystalline or chemical compounds. The various and diverse attempts and methods developed by different research groups have unveiled a sign of potential in this sub-field. However, by far, there is no near-perfect approach to tune the ENZ wavelength by demand within the materials' physical limits. We believe that such an approach should possess the following criteria: (i) low cost and not requiring expensive processing equipment; (ii) being stable and highly reproducible; (iii) flexible and can tune ENZ wavelength over both a small spectral margin (several to tens of nanometers scale) and large spectral margin (hundreds of nanometers scale) with different conditions; and (iv) does not require harsh experimental conditions, such as high temperature, high pressure, and long time. These are the goals we think the ENZ community could work towards. Mastering a good and stable ENZ-wavelength-tuning method, new opportunities will be created in other sub-fields such as ultrafast ENZ laser experiments and ENZ fiber optics.

E. Ultrafast ENZ Experiments and ENZ Fiber Optics

The purpose of ultrafast ENZ laser experiments and ENZ fiber optics is to establish a closer relationship between the fascinating ENZ photonics and state-of-the-art high-intensity ultrafast optics, where new phenomena and applications can emerge by combining the advantages of the two fields. For ultrafast laser experiments, the community has seen the development of the excitation of high nonlinearity and harmonic waves in ENZ materials. The typical application in a laser is to act as a saturable absorber, for example, in Nd:BGO lasers [96], and occasionally implementing some pulse shaping functionalities. For ENZ fiber optics, this area is relatively young due to some previous obstacles in combining ENZ materials into the fibers. In 2019, Yang *et al.* demonstrated the excitation of ENZ mode in D-shaped optical fibers coated with AZO [319]. In 2020, Hossain *et al.* proposed two ENZ PCF designs with ultrahigh birefringence, near-zero flat dispersion, and low loss that operate at the terahertz domain [320]. Kim *et al.* proposed two schemes of ENZ PCFs for the separation of orbital angular momentum modes [321]. In 2021, Yang *et al.* designed and analyzed a single-polarization and single-mode PCF based on ENZ with ultrawide bandwidth in terahertz regime [322]. These instances are indicators of the potentials in this field, especially for experimental realizations. Also, it would be interesting to see some of the ultrafast-related theoretical proposals be implemented in actual experiments.

F. Integration in Complex Systems and Non-Hermitian Optics

The crossroads of different areas of photonics can sometimes spark intriguing optical phenomena, and their underlying physical implications might surpass their own meanings in each field. In recent years, attempts to incorporate more complex systems with ENZ, such as conventional optical waveguide networks [323–328] based on the transmission line theory (TLT), have started to emerge. Pacheco-Peña *et al.* proposed an ENZ sensor based on TLT [296], which introduces, verifies, and broadens the use of TLT in the ENZ case. This example will allow future authors to develop and calculate more complicated ENZ systems, e.g., an ENZ interconnected network.

In ENZ photonics, there is also a tendency to merge with non-Hermitian optics, especially with parity–time-symmetry ($\mathcal{PT}$-symmetry) optics. $\mathcal{PT}$-symmetry first started as a quantum mechanical concept that Hamiltonians should at least be $\mathcal{PT}$-symmetric, and Hermicity is not strictly necessary [329,330]. Above a certain threshold, the $\mathcal{PT}$-symmetry breaks, and the Hamiltonian possesses complex eigenvalues instead of real ones. In 2007, this concept was introduced into optics [331] by El-Ganainy *et al.* In optics, $\mathcal{PT}$-symmetry is implemented by manipulating the refractive index, where a complex conjugate setup is needed, i.e., $n(x) = n^*(-x)$, and gain and loss materials of the same amount are required, often achieved by doping. Below the spontaneous breaking point (SBP, or EP), the system acts as a dissipative optical material with balanced gain and loss. Extraordinary optical phenomena happen above the SBP, such as high-quality single-mode lasing by microring pairs [332,333]. In 2020, optical $\mathcal{PT}$-symmetry and breaking in one spatial unit rather than two was realized [334]. Resembling the non-Hermitian waveguide networks [317,328,335–337], the complexity of the optical system design can take a step up when combining the aforementioned TLT, optical $\mathcal{PT}$-symmetry and breaking, and ENZ properties, to realize logic and processing operations that are not achievable in any of these individual systems.

For zero-index optics, there are early researches on realizing zero-index effects using optical $\mathcal{PT}$-symmetry [338,339]. In 2019, Jin and Argyropoulos achieved nonreciprocal

transmission using defect-doped ENZ media in nonlinear $\mathcal{PT}$-symmetric materials [237]. Their findings can be a candidate for photonic diodes, indicating a different path towards the advancement of previously introduced optical isolators. Li and Argyropoulos investigated the spectral singularities and EPs in active ENZ plasmonic waveguides [340], which could help realize reflectionless ENZ media, all-optical switching, and nanolasers as on-chip light sources. In 2020, inspired by the idea that the high loss of ENZ materials can be compensated for by optical gain, Coppolaro *et al.* showed that non-Hermitian photonic doping can be extended in ENZ media [316], presenting a possibility of reconfigurable nanophotonics platforms controlled by gain.

Conclusively, the ENZ nanophotonic platform is full of potential, and in light of the rapid growth of the integrated CMOS and photonic chip science and industries, we believe that the tendency of ENZ materials and effects to be merged with other photonic platforms is promising and feasible.

6. CONCLUSION

In this review, we introduce the rapid developments, progress, and advancements of ENZ photonics in recent years. First, from the optical concepts induced by ENZ effects, the realization mechanisms, and the nonlinear response of ENZ materials, we present the basics of ENZ photonics. Then, the recent advances in optical physics are analyzed in terms of velocities and chromatic dispersions, pulse dynamics and light–matter interactions, frequency conversion and harmonic waves, nonlinearity and loss, and attempts to align the ENZ wavelength with light sources. Parallelly, for the implementation side, the recent progress for the ENZ systems used in nanophotonic applications is discussed, in aspects of the optical communications of 2 μm, optical isolators, switches, modulators, absorbers, and sensors. Finally, we envision the future academic development of ENZ photonics and share our perspectives in six ENZ-related, young, and fast-growing sub-fields. We believe that the ENZ photonic platform is a novel and promising one for future academics, applications, and products.

Funding. Shenzhen Science and Technology Innovation Commission (GJHZ2018411185015272); Guangdong Basic and Applied Basic Research Foundation (2021A1515011450, 2021A1515012176); Youth Science and Technology Innovation Talent of Guangdong Province (2019TQ05X227).

Disclosures. The authors declare no conflicts of interest.

Data Availability. No new data were generated in the presented research.

REFERENCES

1. I. Liberal and N. Engheta, "Near-zero refractive index photonics," Nat. Photonics **11**, 149–158 (2017).
2. N. Kinsey, C. DeVault, A. Boltasseva, and V. M. Shalaev, "Near-zero-index materials for photonics," Nat. Rev. Mater. **4**, 742–760 (2019).
3. I. Liberal, M. Lobet, Y. Li, and N. Engheta, "Near-zero-index media as electromagnetic ideal fluids," Proc. Natl. Acad. Sci. USA **117**, 24050–24054 (2020).
4. X. Niu, X. Hu, S. Chu, and Q. Gong, "Epsilon-near-zero photonics: a new platform for integrated devices," Adv. Opt. Mater. **6**, 1701292 (2018).
5. G. V. Naik, V. M. Shalaev, and A. Boltasseva, "Alternative plasmonic materials: beyond gold and silver," Adv. Mater. **25**, 3264–3294 (2013).
6. G. Subramania, A. J. Fischer, and T. S. Luk, "Optical properties of metal-dielectric based epsilon near zero metamaterials," Appl. Phys. Lett. **101**, 241107 (2012).
7. S. Feng and K. Halterman, "Parametrically shielding electromagnetic fields by nonlinear metamaterials," Phys. Rev. Lett. **100**, 063901 (2008).
8. D. Felbacq and G. Bouchitté, "Homogenization of a set of parallel fibres," Waves Random Media **7**, 245–256 (1997).
9. B. Edwards, A. Alù, M. E. Young, M. Silveirinha, and N. Engheta, "Experimental verification of epsilon-near-zero metamaterial coupling and energy squeezing using a microwave waveguide," Phys. Rev. Lett. **100**, 033903 (2008).
10. A. Alù and N. Engheta, "Light squeezing through arbitrarily shaped plasmonic channels and sharp bends," Phys. Rev. B **78**, 035440 (2008).
11. E. J. R. Vesseur, T. Coenen, H. Caglayan, N. Engheta, and A. Polman, "Experimental verification of $n = 0$ structures for visible light," Phys. Rev. Lett. **110**, 013902 (2013).
12. L.-G. Wang, Z.-G. Wang, J.-X. Zhang, and S.-Y. Zhu, "Realization of Dirac point with double cones in optics," Opt. Lett. **34**, 1510–1512 (2009).
13. P. Moitra, Y. Yang, Z. Anderson, I. I. Kravchenko, D. P. Briggs, and J. Valentine, "Realization of an all-dielectric zero-index optical metamaterial," Nat. Photonics **7**, 791–795 (2013).
14. S. Kita, Y. Li, P. Camayd-Muñoz, O. Reshef, D. I. Vulis, R. W. Day, E. Mazur, and M. Lončar, "On-chip all-dielectric fabrication-tolerant zero-index metamaterials," Opt. Express **25**, 8326–8334 (2017).
15. B. Askenazi, A. Vasanelli, A. Delteil, Y. Todorov, L. C. Andreani, G. Beaudoin, I. Sagnes, and C. Sirtori, "Ultra-strong light-matter coupling for designer Reststrahlen band," New J. Phys. **16**, 043029 (2014).
16. O. Reshef, I. De Leon, M. Z. Alam, and R. W. Boyd, "Nonlinear optical effects in epsilon-near-zero media," Nat. Rev. Mater. **4**, 535–551 (2019).
17. M. G. Silveirinha and N. Engheta, "Theory of supercoupling, squeezing wave energy, and field confinement in narrow channels and tight bends using ε near-zero metamaterials," Phys. Rev. B **76**, 245109 (2007).
18. A. Ciattoni, A. Marini, C. Rizza, M. Scalora, and F. Biancalana, "Polariton excitation in epsilon-near-zero slabs: transient trapping of slow light," Phys. Rev. A **87**, 053853 (2013).
19. T. Zhai and X. Zhang, "Epsilon-near-zero metamaterials for tailoring ultrashort pulses," Appl. Phys. B **113**, 185–189 (2013).
20. P. Kelly and L. Kuznetsova, "Adaptive pre-shaping for ultrashort pulse control during propagation in AZO/ZnO multilayered metamaterial at the epsilon-near-zero spectral point," OSA Contin. **3**, 143–152 (2020).
21. T. Xu, D. Zhu, and Z. H. Hang, "Pulse reshaping in double-zero-index photonic crystals with Dirac-like-cone dispersion," Sci. Rep. **10**, 8416 (2020).
22. S. Campione, D. de Ceglia, M. A. Vincenti, M. Scalora, and F. Capolino, "Electric field enhancement in ε-near-zero slabs under TM-polarized oblique incidence," Phys. Rev. B **87**, 035120 (2013).
23. G. H. Y. Li, C. M. de Sterke, and A. Tuniz, "Omnidirectional field enhancements drive giant nonlinearities in epsilon-near-zero waveguides," Opt. Lett. **45**, 6514–6517 (2020).
24. A. Baev, P. N. Prasad, M. Z. Alam, and R. W. Boyd, "Dynamically controlling local field enhancement at an epsilon-near-zero/dielectric interface via nonlinearities of an epsilon-near-zero medium," Nanophotonics **9**, 4831–4837 (2020).
25. I. V. A. K. Reddy, J. M. Jornet, A. Baev, and P. N. Prasad, "Extreme local field enhancement by hybrid epsilon-near-zero–plasmon mode in thin films of transparent conductive oxides," Opt. Lett. **45**, 5744–5747 (2020).

26. C. Argyropoulos, P.-Y. Chen, G. D'Aguanno, N. Engheta, and A. Alù, "Boosting optical nonlinearities in ϵ-near-zero plasmonic channels," Phys. Rev. B **85**, 045129 (2012).
27. M. Z. Alam, I. De Leon, and R. W. Boyd, "Large optical nonlinearity of indium tin oxide in its epsilon-near-zero region," Science **352**, 795–797 (2016).
28. A. Ciattoni, C. Rizza, A. Marini, A. D. Falco, D. Faccio, and M. Scalora, "Enhanced nonlinear effects in pulse propagation through epsilon-near-zero media," Laser Photon. Rev. **10**, 517–525 (2016).
29. C. Rizza, A. Ciattoni, and E. Palange, "Two-peaked and flat-top perfect bright solitons in nonlinear metamaterials with epsilon near zero," Phys. Rev. A **83**, 053805 (2011).
30. C. Argyropoulos, P.-Y. Chen, G. D'Aguanno, and A. Alù, "Temporal soliton excitation in an ϵ-near-zero plasmonic metamaterial," Opt. Lett. **39**, 5566–5569 (2014).
31. J. Wu and Q. Li, "Propagation of ultrashort pulses in indium tin oxide epsilon-near-zero subwavelength metamaterial at 2 μm," in *Frontiers in Optics + Laser Science APS/DLS* (OSA, 2019), paper JTu3A.28.
32. J. Wu and Q. Li, "Ultrashort pulses in indium tin oxide thin film at its epsilon-near-zero wavelength," in *Asia Communications and Photonics Conference* (2019), paper M4A.300.
33. J. Wu, Z. T. Xie, Y. Sha, H. Y. Fu, and Q. Li, "Large and complex chromatic dispersion profile in epsilon-near-zero aluminum-doped zinc oxide," in *Frontiers in Optics/Laser Science* (OSA, 2020), paper JTu1A.34.
34. J. Wu, B. A. Malomed, H. Y. Fu, and Q. Li, "Self-interaction of ultrashort pulses in an epsilon-near-zero nonlinear material at the telecom wavelength," Opt. Express **27**, 37298–37306 (2019).
35. J. Wu, Z. T. Xie, Y. Sha, H. Y. Fu, and Q. Li, "Comparative study on epsilon-near-zero transparent conducting oxides: high-order chromatic dispersions and modeling of ultrashort pulse interactions," Phys. Rev. A **102**, 053503 (2020).
36. P. Kelly and L. Kuznetsova, "Pump-probe ultrashort pulse modulation in an AZO/ZnO metamaterial at the epsilon near zero spectral point," OSA Contin. **3**, 3225–3236 (2020).
37. C. Argyropoulos, G. D'Aguanno, and A. Alù, "Giant second-harmonic generation efficiency and ideal phase matching with a double ϵ-near-zero cross-slit metamaterial," Phys. Rev. B **89**, 235401 (2014).
38. A. Capretti, Y. Wang, N. Engheta, and L. Dal Negro, "Comparative study of second-harmonic generation from epsilon-near-zero indium tin oxide and titanium nitride nanolayers excited in the near-infrared spectral range," ACS Photon. **2**, 1584–1591 (2015).
39. C. K. Dass, H. Kwon, S. Vangala, E. M. Smith, J. W. Cleary, J. Guo, A. Alù, and J. R. Hendrickson, "Gap-plasmon-enhanced second-harmonic generation in epsilon-near-zero nanolayers," ACS Photon. **7**, 174–179 (2020).
40. L. Rodríguez-Suné, M. Scalora, A. S. Johnson, C. Cojocaru, N. Akozbek, Z. J. Coppens, D. Perez-Salinas, S. Wall, and J. Trull, "Study of second and third harmonic generation from an indium tin oxide nanolayer: Influence of nonlocal effects and hot electrons," APL Photon. **5**, 010801 (2020).
41. N. C. Passler, I. Razdolski, D. S. Katzer, D. F. Storm, J. D. Caldwell, M. Wolf, and A. Paarmann, "Second harmonic generation from phononic epsilon-near-zero Berreman modes in ultrathin polar crystal films," APL Photon. **6**, 1365–1371 (2019).
42. P. G. Vianna, A. d. S. Almeida, R. M. Gerosa, D. A. Bahamon, and C. J. S. de Matos, "Second-harmonic generation enhancement in monolayer transition-metal dichalcogenides by an epsilon-near-zero substrate," Nano. Adv. **3**, 272–278 (2020).
43. I. A. Kolmychek, V. B. Novikov, I. V. Malysheva, A. P. Leontiev, K. S. Napolskii, and T. V. Murzina, "Second-harmonic generation spectroscopy in gold nanorod-based epsilon-near-zero metamaterials," Opt. Lett. **45**, 1866–1869 (2020).
44. T. S. Luk, D. de Ceglia, S. Liu, G. A. Keeler, R. P. Prasankumar, M. A. Vincenti, M. Scalora, M. B. Sinclair, and S. Campione, "Enhanced third harmonic generation from the epsilon-near-zero modes of ultrathin films," Appl. Phys. Lett. **106**, 151103 (2015).
45. A. Capretti, Y. Wang, N. Engheta, and L. Dal Negro, "Enhanced third-harmonic generation in Si-compatible epsilon-near-zero indium tin oxide nanolayers," Opt. Lett. **40**, 1500–1503 (2015).
46. Y. Yang, J. Lu, A. Manjavacas, T. S. Luk, H. Liu, K. Kelley, J.-P. Maria, E. L. Runnerstrom, M. B. Sinclair, S. Ghimire, and I. Brener, "High-harmonic generation from an epsilon-near-zero material," Nat. Phys. **15**, 1022–1026 (2019).
47. Y. Yang, J. Lu, A. Manjavacas, T. S. Luk, H. Liu, K. Kelley, J.-P. Maria, M. B. Sinclair, E. L. Runnerstrom, S. Ghimire, and I. Brener, "High-harmonic generation from an epsilon-near-zero material," Proc. SPIE **11080**, 110800D (2019).
48. J. Wu, Z. T. Xie, H. Fu, and Q. Li, "Numerical investigations on the cascaded high harmonic and quasi-supercontinuum generations in epsilon-near-zero aluminum-doped zinc oxide nanolayers," Results Phys. **24**, 104086 (2021).
49. J. Wu, Z. T. Xie, H. Y. Fu, and Q. Li, "High-order harmonic generations in epsilon-near-zero aluminum-doped zinc oxide nanopyramid array," in *12th International Conference on Advanced Infocomm Technology (ICAIT)* (IEEE, 2020), pp. 5–9.
50. Z. T. Xie, J. Wu, H. Y. Fu, and Q. Li, "Giant enhancement of third- and fifth-harmonic generations in epsilon-near-zero nanolayer," in *Asia Communications and Photonics Conference/International Conference on Information Photonics and Optical Communications (ACP/IPOC)* (OSA, 2020), paper M4A.15.
51. W. Tian, F. Liang, D. Lu, H. Yu, and H. Zhang, "Highly efficient ultraviolet high-harmonic generation from epsilon-near-zero indium tin oxide films," Photon. Res. **9**, 317–323 (2021).
52. J. B. Khurgin, M. Clerici, V. Bruno, L. Caspani, C. DeVault, J. Kim, A. Shaltout, A. Boltasseva, V. M. Shalaev, M. Ferrera, D. Faccio, and N. Kinsey, "Adiabatic frequency shifting in epsilon-near-zero materials: the role of group velocity," Optica **7**, 226–231 (2020).
53. Y. Zhou, M. Z. Alam, M. Karimi, J. Upham, O. Reshef, C. Liu, A. E. Willner, and R. W. Boyd, "Broadband frequency translation through time refraction in an epsilon-near-zero material," Nat. Commun. **11**, 2180 (2020).
54. D. Yoo, F. Vidal-Codina, C. Ciracì, N.-C. Nguyen, D. R. Smith, J. Peraire, and S.-H. Oh, "Modeling and observation of mid-infrared nonlocality in effective epsilon-near-zero ultranarrow coaxial apertures," Nat. Commun. **10**, 4476 (2019).
55. Y. He, Y. Li, Z. Zhou, H. Li, Y. Hou, S. Liao, and P. Chen, "Wideband epsilon-near-zero supercoupling control through substrate-integrated impedance surface," Adv. Theor. Simul. **2**, 1900059 (2019).
56. Y. Wang, H. Luong, Z. Zhang, and Y. Zhao, "Coupling between plasmonic nanohole array and nanorod array: the emerging of a new extraordinary optical transmission mode and epsilon-near-zero property," J. Phys. D **53**, 275202 (2020).
57. I. V. Bondarev, H. Mousavi, and V. M. Shalaev, "Transdimensional epsilon-near-zero modes in planar plasmonic nanostructures," Phys. Rev. Res. **2**, 013070 (2020).
58. Y. G. Lee and C.-S. Kee, "Defect modes of two-dimensional photonic crystals composed of epsilon-near-zero metamaterials," J. Opt. **22**, 045102 (2020).
59. O. Dominguez, L. Nordin, J. Lu, K. Feng, D. Wasserman, and A. J. Hoffman, "Monochromatic multimode antennas on epsilon-near-zero materials," Adv. Opt. Mater. **7**, 1800826 (2019).
60. W. Zhu and W. She, "Enhanced spin Hall effect of transmitted light through a thin epsilon-near-zero slab," Opt. Lett. **40**, 2961–2964 (2015).
61. A. Ciattoni, A. Marini, and C. Rizza, "Efficient vortex generation in subwavelength epsilon-near-zero slabs," Phys. Rev. Lett. **118**, 104301 (2017).
62. R. J. Pollard, A. Murphy, W. R. Hendren, P. R. Evans, R. Atkinson, G. A. Wurtz, A. V. Zayats, and V. A. Podolskiy, "Optical nonlocalities and additional waves in epsilon-near-zero metamaterials," Phys. Rev. Lett. **102**, 127405 (2009).
63. C. Rizza, A. Di Falco, M. Scalora, and A. Ciattoni, "One-dimensional chirality: strong optical activity in epsilon-near-zero metamaterials," Phys. Rev. Lett. **115**, 057401 (2015).
64. M. G. Wood, S. Campione, S. Parameswaran, T. S. Luk, J. R. Wendt, D. K. Serkland, and G. A. Keeler, "Gigahertz speed operation of epsilon-near-zero silicon photonic modulators," Optica **5**, 233–236 (2018).

65. Z. T. Xie, J. Wu, H. Y. Fu, and Q. Li, "Tunable electro- and all-optical switch based on epsilon-near-zero metasurface," IEEE Photon. J. **12**, 4501510 (2020).
66. A. P. Vasudev, J.-H. Kang, J. Park, X. Liu, and M. L. Brongersma, "Electro-optical modulation of a silicon waveguide with an "epsilon-near-zero" material," Opt. Express **21**, 26387–26397 (2013).
67. H. Wang, X. Dai, K. Du, K. Gao, W. Zhang, S. J. Chua, and T. Mei, "Tuning epsilon-near-zero wavelength of indium tin oxide film via annealing," J. Phys. D **53**, 225108 (2020).
68. B. Johns, N. M. Puthoor, H. Gopalakrishnan, A. Mishra, R. Pant, and J. Mitra, "Epsilon-near-zero response in indium tin oxide thin films: octave span tuning and IR plasmonics," J. Appl. Phys. **127**, 043102 (2020).
69. R. Hong, T. Yan, C. Tao, Q. Wang, H. Lin, and D. Zhang, "Laser induced the tunable permittivity of epsilon-near-zero induced in indium tin oxide thin films," Opt. Mater. **107**, 110137 (2020).
70. J. Wu, H. Fu, Y. Zheng, K.-C. Chang, S. Zhang, H. Y. Fu, and Q. Li, "Precise tuning of epsilon-near-zero properties in indium tin oxide nanolayer by supercritical carbon dioxide," in *14th Pacific Rim Conference on Lasers and Electro-Optics (CLEO PR)* (OSA, 2020), paper C4G_3.
71. I. Liberal and N. Engheta, "Manipulating thermal emission with spatially static fluctuating fields in arbitrarily shaped epsilon-near-zero bodies," Proc. Natl. Acad. Sci. USA **115**, 2878–2883 (2018).
72. C. Zhang, Y. Zu, W. Yang, S. Jiang, and J. Liu, "Epsilon-near-zero medium for optical switches in Ho solid-state laser at 2.06 μm," Opt. Laser Technol. **129**, 106271 (2020).
73. L. Vertchenko, N. Akopian, and A. V. Lavrinenko, "Epsilon-near-zero grids for on-chip quantum networks," Sci. Rep. **9**, 6053 (2019).
74. Q. Guo, Y. Cui, Y. Yao, Y. Ye, Y. Yang, X. Liu, S. Zhang, X. Liu, J. Qiu, and H. Hosono, "A solution-processed ultrafast optical switch based on a nanostructured epsilon-near-zero medium," Adv. Mater. **29**, 1700754 (2017).
75. Z. T. Xie, J. Wu, H. Y. Fu, and Q. Li, "Tunable electro-optical metasurface based on an ultra-strong coupling epsilon-near-zero system," in *Frontiers in Optics/Laser Science* (OSA, 2020), paper JTu1A.41.
76. F. Hu, W. Jia, Y. Meng, M. Gong, and Y. Yang, "High-contrast optical switching using an epsilon-near-zero material coupled to a Bragg microcavity," Opt. Express **27**, 26405–26414 (2019).
77. Z. Zhang, J. Liu, Q. Hao, and J. Liu, "Sensitive saturable absorber and optical switch of epsilon-near-zero medium," Appl. Phys. Express **12**, 065504 (2019).
78. E. Li and A. X. Wang, "Femto-Joule all-optical switching using epsilon-near-zero high-mobility conductive oxide," IEEE J. Sel. Top. Quantum Electron. **27**, 3600109 (2021).
79. J. Kuttruff, D. Garoli, J. Allerbeck, R. Krahne, A. De Luca, D. Brida, V. Caligiuri, and N. Maccaferri, "Ultrafast all-optical switching enabled by epsilon-near-zero-tailored absorption in metal-insulator nanocavities," Commun. Phys. **3**, 114 (2020).
80. Y. Kuang, Y. Liu, L. Tian, W. Han, and Z. Li, "A dual-slot electro-optic modulator based on an epsilon-near-zero oxide," IEEE Photon. J. **11**, 2200912 (2019).
81. B. Zhou, E. Li, Y. Bo, and A. X. Wang, "High-speed plasmonic-conductive oxide-silicon modulator by epsilon-near-zero electro-absorption," in *IEEE 16th International Conference on Group IV Photonics (GFP)* (IEEE, 2019), pp. 1–2.
82. Q. Gao, E. Li, and A. X. Wang, "Ultra-compact and broadband electro-absorption modulator using an epsilon-near-zero conductive oxide," Photon. Res. **6**, 277–281 (2018).
83. Y. Sha, J. Wu, Z. T. Xie, and Q. Li, "Optimization of slot waveguide modulator based on epsilon-near-zero effect," in *Frontiers in Optics/Laser Science* (OSA, 2020), paper JTu1B.9.
84. X. Liu, K. Zang, J.-H. Kang, J. Park, J. S. Harris, P. G. Kik, and M. L. Brongersma, "Epsilon-near-zero Si slot-waveguide modulator," ACS Photon. **5**, 4484–4490 (2018).
85. L. Tao, A. Anopchenko, S. Gurung, J. Zhang, and H. W. H. Lee, "Gate-tunable plasmon-induced transparency modulator based on stub-resonator waveguide with epsilon-near-zero materials," Sci. Rep. **9**, 2789 (2019).
86. E. Alvear-Cabezón, T. Taliercio, S. Blin, R. Smaali, F. Gonzalez-Posada, A. Baranov, R. Teissier, and E. Centeno, "Epsilon near-zero all-optical terahertz modulator," Appl. Phys. Lett. **117**, 111101 (2020).
87. M. A. Swillam, A. O. Zaki, K. Kirah, and L. A. Shahada, "On chip optical modulator using epsilon-near-zero hybrid plasmonic platform," Sci. Rep. **9**, 6669 (2019).
88. B. Zhou, E. Li, Y. Bo, and A. X. Wang, "High-speed plasmonic-silicon modulator driven by epsilon-near-zero conductive oxide," J. Lightwave Technol. **38**, 3338–3345 (2020).
89. B. Zhou, E. Li, Y. Bo, W.-C. Hsu, and A. X. Wang, "High-speed broadband plasmonic-silicon modulator integrated with epsilon-near-zero conductive oxide," in *Conference on Lasers and Electro-Optics* (OSA, 2020), paper STh3O.5.
90. J. Park, J.-H. Kang, X. Liu, and M. L. Brongersma, "Electrically tunable epsilon-near-zero (ENZ) metafilm absorbers," Sci. Rep. **5**, 15754 (2015).
91. E. Nahvi, I. Liberal, and N. Engheta, "Nonlinear metamaterial absorbers enabled by photonic doping of epsilon-near-zero metastructures," Phys. Rev. B **102**, 035404 (2020).
92. Z. Meng, H. Cao, and X. Wu, "New design strategy for broadband perfect absorber by coupling effects between metamaterial and epsilon-near-zero mode," Opt. Mater. **96**, 109347 (2019).
93. E. M. Smith, J. Chen, J. R. Hendrickson, J. W. Cleary, C. Dass, A. N. Reed, S. Vangala, and J. Guo, "Epsilon-near-zero thin-film metamaterials for wideband near-perfect light absorption," Opt. Mater. Express **10**, 2439–2446 (2020).
94. W. Ji, D. Wang, S. Li, Y. Shang, W. Xiong, L. Zhang, and J. Luo, "Photonic-doped epsilon-near-zero media for coherent perfect absorption," Appl. Phys. A **125**, 129 (2019).
95. X. Chai, Y. Zhang, Y. Cao, L. Wu, J. Ma, Y. Liu, and L. Song, "Modulation of photoelectric properties of indium tin oxide thin films via oxygen control, and its application to epsilon-near-zero properties for an infrared absorber," J. Appl. Phys. **128**, 185301 (2020).
96. Q.-H. Xiao, X.-Y. Feng, W. Yang, Y.-K. Lin, Q.-Q. Peng, S.-Z. Jiang, J. Liu, and L.-B. Su, "Epsilon-near-zero indium tin oxide nanocolumns array as a saturable absorber for a Nd:BGO laser," Laser Phys. **30**, 055802 (2020).
97. W.-B. Liao, C.-C. Lee, Y.-C. Chang, W.-H. Cho, H.-P. Chen, and C.-C. Kuo, "Admittance analysis of broadband omnidirectional near-perfect absorber in epsilon-near-zero mode," Appl. Opt. **59**, 10138–10142 (2020).
98. A. R. Davoyan, A. M. Mahmoud, and N. Engheta, "Optical isolation with epsilon-near-zero metamaterials," Opt. Express **21**, 3279–3286 (2013).
99. J. Parra, I. Olivares, A. Brimont, and P. Sanchis, "Non-volatile epsilon-near-zero readout memory," Opt. Lett. **44**, 3932–3935 (2019).
100. M. Kim, S. Kim, and S. Kim, "Resonator-free optical bistability based on epsilon-near-zero mode," Sci. Rep. **9**, 6552 (2019).
101. Y. Wu, X. Hu, F. Wang, J. Yang, C. Lu, Y.-C. Liu, H. Yang, and Q. Gong, "Ultracompact and unidirectional on-chip light source based on epsilon-near-zero materials in an optical communication range," Phys. Rev. Appl. **12**, 054021 (2019).
102. X. Duan, F. Zhang, Z. Qian, H. Hao, L. Shan, Q. Gong, and Y. Gu, "Accumulation and directionality of large spontaneous emission enabled by epsilon-near-zero film," Opt. Express **27**, 7426–7434 (2019).
103. J.-K. So, G. H. Yuan, C. Soci, and N. I. Zheludev, "Enhancement of luminescence of quantum emitters in epsilon-near-zero waveguides," Appl. Phys. Lett. **117**, 181104 (2020).
104. K. Minn, A. Anopchenko, C.-W. Chang, J. Kim, Y.-J. Lu, S. Gwo, and H. W. H. Lee, "Enhanced spontaneous emission of 2D materials on epsilon-near-zero substrates," Proc. SPIE **11462**, 114620O (2020).
105. Z. Zhou, Y. Li, E. Nahvi, H. Li, Y. He, I. Liberal, and N. Engheta, "General impedance matching via doped epsilon-near-zero media," Phys. Rev. Appl. **13**, 034005 (2020).
106. Y. Lin, X. Liu, H. Chen, X. Guo, J. Pan, J. Yu, H. Zheng, H. Guan, H. Lu, Y. Zhong, Y. Chen, Y. Luo, W. Zhu, and Z. Chen, "Tunable

asymmetric spin splitting by black phosphorus sandwiched epsilon-near-zero-metamaterial in the terahertz region," Opt. Express **27**, 15868–15879 (2019).
107. T. Suzuki, T. Sato, M. Sekiya, and J. C. Young, "Epsilon-near-zero three-dimensional metamaterial for manipulation of terahertz beams," Appl. Opt. **58**, 3029–3035 (2019).
108. W. Jia, M. Liu, Y. Lu, X. Feng, Q. Wang, X. Zhang, Y. Ni, F. Hu, M. Gong, X. Xu, Y. Huang, W. Zhang, Y. Yang, and J. Han, "Broadband terahertz wave generation from an epsilon-near-zero material," Light Sci. Appl. **10**, 11 (2021).
109. J. Dai, H. Luo, M. Moloney, and J. Qiu, "Adjustable graphene/polyolefin elastomer epsilon-near-zero metamaterials at radiofrequency range," ACS Appl. Mater. Interfaces **12**, 22019–22028 (2020).
110. D. M. George and A. Chandroth, "5 GHz high gain slotted SIW epsilon near zero antenna array for wireless communications," Eng. Res. Express **2**, 045014 (2020).
111. A. Nieminen, A. Marini, and M. Ornigotti, "Goos–Hänchen and Imbert–Fedorov shifts for epsilon-near-zero materials," J. Opt. **22**, 035601 (2020).
112. R. K. Saripalli, N. Chaitanya, A. Ghosh, V. Sharma, I. De Leon, and G. Samanta, "Experimental verification of vortex generation through spin-orbit coupling in epsilon-near-zero films," in *Conference on Lasers and Electro-Optics* (OSA, 2020), paper FM2B.8.
113. A. Ghosh, R. Saripalli, K. Subith, N. A. Chaitanya, V. Sharma, I. D. Leon, and G. Samanta, "Generation of non-collinear Poincaré beam through the spin-orbit interaction in epsilon-near-zero film," in *Frontiers in Optics/Laser Science* (OSA, 2020), paper FM7C.3.
114. S. Benis, N. Munera, E. W. V. Stryland, and D. J. Hagan, "Transient nonlinear phase-shift in epsilon-near-zero materials," in *IEEE Research and Applications of Photonics in Defense Conference (RAPID)* (IEEE, 2020), pp. 1–2.
115. G. E. Lio, A. Ferraro, M. Giocondo, R. Caputo, and A. De Luca, "Color gamut behavior in epsilon near-zero nanocavities during propagation of gap surface plasmons," Adv. Opt. Mater. **8**, 2000487 (2020).
116. K. Manukyan, M. Z. Alam, C. Liu, K. Pang, Y. Zhou, Z. Zhao, H. Song, M. Tur, R. W. Boyd, and A. E. Willner, "Generation of pulses with dynamic polarization evolution using time-varying epsilon-near-zero metasurface," in *IEEE Photonics Conference (IPC)* (IEEE, 2020), pp. 1–2.
117. G. E. Lio, A. Ferraro, T. Ritacco, D. M. Aceti, A. De Luca, M. Giocondo, and R. Caputo, "Leveraging on ENZ metamaterials to achieve 2D and 3D hyper-resolution in two-photon direct laser writing," Adv. Mater. **33**, 2008644 (2021).
118. Q. Jin, G. Liang, G. Chen, F. Zhao, S. Yan, K. Zhang, M. Yang, Q. Zhang, Z. Wen, and Z. Zhang, "Enlarging focal depth using epsilon-near-zero metamaterial for plasmonic lithography," Opt. Lett. **45**, 3159–3162 (2020).
119. H. Luo, J. Qin, E. Kinzel, and L. Wang, "Deep plasmonic direct writing lithography with ENZ metamaterials and nanoantenna," Nanotechnology **30**, 425303 (2019).
120. G. D'Aguanno, N. Mattiucci, M. Scalora, and M. J. Bloemer, "Bright and dark gap solitons in a negative index Fabry-Pérot etalon," Phys. Rev. Lett. **93**, 213902 (2004).
121. N. Mattiucci, G. D'Aguanno, M. J. Bloemer, and M. Scalora, "Second-harmonic generation from a positive-negative index material heterostructure," Phys. Rev. E **72**, 066612 (2005).
122. G. D'Aguanno, N. Mattiucci, M. J. Bloemer, and M. Scalora, "Large enhancement of interface second-harmonic generation near the zero-$\bar{n}$ gap of a negative-index Bragg grating," Phys. Rev. E **73**, 036603 (2006).
123. G. D'Aguanno, N. Mattiucci, M. Scalora, and M. J. Bloemer, "Second-harmonic generation at angular incidence in a negative-positive index photonic band-gap structure," Phys. Rev. E **74**, 026608 (2006).
124. M. Kamandi, C. Guclu, T. S. Luk, G. T. Wang, and F. Capolino, "Giant field enhancement in longitudinal epsilon-near-zero films," Phys. Rev. B **95**, 161105 (2017).
125. M. Silveirinha and N. Engheta, "Tunneling of electromagnetic energy through subwavelength channels and bends using ε-near-zero materials," Phys. Rev. Lett. **97**, 157403 (2006).
126. V. Caligiuri, M. Palei, G. Biffi, S. Artyukhin, and R. Krahne, "A semi-classical view on epsilon-near-zero resonant tunneling modes in metal/insulator/metal nanocavities," Nano Lett. **19**, 3151–3160 (2019).
127. S. Enoch, G. Tayeb, P. Sabouroux, N. Guérin, and P. Vincent, "A metamaterial for directive emission," Phys. Rev. Lett. **89**, 213902 (2002).
128. S. S. M. Khaleghi, G. Moradi, R. S. Shirazi, and A. Jafargholi, "Microstrip line impedance matching using ENZ metamaterials, design, and application," IEEE Trans. Antennas Propag. **67**, 2243–2251 (2019).
129. G. D'Aguanno, N. Mattiucci, M. J. Bloemer, R. Trimm, N. Aközbek, and A. Alù, "Frozen light in a near-zero index metasurface," Phys. Rev. B **90**, 054202 (2014).
130. J. B. Khurgin, M. Clerici, and N. Kinsey, "Fast and slow nonlinearities in ENZ materials," arXiv:2007.05613 (2020).
131. G. D'Aguanno, N. Mattiucci, and M. J. Bloemer, "Ultraslow light pulses in a nonlinear metamaterial," J. Opt. Soc. Am. B **25**, 1236–1241 (2008).
132. A. Alù, M. G. Silveirinha, A. Salandrino, and N. Engheta, "Epsilon-near-zero metamaterials and electromagnetic sources: tailoring the radiation phase pattern," Phys. Rev. B **75**, 155410 (2007).
133. S. Vassant, J.-P. Hugonin, F. Marquier, and J.-J. Greffet, "Berreman mode and epsilon near zero mode," Opt. Express **20**, 23971–23977 (2012).
134. S. Campione, I. Brener, and F. Marquier, "Theory of epsilon-near-zero modes in ultrathin films," Phys. Rev. B **91**, 121408 (2015).
135. S. Vassant, J.-P. Hugonin, and J.-J. Greffet, "Quasi-confined ENZ mode in an anisotropic uniaxial thin slab," Opt. Express **27**, 12317–12335 (2019).
136. W. Tian, F. Liang, S. Chi, C. Li, H. Yu, H. Zhang, and H. Zhang, "Highly efficient super-continuum generation on an epsilon-near-zero surface," ACS Omega **5**, 2458–2464 (2020).
137. G. P. Agrawal, *Nonlinear Fiber Optics*, 5th ed. (Academic, 2013).
138. N. Kinsey and J. Khurgin, "Nonlinear epsilon-near-zero materials explained: opinion," Opt. Mater. Express **9**, 2793–2796 (2019).
139. E. Nahvi, I. Liberal, and N. Engheta, "Nonperturbative effective magnetic nonlinearity in ENZ media doped with Kerr dielectric inclusions," ACS Photon. **6**, 2823–2831 (2019).
140. M. A. Vincenti, D. de Ceglia, and M. Scalora, "ENZ materials and anisotropy: enhancing nonlinear optical interactions at the nanoscale," Opt. Express **28**, 31180–31196 (2020).
141. J. Deng, Y. Tang, S. Chen, K. Li, A. V. Zayats, and G. Li, "Giant enhancement of second-order nonlinearity of epsilon-near- zero medium by a plasmonic metasurface," Nano Lett. **20**, 5421–5427 (2020).
142. S. Benis, N. Munera, D. J. Hagan, and E. W. Van Stryland, "Spectral and angular dependence of the giant nonlinear refraction of indium tin oxide excited at epsilon-near-zero," in *Conference on Lasers and Electro-Optics* (OSA, 2019), paper FF3D.3.
143. D. M. Solis and N. Engheta, "A theoretical explanation for enhanced nonlinear response in epsilon-near-zero media," in *Conference on Lasers and Electro-Optics* (OSA, 2020), paper JW2D.15.
144. C. Liu, M. Z. Alam, K. Manukyan, K. Pang, Y. Zhou, H. Song, X. Su, J. R. Hendrickson, E. M. Smith, M. Tur, R. W. Boyd, and A. E. Willner, "Nonlinear response of ENZ plasmon modes near 1550 nm," in *IEEE Photonics Conference (IPC)* (IEEE, 2020), pp. 1–2.
145. H. Wang, K. Du, R. Liu, X. Dai, W. Zhang, S. J. Chua, and T. Mei, "Role of hot electron scattering in epsilon-near-zero optical nonlinearity," Nanophotonics **9**, 4287–4293 (2020).
146. S. Suresh, O. Reshef, M. Z. Alam, J. Upham, M. Karimi, and R. W. Boyd, "Enhanced nonlinear optical responses of layered epsilon-near-zero metamaterials at visible frequencies," ACS Photon. **8**, 125–129 (2021).
147. S. Suresh, O. Reshef, M. Z. Alam, J. Upham, M. Karimi, and R. W. Boyd, "Large optical nonlinearity in epsilon-near-zero metamaterials in the visible regime," in *Frontiers in Optics + Laser Science APS/DLS* (OSA, 2019), paper JW3A.21.
148. X. Niu, X. Hu, Q. Sun, C. Lu, Y. Yang, H. Yang, and Q. Gong, "Polarization-selected nonlinearity transition in gold dolmens

coupled to an epsilon-near-zero material," Nanophotonics **9**, 4839–4851 (2020).
149. A. Ciattoni, C. Rizza, and E. Palange, "Transmissivity directional hysteresis of a nonlinear metamaterial slab with very small linear permittivity," Opt. Lett. **35**, 2130–2132 (2010).
150. A. Ciattoni, C. Rizza, and E. Palange, "Extreme nonlinear electrodynamics in metamaterials with very small linear dielectric permittivity," Phys. Rev. A **81**, 043839 (2010).
151. R. M. Kaipurath, M. Pietrzyk, L. Caspani, T. Roger, M. Clerici, C. Rizza, A. Ciattoni, A. Di Falco, and D. Faccio, "Optically induced metal-to-dielectric transition in epsilon-near-zero metamaterials," Sci. Rep. **6**, 27700 (2016).
152. P. Drude, "Zur Elektronentheorie der Metalle," Ann. Phys. (Leipzig) **306**, 566–613 (1900).
153. S. Ray, R. Banerjee, N. Basu, A. K. Batabyal, and A. K. Barua, "Properties of tin doped indium oxide thin films prepared by magnetron sputtering," J. Appl. Phys. **54**, 3497–3501 (1983).
154. H. Agura, A. Suzuki, T. Matsushita, T. Aoki, and M. Okuda, "Low resistivity transparent conducting Al-doped ZnO films prepared by pulsed laser deposition," Thin Solid Films **445**, 263–267 (2003).
155. S.-M. Park, T. Ikegami, and K. Ebihara, "Effects of substrate temperature on the properties of Ga-doped ZnO by pulsed laser deposition," Thin Solid Films **513**, 90–94 (2006).
156. B. T. Diroll, P. Guo, R. P. H. Chang, and R. D. Schaller, "Large transient optical modulation of epsilon-near-zero colloidal nanocrystals," ACS Nano **10**, 10099–10105 (2016).
157. Y. Yang, K. Kelley, E. Sachet, S. Campione, T. S. Luk, J.-P. Maria, M. B. Sinclair, and I. Brener, "Femtosecond optical polarization switching using a cadmium oxide-based perfect absorber," Nat. Photonics **11**, 390–395 (2017).
158. K. M. Yu, D. M. Detert, G. Chen, W. Zhu, C. Liu, S. Grankowska, L. Hsu, O. D. Dubon, and W. Walukiewicz, "Defects and properties of cadmium oxide based transparent conductors," J. Appl. Phys. **119**, 181501 (2016).
159. E. L. Runnerstrom, K. P. Kelley, E. Sachet, C. T. Shelton, and J.-P. Maria, "Epsilon-near-zero modes and surface plasmon resonance in fluorine-doped cadmium oxide thin films," ACS Photon. **4**, 1885–1892 (2017).
160. C. P. Liu, Y. Foo, M. Kamruzzaman, C. Y. Ho, J. A. Zapien, W. Zhu, Y. J. Li, W. Walukiewicz, and K. M. Yu, "Effects of free carriers on the optical properties of doped CdO for full-spectrum photovoltaics," Phys. Rev. Appl. **6**, 064018 (2016).
161. S. Jin, Y. Yang, J. E. Medvedeva, J. R. Ireland, A. W. Metz, J. Ni, C. R. Kannewurf, A. J. Freeman, and T. J. Marks, "Dopant ion size and electronic structure effects on transparent conducting oxides. Sc-doped CdO thin films grown by MOCVD," J. Am. Chem. Soc. **126**, 13787–13793 (2004).
162. R. G. Bikbaev, S. Y. Vetrov, and I. V. Timofeev, "Transparent conductive oxides for the epsilon-near-zero Tamm plasmon polaritons," J. Opt. Soc. Am. B **36**, 2817–2823 (2019).
163. Y.-W. Huang, H. W. H. Lee, R. Sokhoyan, R. A. Pala, K. Thyagarajan, S. Han, D. P. Tsai, and H. A. Atwater, "Gate-tunable conducting oxide metasurfaces," Nano Lett. **16**, 5319–5325 (2016).
164. E. Yablonovitch, "Inhibited spontaneous emission in solid-state physics and electronics," Phys. Rev. Lett. **58**, 2059–2062 (1987).
165. S. John, "Strong localization of photons in certain disordered dielectric superlattices," Phys. Rev. Lett. **58**, 2486–2489 (1987).
166. E. Rephaeli, A. P. Raman, and S. Fan, "Ultrabroadband photonic structures to achieve high-performance daytime radiative cooling," Nano Lett. **13**, 1457–1461 (2013).
167. A. P. Raman, M. A. Anoma, L. Zhu, E. Rephaeli, and S. Fan, "Passive radiative cooling below ambient air temperature under direct sunlight," Nature **515**, 540–544 (2014).
168. J.-Y. Wu, Y.-Z. Gong, P.-R. Huang, G.-J. Ma, and Q.-F. Dai, "Diurnal cooling for continuous thermal sources under direct subtropical sunlight produced by quasi-Cantor structure," Chin. Phys. B **26**, 104201 (2017).
169. J. Wu and Y. Chen, "Broadband radiative cooling and decoration for passively dissipated portable electronic devices by aperiodic photonic multilayers," Ann. Phys. (Leipzig) **532**, 2000001 (2020).
170. M. Habib, D. Briukhanova, N. Das, B. C. Yildiz, and H. Caglayan, "Controlling the plasmon resonance via epsilon-near-zero multilayer metamaterials," Nanophotonics **9**, 3637–3644 (2020).
171. T. G. Folland, G. Lu, A. Bruncz, J. R. Nolen, M. Tadjer, and J. D. Caldwell, "Vibrational coupling to epsilon-near-zero waveguide modes," ACS Photon. **7**, 614–621 (2020).
172. C. Rizza, A. Di Falco, and A. Ciattoni, "Gain assisted nanocomposite multilayers with near zero permittivity modulus at visible frequencies," Appl. Phys. Lett. **99**, 221107 (2011).
173. R. Maas, J. Parsons, N. Engheta, and A. Polman, "Experimental realization of an epsilon-near-zero metamaterial at visible wavelengths," Nat. Photonics **7**, 907–912 (2013).
174. L. Zhao and H. Xie, "A novel optical ε-near-zero material realized by multi-layered Ag/SiC film structures," Optik **183**, 513–522 (2019).
175. K. P. Kelley, E. L. Runnerstrom, E. Sachet, C. T. Shelton, E. D. Grimley, A. Klump, J. M. LeBeau, Z. Sitar, J. Y. Suen, W. J. Padilla, and J.-P. Maria, "Multiple epsilon-near-zero resonances in multilayered cadmium oxide: designing metamaterial-like optical properties in monolithic materials," ACS Photon. **6**, 1139–1145 (2019).
176. D. Dai and M. Zhang, "Mode hybridization and conversion in silicon-on-insulator nanowires with angled sidewalls," Opt. Express **23**, 32452–32464 (2015).
177. V. Caligiuri, M. Palei, G. Biffi, and R. Krahne, "Hybridization of epsilon-near-zero modes via resonant tunneling in layered metal-insulator double nanocavities," Nanophotonics **8**, 1505–1512 (2019).
178. A. R. Rashed, B. C. Yildiz, S. R. Ayyagari, and H. Caglayan, "Hot electron dynamics in ultrafast multilayer epsilon-near-zero metamaterials," Phys. Rev. B **101**, 165301 (2020).
179. M. Koivurova, T. Hakala, J. Turunen, A. T. Friberg, M. Ornigotti, and H. Caglayan, "Metamaterials designed for enhanced ENZ properties," New J. Phys. **22**, 093054 (2020).
180. Y. G. Lee and C.-S. Kee, "Constant cutoff frequency of a two-dimensional photonic crystal composed of metallic rods and epsilon-near-zero materials," Physica B **600**, 412598 (2021).
181. Z. Zhou and Y. Li, "Effective epsilon-near-zero (ENZ) antenna based on transverse cutoff mode," IEEE Trans. Antennas Propag. **67**, 2289–2297 (2019).
182. W. Ji, J. Luo, and Y. Lai, "Extremely anisotropic epsilon-near-zero media in waveguide metamaterials," Opt. Express **27**, 19463–19473 (2019).
183. S. Benis, N. Munera, E. W. Van Stryland, and D. J. Hagan, "Enhanced nonlinear phase-shift in epsilon-near-zero materials: the effect of group and phase velocity," in *14th Pacific Rim Conference on Lasers and Electro-Optics (CLEO PR)* (OSA, 2020), paper C8B_4.
184. S. A. Benis, N. Munera, E. W. Van Stryland, and D. J. Hagan, "Large nonlinear phase shift in epsilon-near-zero materials: the effect of group and phase velocity," Proc. SPIE **11460**, 1146010 (2020).
185. J. O. Kjellman, R. Stabile, and K. A. Williams, "Broadband giant group velocity dispersion in asymmetric InP dual layer, dual width waveguides," J. Lightwave Technol. **35**, 3791–3800 (2017).
186. J. Wu and Q. Li, "Highly efficient self-similar spectral compression of hyperbolic secant pulses enhanced by pre-chirping in nonlinear fibres," J. Opt. **21**, 085503 (2019).
187. J. Wu and Q. Li, "Efficient self-similar spectral compression of chirped soliton pulses in nonlinear fibers with exponentially increasing dispersion," in *Frontiers in Optics + Laser Science APS/DLS* (OSA, 2019), paper JTu4A.63.
188. P. Kelly and L. Kuznetsova, "Pulse shaping in the presence of enormous second-order dispersion in Al:ZnO/ZnO epsilon-near-zero metamaterial," Appl. Phys. B **124**, 60 (2018).
189. N. Smith, N. Doran, W. Forysiak, and F. Knox, "Soliton transmission using periodic dispersion compensation," J. Lightwave Technol. **15**, 1808–1822 (1997).
190. B. E. A. Saleh and M. C. Teich, *Fundamentals of Photonics*, 1st ed. (Wiley, 1991).
191. P. A. Belov, R. Marqués, S. I. Maslovski, I. S. Nefedov, M. Silveirinha, C. R. Simovski, and S. A. Tretyakov, "Strong spatial

dispersion in wire media in the very large wavelength limit," Phys. Rev. B **67**, 113103 (2003).
192. F. Capolino, *Theory and Phenomena of Metamaterials* (CRC Press, 2010).
193. K.-S. Lee and M. A. El-Sayed, "Gold and silver nanoparticles in sensing and imaging: sensitivity of plasmon response to size, shape, and metal composition," J. Phys. Chem. B **110**, 19220–19225 (2006).
194. J. B. González-Díaz, A. García-Martín, J. M. García-Martín, A. Cebollada, G. Armelles, B. Sepúlveda, Y. Alaverdyan, and M. Käll, "Plasmonic Au/Co/Au nanosandwiches with enhanced magneto-optical activity," Small **4**, 202–205 (2008).
195. E. Hutter and J. H. Fendler, "Exploitation of localized surface plasmon resonance," Adv. Mater. **16**, 1685–1706 (2004).
196. F. Kusa and S. Ashihara, "Spectral response of localized surface plasmon in resonance with mid-infrared light," J. Appl. Phys. **116**, 153103 (2014).
197. J. Doster, G. Baraldi, J. Gonzalo, J. Solis, J. Hernandez-Rueda, and J. Siegel, "Tailoring the surface plasmon resonance of embedded silver nanoparticles by combining nano- and femtosecond laser pulses," Appl. Phys. Lett. **104**, 153106 (2014).
198. R. Rosei, "Temperature modulation of the optical transitions involving the Fermi surface in Ag: theory," Phys. Rev. B **10**, 474–483 (1974).
199. N. Del Fatti, C. Voisin, M. Achermann, S. Tzortzakis, D. Christofilos, and F. Vallée, "Nonequilibrium electron dynamics in noble metals," Phys. Rev. B **61**, 16956–16966 (2000).
200. G. Della Valle, M. Conforti, S. Longhi, G. Cerullo, and D. Brida, "Real-time optical mapping of the dynamics of nonthermal electrons in thin gold films," Phys. Rev. B **86**, 155139 (2012).
201. N. Kinsey, C. DeVault, J. Kim, M. Ferrera, V. M. Shalaev, and A. Boltasseva, "Epsilon-near-zero Al-doped ZnO for ultrafast switching at telecom wavelengths," Optica **2**, 616–622 (2015).
202. H. Wang, K. Du, C. Jiang, Z. Yang, L. Ren, W. Zhang, S. J. Chua, and T. Mei, "Extended Drude model for intraband-transition-induced optical nonlinearity," Phys. Rev. Appl. **11**, 064062 (2019).
203. B. C. Yildiz and H. Caglayan, "Epsilon-near-zero media coupled with localized surface plasmon modes," Phys. Rev. B **102**, 165303 (2020).
204. H. F. Arnoldus and Z. Xu, "Force on an electric dipole near an ENZ interface," J. Opt. Soc. Am. B **36**, F18–F24 (2019).
205. I. S. Nefedov and J. M. Rubi, "Casimir forces exerted by epsilon-near-zero hyperbolic materials," Sci. Rep. **10**, 16831 (2020).
206. C. S. Castro, E. R. Méndez, A. Vial, G. Lerondel, Y. Battie, A. Bruyant, and R. Vincent, "Optical density of states near planar ENZ materials," Opt. Lett. **45**, 3593–3596 (2020).
207. Y. Zhou, M. Karimi, J. Upham, O. Reshef, C. Liu, A. E. Willner, M. Z. Alam, and R. W. Boyd, "Frequency conversion through time refraction using an epsilon-near-zero material," in *Conference on Lasers and Electro-Optics* (OSA, 2019), paper FF1B.3.
208. C. Liu, M. Z. Alam, K. Pang, K. Manukyan, J. R. Hendrickson, E. M. Smith, Y. Zhou, O. Reshef, H. Song, R. Zhang, H. Song, F. Alishahi, A. Fallahpour, A. Almaiman, R. W. Boyd, M. Tur, and A. E. Willner, "Experimental demonstration of self-phase-modulation induced wavelength shift in an 80-nm thick ITO-ENZ material in the telecom C band," in *Conference on Lasers and Electro-Optics* (OSA, 2020), paper FTu3Q.5.
209. K. Pang, M. Z. Alam, Y. Zhou, O. Reshef, C. Liu, K. Manukyan, M. Voegtle, A. Pennathur, C. Tseng, X. Su, H. Song, Z. Zhao, R. Zhang, H. Song, N. Hu, A. Almaiman, J. M. Dawlaty, R. W. Boyd, M. Tur, and A. E. Willner, "Plasmonic nanoantenna-enhanced adiabatic wavelength conversion using a time-varying epsilon-near-zero-based metasurface," in *Conference on Lasers and Electro-Optics* (OSA, 2020), paper FTh4Q.6.
210. M. Z. Alam, Y. Zhou, M. Karimi, J. Upham, O. Reshef, C. Liu, A. E. Willner, and R. W. Boyd, "Epsilon-near-zero material for time refraction," in *Nonlinear Optics (NLO)* (OSA, 2019), paper NTh3A.4.
211. V. Bruno, S. Vezzoli, C. DeVault, E. Carnemolla, M. Ferrera, A. Boltasseva, V. M. Shalaev, D. Faccio, and M. Clerici, "Broad frequency shift of parametric processes in epsilon-near-zero time-varying media," Appl. Sci. **10**, 1318 (2020).
212. V. Bruno, C. DeVault, S. Vezzoli, Z. Kudyshev, T. Huq, S. Mignuzzi, A. Jacassi, S. Saha, Y. D. Shah, S. A. Maier, D. R. S. Cumming, A. Boltasseva, M. Ferrera, M. Clerici, D. Faccio, R. Sapienza, and V. M. Shalaev, "Negative refraction in time-varying strongly coupled plasmonic-antenna–epsilon-near-zero systems," Phys. Rev. Lett. **124**, 043902 (2020).
213. M. Bellini, C. Lyngå, A. Tozzi, M. B. Gaarde, T. W. Hänsch, A. L'Huillier, and C.-G. Wahlström, "Temporal coherence of ultrashort high-order harmonic pulses," Phys. Rev. Lett. **81**, 297–300 (1998).
214. E. Hemsing, M. Dunning, C. Hast, T. O. Raubenheimer, S. Weathersby, and D. Xiang, "Highly coherent vacuum ultraviolet radiation at the 15th harmonic with echo-enabled harmonic generation technique," Phys. Rev. Spec. Top. Accel. Beams **17**, 070702 (2014).
215. M. Z. Alam, S. A. Schulz, J. Upham, I. De Leon, and R. W. Boyd, "Large optical nonlinearity of nanoantennas coupled to an epsilon-near-zero material," Nat. Photonics **12**, 79–83 (2018).
216. R. Secondo and N. Kinsey, "Modelling nonlinear near-zero-index media through carrier kinetic models," in *Frontiers in Optics + Laser Science APS/DLS* (OSA, 2019), paper JTu4A.34.
217. N. Kinsey, R. Secondo, and D. Fomra, "Optical nonlinearities in transparent conducting oxides–the role of loss," in *IEEE Research and Applications of Photonics in Defense Conference (RAPID)* (IEEE, 2019), pp. 1–4.
218. R. Secondo, J. Khurgin, and N. Kinsey, "Absorptive loss and band non-parabolicity as a physical origin of large nonlinearity in epsilon-near-zero materials," Opt. Mater. Express **10**, 1545–1560 (2020).
219. D. Rocco, C. De Angelis, D. de Ceglia, L. Carletti, M. Scalora, and M. Vincenti, "Dielectric nanoantennas on epsilon-near-zero substrates: impact of losses on second order nonlinear processes," Opt. Commun. **456**, 124570 (2020).
220. H. Liu, S. Zhong, Y. Gao, J. Huang, T. Liu, and G. Xu, "Tailoring absorption spectrum by inserting an epsilon-near-zero film into metal-dielectric-metal assembly," Solid State Commun. **289**, 17–21 (2019).
221. Y. Li, I. Liberal, and N. Engheta, "Structural dispersion–based reduction of loss in epsilon-near-zero and surface plasmon polariton waves," Sci. Adv. **5**, eaav3764 (2019).
222. H. Ma, Y. Zhao, Y. Shao, Y. Lian, W. Zhang, G. Hu, Y. Leng, and J. Shao, "Principles to tailor the saturable and reverse saturable absorption of epsilon-near-zero material," Photon. Res. **9**, 678–686 (2021).
223. S. Xian, L. Nie, J. Qin, T. Kang, C. Li, J. Xie, L. Deng, and L. Bi, "Effect of oxygen stoichiometry on the structure, optical and epsilon-near-zero properties of indium tin oxide films," Opt. Express **27**, 28618–28628 (2019).
224. S. Gurung, A. Anopchenko, S. Bej, J. Joyner, J. D. Myers, J. Frantz, and H. W. H. Lee, "Atomic layer engineering of epsilon-near-zero ultrathin films with controllable field enhancement," Adv. Mater. Interfaces **7**, 2000844 (2020).
225. X. Qiu, J. Shi, Y. Li, and F. Zhang, "All-dielectric multifunctional transmittance-tunable metasurfaces based on guided-mode resonance and ENZ effect," Nanotechnology **32**, 065202 (2021).
226. X. Qiu, F. Yang, Y. Li, and F. Zhang, "All-dielectric tunable metasurface based on guide-mode resonance and ENZ effects," in *Conference on Lasers and Electro-Optics* (OSA, 2020), paper JW2D.16.
227. H. Zheng, R.-J. Zhang, D.-H. Li, X. Chen, S.-Y. Wang, Y.-X. Zheng, M.-J. Li, Z.-G. Hu, N. Dai, and L.-Y. Chen, "Optical properties of Al-doped ZnO films in the infrared region and their absorption applications," Nano. Res. Lett. **13**, 149 (2018).
228. M. Herrero, J. A. Mendiola, A. Cifuentes, and E. Ibáñez, "Supercritical fluid extraction: recent advances and applications," J. Chromatogr. A **1217**, 2495–2511 (2010).
229. F. Maxim, C. Contescu, P. Boillat, B. Niceno, K. Karalis, A. Testino, and C. Ludwig, "Visualization of supercritical water pseudo-boiling at Widom line crossover," Nat. Commun. **10**, 4114 (2019).
230. K.-C. Chang, T.-M. Tsai, T.-C. Chang, Y.-E. Syu, C.-C. Wang, S.-L. Chuang, C.-H. Li, D.-S. Gan, and S. M. Sze, "Reducing operation current of Ni-doped silicon oxide resistance random access memory by supercritical CO_2 fluid treatment," Appl. Phys. Lett. **99**, 263501 (2011).

231. T.-M. Tsai, K.-C. Chang, T.-C. Chang, Y.-E. Syu, K.-H. Liao, B.-H. Tseng, and S. M. Sze, "Dehydroxyl effect of Sn-doped silicon oxide resistance random access memory with supercritical CO_2 fluid treatment," Appl. Phys. Lett. **101**, 112906 (2012).
232. K.-C. Chang, T.-M. Tsai, R. Zhang, T.-C. Chang, K.-H. Chen, J.-H. Chen, T.-F. Young, J. C. Lou, T.-J. Chu, C.-C. Shih, J.-H. Pan, Y.-T. Su, Y.-E. Syu, C.-W. Tung, M.-C. Chen, J.-J. Wu, Y. Hu, and S. M. Sze, "Electrical conduction mechanism of Zn:SiO_x resistance random access memory with supercritical CO_2 fluid process," Appl. Phys. Lett. **103**, 083509 (2013).
233. K.-C. Chang, C.-H. Pan, T.-C. Chang, T.-M. Tsai, R. Zhang, J.-C. Lou, T.-F. Young, J.-H. Chen, C.-C. Shih, T.-J. Chu, J.-Y. Chen, Y.-T. Su, J.-P. Jiang, K.-H. Chen, H.-C. Huang, Y.-E. Syu, D.-S. Gan, and S. M. Sze, "Hopping effect of hydrogen-doped silicon oxide insert RRAM by supercritical CO_2 fluid treatment," IEEE Electron Device Lett. **34**, 617–619 (2013).
234. K.-H. Chen, K.-C. Chang, T.-C. Chang, T.-M. Tsai, S.-P. Liang, T.-F. Young, Y.-E. Syu, and S. M. Sze, "Improvement of bipolar switching properties of Gd:SiO_x RRAM devices on indium tin oxide electrode by low-temperature supercritical CO_2 treatment," Nano. Res. Lett. **11**, 52 (2016).
235. C. Ye, J.-J. Wu, C.-H. Pan, T.-M. Tsai, K.-C. Chang, H. Wu, N. Deng, and H. Qian, "Boosting the performance of resistive switching memory with a transparent ITO electrode using supercritical fluid nitridation," RSC Adv. **7**, 11585–11590 (2017).
236. D. Jalas, A. Petrov, M. Eich, W. Freude, S. Fan, Z. Yu, R. Baets, M. Popović, A. Melloni, J. D. Joannopoulos, M. Vanwolleghem, C. R. Doerr, and H. Renner, "What is–and what is not–an optical isolator," Nat. Photonics **7**, 579–582 (2013).
237. B. Jin and C. Argyropoulos, "Nonreciprocal transmission in nonlinear PT-symmetric metamaterials using epsilon-near-zero media doped with defects," Adv. Opt. Mater. **7**, 1901083 (2019).
238. X. Jiang, H. Lu, Q. Li, H. Zhou, S. Zhang, and H. Zhang, "Epsilon-near-zero medium for optical switches in a monolithic waveguide chip at 1.9 μm," Nanophotonics **7**, 1835–1843 (2018).
239. S. Saha, B. T. Diroll, J. Shank, Z. Kudyshev, A. Dutta, S. N. Chowdhury, T. S. Luk, S. Campione, R. D. Schaller, V. M. Shalaev, A. Boltasseva, and M. G. Wood, "Broadband, high-speed, and large-amplitude dynamic optical switching with yttrium-doped cadmium oxide," Adv. Funct. Mater. **30**, 1908377 (2020).
240. A. D. Neira, G. A. Wurtz, and A. V. Zayats, "All-optical switching in silicon photonic waveguides with an epsilon-near-zero resonant cavity," Photon. Res. **6**, B1–B5 (2018).
241. W. Wang, Z. Guan, and H. Xu, "A high speed electrically switching reflective structural color display with large color gamut," Nanoscale **13**, 1164–1171 (2021).
242. J. Bohn, T. S. Luk, C. Tollerton, S. W. Hutchings, I. Brener, S. Horsley, W. L. Barnes, and E. Hendry, "All-optical switching of an epsilon-near-zero plasmon resonance in indium tin oxide," Nat. Commun. **12**, 1017 (2021).
243. Z. Chai, X. Hu, F. Wang, C. Li, Y. Ao, Y. Wu, K. Shi, H. Yang, and Q. Gong, "Ultrafast on-chip remotely-triggered all-optical switching based on epsilon-near-zero nanocomposites," Laser Photon. Rev. **11**, 1700042 (2017).
244. Z. Lu, W. Zhao, and K. Shi, "Ultracompact electroabsorption modulators based on tunable epsilon-near-zero-slot waveguides," IEEE Photon. J. **4**, 735–740 (2012).
245. H. W. Lee, G. Papadakis, S. P. Burgos, K. Chander, A. Kriesch, R. Pala, U. Peschel, and H. A. Atwater, "Nanoscale conducting oxide PlasMOStor," Nano Lett. **14**, 6463–6468 (2014).
246. H. Zhao, Y. Wang, A. Capretti, L. D. Negro, and J. Klamkin, "Broadband electroabsorption modulators design based on epsilon-near-zero indium tin oxide," IEEE J. Sel. Top. Quantum Electron. **21**, 192–198 (2015).
247. J. Baek, J.-B. You, and K. Yu, "Free-carrier electro-refraction modulation based on a silicon slot waveguide with ITO," Opt. Express **23**, 15863–15876 (2015).
248. U. Koch, C. Hoessbacher, J. Niegemann, C. Hafner, and J. Leuthold, "Digital plasmonic absorption modulator exploiting epsilon-near-zero in transparent conducting oxides," IEEE Photon. J. **8**, 4800813 (2016).
249. G. Sinatkas, A. Pitilakis, D. C. Zografopoulos, R. Beccherelli, and E. E. Kriezis, "Transparent conducting oxide electro-optic modulators on silicon platforms: a comprehensive study based on the drift-diffusion semiconductor model," J. Appl. Phys. **121**, 023109 (2017).
250. S. Campione, M. G. Wood, D. K. Serkland, S. Parameswaran, J. Ihlefeld, T. S. Luk, J. R. Wendt, K. M. Geib, and G. A. Keeler, "Submicrometer epsilon-near-zero electroabsorption modulators enabled by high-mobility cadmium oxide," IEEE Photon. J. **9**, 6601307 (2017).
251. E. Li, Q. Gao, R. T. Chen, and A. X. Wang, "Ultracompact silicon-conductive oxide nanocavity modulator with 0.02 lambda-cubic active volume," Nano Lett. **18**, 1075–1081 (2018).
252. M. H. Tahersima, Z. Ma, Y. Gui, S. Sun, H. Wang, R. Amin, H. Dalir, R. Chen, M. Miscuglio, and V. J. Sorger, "Coupling-enhanced dual ITO layer electro-absorption modulator in silicon photonics," Nanophotonics **8**, 1559–1566 (2019).
253. R. Amin, R. Maiti, Y. Gui, C. Suer, M. Miscuglio, E. Heidari, R. T. Chen, H. Dalir, and V. J. Sorger, "Sub-wavelength GHz-fast broadband ITO Mach–Zehnder modulator on silicon photonics," Optica **7**, 333–335 (2020).
254. Q. Gao, E. Li, and A. X. Wang, "Comparative analysis of transparent conductive oxide electro-absorption modulators," Opt. Mater. Express **8**, 2850–2862 (2018).
255. Q. Gao, E. Li, B. Zhou, and A. X. Wang, "Hybrid silicon-conductive oxide-plasmonic electro-absorption modulator with 2-V swing voltage," J. Nanophoton. **13**, 036005 (2019).
256. A. Forouzmand and H. Mosallaei, "Electro-optical amplitude and phase modulators based on tunable guided-mode resonance effect," ACS Photon. **6**, 2860–2869 (2019).
257. S. Rajput, V. Kaushik, S. Jain, P. Tiwari, A. K. Srivastava, and M. Kumar, "Optical modulation in hybrid waveguide based on Si-ITO heterojunction," J. Lightwave Technol. **38**, 1365–1371 (2020).
258. Y. Sha, J. Wu, Z. T. Xie, H. Y. Fu, and Q. Li, "Comparison study of multi-slot designs in epsilon-near-zero waveguide-based electro-optical modulators," IEEE Photon. J. **13**, 4800412 (2021).
259. S. Zhu, G. Q. Lo, and D. L. Kwong, "Design of an ultra-compact electro-absorption modulator comprised of a deposited TiN/HfO_2/ITO/Cu stack for CMOS backend integration," Opt. Express **22**, 17930–17947 (2014).
260. M. Ayata, Y. Nakano, and T. Tanemura, "Silicon rib waveguide electro-absorption optical modulator using transparent conductive oxide bilayer," Jpn. J. Appl. Phys. **55**, 042201 (2016).
261. L. Jin, Q. Chen, W. Liu, and S. Song, "Electro-absorption modulator with dual carrier accumulation layers based on epsilon-near-zero ITO," Plasmonics **11**, 1087–1092 (2016).
262. J.-S. Kim and J. T. Kim, "Silicon electro-optic modulator based on an ITO-integrated tunable directional coupler," J. Phys. D **49**, 075101 (2016).
263. M. Y. Abdelatty, M. M. Badr, and M. A. Swillam, "Compact silicon electro-optical modulator using hybrid ITO tri-coupled waveguides," J. Lightwave Technol. **36**, 4198–4204 (2018).
264. X. Qiu, X. Ruan, Y. Li, and F. Zhang, "Multi-layer MOS capacitor based polarization insensitive electro-optic intensity modulator," Opt. Express **26**, 13902–13914 (2018).
265. L. Jin, L. Wen, L. Liang, Q. Chen, and Y. Sun, "Polarization-insensitive surface plasmon polarization electro-absorption modulator based on epsilon-near-zero indium tin oxide," Nano. Res. Lett. **13**, 39 (2018).
266. M. M. Badr, M. M. Elgarf, and M. A. Swillam, "Silicon ring resonator electro-optical modulator utilizing epsilon-near-zero characteristics of indium tin oxide," Phys. Scr. **94**, 125507 (2019).
267. S. Feng and K. Halterman, "Coherent perfect absorption in epsilon-near-zero metamaterials," Phys. Rev. B **86**, 165103 (2012).
268. T. S. Luk, S. Campione, I. Kim, S. Feng, Y. C. Jun, S. Liu, J. B. Wright, I. Brener, P. B. Catrysse, S. Fan, and M. B. Sinclair, "Directional perfect absorption using deep subwavelength low-permittivity films," Phys. Rev. B **90**, 085411 (2014).
269. S. Zhong, Y. Ma, and S. He, "Perfect absorption in ultrathin anisotropic ε-near-zero metamaterials," Appl. Phys. Lett. **105**, 023504 (2014).

270. J. Yoon, M. Zhou, M. A. Badsha, T. Y. Kim, Y. C. Jun, and C. K. Hwangbo, "Broadband epsilon-near-zero perfect absorption in the near-infrared," Sci. Rep. **5**, 12788 (2015).
271. T. Y. Kim, M. A. Badsha, J. Yoon, S. Y. Lee, Y. C. Jun, and C. K. Hwangbo, "General strategy for broadband coherent perfect absorption and multi-wavelength all-optical switching based on epsilon-near-zero multilayer films," Sci. Rep. **6**, 22941 (2016).
272. J. Rensberg, Y. Zhou, S. Richter, C. Wan, S. Zhang, P. Schöppe, R. Schmidt-Grund, S. Ramanathan, F. Capasso, M. A. Kats, and C. Ronning, "Epsilon-near-zero substrate engineering for ultrathin-film perfect absorbers," Phys. Rev. Appl. **8**, 014009 (2017).
273. V. Bruno, S. Vezzoli, C. DeVault, T. Roger, M. Ferrera, A. Boltasseva, V. M. Shalaev, and D. Faccio, "Dynamical control of broadband coherent absorption in ENZ films," Micromachines (Basel) **11**, 110 (2020).
274. J. R. Hendrickson, S. Vangala, C. Dass, R. Gibson, J. Goldsmith, K. Leedy, D. E. Walker, J. W. Cleary, W. Kim, and J. Guo, "Coupling of epsilon-near-zero mode to gap plasmon mode for flat-top wideband perfect light absorption," ACS Photon. **5**, 776–781 (2018).
275. J. Kim, E. G. Carnemolla, C. DeVault, A. M. Shaltout, D. Faccio, V. M. Shalaev, A. V. Kildishev, M. Ferrera, and A. Boltasseva, "Dynamic control of nanocavities with tunable metal oxides," Nano Lett. **18**, 740–746 (2018).
276. P. Zhou, G. Zheng, F. Xian, and L. Xu, "Dynamically switchable polarization-independent and broadband metasurface perfect absorber in the visible and near-infrared spectra regime," Results Phys. **11**, 278–282 (2018).
277. Z. Wang, P. Zhou, and G. Zheng, "Electrically switchable highly efficient epsilon-near-zero metasurfaces absorber with broadband response," Results Phys. **14**, 102376 (2019).
278. K. Chaudhuri, M. Alhabeb, Z. Wang, V. M. Shalaev, Y. Gogotsi, and A. Boltasseva, "Highly broadband absorber using plasmonic titanium carbide (MXene)," ACS Photon. **5**, 1115–1122 (2018).
279. S. Lee, T. Q. Tran, M. Kim, H. Heo, J. Heo, and S. Kim, "Angle- and position-insensitive electrically tunable absorption in graphene by epsilon-near-zero effect," Opt. Express **23**, 33350–33358 (2015).
280. M. Lobet, B. Majerus, L. Henrard, and P. Lambin, "Perfect electromagnetic absorption using graphene and epsilon-near-zero metamaterials," Phys. Rev. B **93**, 235424 (2016).
281. S. S. Mirshafieyan and D. A. Gregory, "Electrically tunable perfect light absorbers as color filters and modulators," Sci. Rep. **8**, 2635 (2018).
282. K. Halterman, M. Alidoust, and A. Zyuzin, "Epsilon-near-zero response and tunable perfect absorption in Weyl semimetals," Phys. Rev. B **98**, 085109 (2018).
283. P. T. Dang, K. Q. Le, J.-H. Lee, and T. K. Nguyen, "A designed broadband absorber based on ENZ mode incorporating plasmonic metasurfaces," Micromachines (Basel) **10**, 673 (2019).
284. L. Zhang, K. Wang, H. Chen, and Y. Zhang, "Robust conformal perfect absorber involving lossy ultrathin film," Photonics **7**, 57 (2020).
285. R. Bikbaev, S. Vetrov, and I. Timofeev, "Epsilon-near-zero absorber by Tamm plasmon polariton," Photonics **6**, 28 (2019).
286. Y. Li and C. Argyropoulos, "Tunable nonlinear coherent perfect absorption with epsilon-near-zero plasmonic waveguides," Opt. Lett. **43**, 1806–1809 (2018).
287. B. X. Wang, M. Q. Liu, T. C. Huang, and C. Y. Zhao, "Micro/nanostructures for far-field thermal emission control: an overview," ES Energy Environ. **6**, 18–38 (2019).
288. V. Caligiuri, M. Palei, M. Imran, L. Manna, and R. Krahne, "Planar double-epsilon-near-zero cavities for spontaneous emission and Purcell effect enhancement," ACS Photon. **5**, 2287–2294 (2018).
289. A. R. Davoyan and N. Engheta, "Nonreciprocal emission in magnetized epsilon-near-zero metamaterials," ACS Photon. **6**, 581–586 (2019).
290. X. Duan, F. Zhang, Z. Qian, H. Hao, L. Shan, Q. Gong, and Y. Gu, "Accumulation and directionality of large spontaneous emission enabled by epsilon-near-zero film," in *Frontiers in Optics + Laser Science APS/DLS* (OSA, 2019), paper JW4A.69.
291. V. Caligiuri, G. Biffi, M. Palei, B. Martín-García, R. D. Pothuraju, Y. Bretonnière, and R. Krahne, "Angle and polarization selective spontaneous emission in dye-doped metal/insulator/metal nanocavities," Adv. Opt. Mater. **8**, 1901215 (2020).
292. Z. Sakotic, A. Krasnok, N. Cselyuszka, N. Jankovic, and A. Alú, "Berreman embedded eigenstates for narrow-band absorption and thermal emission," Phys. Rev. Appl. **13**, 064073 (2020).
293. A. Alù and N. Engheta, "Dielectric sensing in ε-near-zero narrow waveguide channels," Phys. Rev. B **78**, 045102 (2008).
294. H. Lobato-Morales, D. V. B. Murthy, A. Corona-Chavez, J. L. Olvera-Cervantes, J. Martinez-Brito, and L. G. Guerrero-Ojeda, "Permittivity measurements at microwave frequencies using epsilon-near-zero (ENZ) tunnel structure," IEEE Trans. Microw. Theory Tech. **59**, 1863–1868 (2011).
295. A. K. Jha and M. J. Akhtar, "Design of multilayered epsilon-near-zero microwave planar sensor for testing of dispersive materials," IEEE Trans. Microw. Theory Tech. **63**, 2418–2426 (2015).
296. V. Pacheco-Peña, M. Beruete, P. Rodríguez-Ulibarri, and N. Engheta, "On the performance of an ENZ-based sensor using transmission line theory and effective medium approach," New J. Phys. **21**, 043056 (2019).
297. Z. Fusco, M. Taheri, R. Bo, T. Tran-Phu, H. Chen, X. Guo, Y. Zhu, T. Tsuzuki, T. P. White, and A. Tricoli, "Non-periodic epsilon-near-zero metamaterials at visible wavelengths for efficient non-resonant optical sensing," Nano Lett. **20**, 3970–3977 (2020).
298. Z. Meng, H. Cao, R. Liu, and X. Wu, "An electrically tunable dual-wavelength refractive index sensor based on a metagrating structure integrating epsilon-near-zero materials," Sensors **20**, 2301 (2020).
299. T. Yang, C. Ding, R. W. Ziolkowski, and Y. J. Guo, "A controllable plasmonic resonance in a SiC-loaded single-polarization single-mode photonic crystal fiber enables its application as a compact LWIR environmental sensor," Materials (Basel) **13**, 3915 (2020).
300. W.-C. Hsu, E. Li, B. Zhou, and A. X. Wang, "Characterization of field-effect mobility at optical frequency by microring resonators," Photon. Res. **9**, 615–621 (2021).
301. M. Maier, M. Mattheakis, E. Kaxiras, M. Luskin, and D. Margetis, "Homogenization of plasmonic crystals: seeking the epsilon-near-zero effect," Proc. R. Soc. A **475**, 20190220 (2019).
302. Y. Zhang, C.-K. Lim, Z. Dai, G. Yu, J. W. Haus, H. Zhang, and P. N. Prasad, "Photonics and optoelectronics using nano-structured hybrid perovskite media and their optical cavities," Phys. Rep. **795**, 1–51 (2019).
303. I. Abdelwahab, P. Dichtl, G. Grinblat, K. Leng, X. Chi, I. Park, M. P. Nielsen, R. F. Oulton, K. P. Loh, and S. A. Maier, "Giant and tunable optical nonlinearity in single-crystalline 2D perovskites due to excitonic and plasma effects," Adv. Mater. **31**, 1902685 (2019).
304. H. Kim, N. A. Charipar, and A. Piqué, "Tunable permittivity of La-doped $BaSnO_3$ thin films for near- and mid-infrared plasmonics," J. Phys. D **53**, 365103 (2020).
305. P. Zheng, Y. G. Shi, A. F. Fang, T. Dong, K. Yamaura, and N. L. Wang, "The charge carrier localization in the cubic perovskite $BaOsO_3$ revealed by an optical study," J. Phys. Condens. Matter **26**, 435601 (2014).
306. S. S. Kharintsev, A. V. Kharitonov, A. M. Alekseev, and S. G. Kazarian, "Superresolution stimulated Raman scattering microscopy using 2-ENZ nano-composites," Nanoscale **11**, 7710–7719 (2019).
307. Y. Ran, H. Lu, S. Zhao, Q. Guo, C. Gao, Z. Jiang, and Z. Wang, "Stoichiometry-modulated dual epsilon-near-zero characteristics of niobium nitride films," Appl. Surf. Sci. **537**, 147981 (2021).
308. X. Li, C. Rizza, S. A. Schulz, A. Ciattoni, and A. Di Falco, "Conformable optical coatings with epsilon near zero response," APL Photon. **4**, 056107 (2019).
309. E. Nahvi, I. Liberal, and N. Engheta, "Soft surfaces and enhanced nonlinearity enabled via epsilon-near-zero media doped with zero-area perfect electric conductor inclusions," Opt. Lett. **45**, 4591–4594 (2020).
310. L. Shen, X. Lin, B. Zheng, M. Y. Musa, Z. Xu, X. Zhang, and H. Wang, "Analog of giant magnetoimpedance in magnetized ε-near-zero plasma," Opt. Lett. **44**, 991–994 (2019).
311. L. Zhao, Y. Feng, B. Zhu, and J. Zhao, "Electromagnetic properties of magnetic epsilon-near-zero medium with dielectric dopants," Opt. Express **27**, 20073–20083 (2019).

312. A. Forouzmand and H. Mosallaei, "Tunable dual-band amplitude modulation with a double epsilon-near-zero metasurface," J. Opt. **22**, 094001 (2020).
313. V. Popov, S. Tretyakov, and A. Novitsky, "Brewster effect when approaching exceptional points of degeneracy: epsilon-near-zero behavior," Phys. Rev. B **99**, 045146 (2019).
314. K. Ito, Y. Yamada, A. Miura, and H. Iizuka, "High-aspect-ratio mushroom-like silica nanopillars immersed in air: epsilon-near-zero metamaterials mediated by a phonon-polaritonic anisotropy," RSC Adv. **9**, 16431–16438 (2019).
315. I. A. Kolmychek, A. R. Pomozov, V. B. Novikov, A. P. Leontiev, K. S. Napolskii, and T. V. Murzina, "Anomalous birefringence and enhanced magneto-optical effects in epsilon-near-zero metamaterials based on nanorods' arrays," Opt. Express **27**, 32069–32074 (2019).
316. M. Coppolaro, M. Moccia, G. Castaldi, N. Engheta, and V. Galdi, "Non-Hermitian doping of epsilon-near-zero media," Proc. Natl. Acad. Sci. USA **117**, 13921–13928 (2020).
317. J. Wu and X. Yang, "Ultrastrong extraordinary transmission and reflection in PT-symmetric Thue-Morse optical waveguide networks," Opt. Express **25**, 27724–27735 (2017).
318. J. Wu, "Beat-like frequency pattern of extraordinary transmission and reflection in PT-symmetric Fibonacci aperiodic optical networks of waveguide rings," Phys. Lett. A **383**, 125915 (2019).
319. J. Yang, K. Minn, A. Anopchenko, S. Gurung, and H. W. H. Lee, "Excitation of epsilon-near-zero mode in optical fiber," in *IEEE Photonics Conference (IPC)* (IEEE, 2019), pp. 1–2.
320. M. S. Hossain, S. M. A. Razzak, C. Markos, N. H. Hai, M. S. Habib, and M. S. Habib, "Highly birefringent, low-loss, and near-zero flat dispersion ENZ based THz photonic crystal fibers," IEEE Photon. J. **12**, 7202109 (2020).
321. M. Kim and S. Kim, "Epsilon-near-zero photonic crystal fibers for a large mode separation of orbital angular momentum modes," Optik **204**, 164209 (2020).
322. T. Yang, C. Ding, R. W. Ziolkowski, and Y. J. Guo, "An epsilon-near-zero (ENZ) based, ultra-wide bandwidth terahertz single-polarization single-mode photonic crystal fiber," J. Lightwave Technol. **39**, 223–232 (2021).
323. Z.-Q. Zhang and P. Sheng, "Wave localization in random networks," Phys. Rev. B **49**, 83–89 (1994).
324. M. Li, Y. Liu, and Z.-Q. Zhang, "Photonic band structure of Sierpinski waveguide networks," Phys. Rev. B **61**, 16193–16200 (2000).
325. S.-K. Cheung, T.-L. Chan, Z.-Q. Zhang, and C. T. Chan, "Large photonic band gaps in certain periodic and quasiperiodic networks in two and three dimensions," Phys. Rev. B **70**, 125104 (2004).
326. Z.-Y. Wang and X. Yang, "Strong attenuation within the photonic band gaps of multiconnected networks," Phys. Rev. B **76**, 235104 (2007).
327. J. Wu and X. Yang, "Theoretical design of a pump-free ultrahigh efficiency all-optical switching based on a defect ring optical waveguide network," Ann. Phys. (Leipzig) **531**, 1800258 (2019).
328. T.-S. Jiang, M. Xiao, Z.-Q. Zhang, and C.-T. Chan, "Physics and topological properties of periodic and aperiodic transmission line networks," Acta Phys. Sin. **69**, 150301 (2020).
329. C. M. Bender and S. Boettcher, "Real spectra in non-Hermitian Hamiltonians having PT symmetry," Phys. Rev. Lett. **80**, 5243–5246 (1998).
330. C. M. Bender, D. C. Brody, and H. F. Jones, "Complex extension of quantum mechanics," Phys. Rev. Lett. **89**, 270401 (2002).
331. R. El-Ganainy, K. G. Makris, D. N. Christodoulides, and Z. H. Musslimani, "Theory of coupled optical PT-symmetric structures," Opt. Lett. **32**, 2632–2634 (2007).
332. L. Feng, Z. J. Wong, R.-M. Ma, Y. Wang, and X. Zhang, "Single-mode laser by parity-time symmetry breaking," Science **346**, 972–975 (2014).
333. H. Hodaei, M.-A. Miri, M. Heinrich, D. N. Christodoulides, and M. Khajavikhan, "Parity-time-symmetric microring lasers," Science **346**, 975–978 (2014).
334. L. Li, Y. Cao, Y. Zhi, J. Zhang, Y. Zou, X. Feng, B.-O. Guan, and J. Yao, "Polarimetric parity-time symmetry in a photonic system," Light Sci. Appl. **9**, 169 (2020).
335. Y. Zhi, X. Yang, J. Wu, S. Du, P. Cao, D. Deng, and C. T. Liu, "Extraordinary characteristics for one-dimensional parity-time-symmetric periodic ring optical waveguide networks," Photon. Res. **6**, 579–586 (2018).
336. J.-Y. Wu, X.-H. Wu, X.-B. Yang, and H.-Y. Li, "Extraordinary transmission and reflection in PT-symmetric two-segment-connected triangular optical waveguide networks with perfect and broken integer waveguide length ratios," Chin. Phys. B **28**, 104208 (2019).
337. H. Li, X. Yang, J. Wu, and X. Wu, "Extraordinary characteristics of one-dimensional PT-symmetric ring optical waveguide networks with near-isometric and isometric arms," Europhys. Lett. **131**, 54001 (2020).
338. Y. Fu, Y. Xu, and H. Chen, "Zero index metamaterials with PT symmetry in a waveguide system," Opt. Express **24**, 1648–1657 (2016).
339. Y. Fu, X. Zhang, Y. Xu, and H. Chen, "Design of zero index metamaterials with PT symmetry using epsilon-near-zero media with defects," J. Appl. Phys. **121**, 094503 (2017).
340. Y. Li and C. Argyropoulos, "Exceptional points and spectral singularities in active epsilon-near-zero plasmonic waveguides," Phys. Rev. B **99**, 075413 (2019).